

University of Alberta

**DYNAMIC SPATIAL MODELLING
FOR NATURAL RESOURCES MANAGEMENT**

by

Patrick Emiel Van Laake



A thesis submitted to the Faculty of Graduate Studies and Research in partial
fulfillment of the requirements for the degree of Doctor of Philosophy

Department of Earth and Atmospheric Sciences

Edmonton, Alberta

Fall 2004



Library and
Archives Canada

Bibliothèque et
Archives Canada

Published Heritage
Branch

Direction du
Patrimoine de l'édition

395 Wellington Street
Ottawa ON K1A 0N4
Canada

395, rue Wellington
Ottawa ON K1A 0N4
Canada

Your file *Votre référence*
ISBN: 0-612-96034-X
Our file *Notre référence*
ISBN: 0-612-96034-X

The author has granted a non-exclusive license allowing the Library and Archives Canada to reproduce, loan, distribute or sell copies of this thesis in microform, paper or electronic formats.

L'auteur a accordé une licence non exclusive permettant à la Bibliothèque et Archives Canada de reproduire, prêter, distribuer ou vendre des copies de cette thèse sous la forme de microfiche/film, de reproduction sur papier ou sur format électronique.

The author retains ownership of the copyright in this thesis. Neither the thesis nor substantial extracts from it may be printed or otherwise reproduced without the author's permission.

L'auteur conserve la propriété du droit d'auteur qui protège cette thèse. Ni la thèse ni des extraits substantiels de celle-ci ne doivent être imprimés ou autrement reproduits sans son autorisation.

In compliance with the Canadian Privacy Act some supporting forms may have been removed from this thesis.

Conformément à la loi canadienne sur la protection de la vie privée, quelques formulaires secondaires ont été enlevés de cette thèse.

While these forms may be included in the document page count, their removal does not represent any loss of content from the thesis.

Bien que ces formulaires aient inclus dans la pagination, il n'y aura aucun contenu manquant.

Canada



In acquiring knowledge we all make mistakes.

Through mistakes we learn.

There is beauty in failure.

ACKNOWLEDGEMENTS

A thesis that takes more than four years to complete can not be fully attributed to a single person. Without the support of the people close to me, in my private life and at the University, this work would not have been completed.

To Anneke, who has endured my sometimes erratic lifestyle in the pursuit of producing this thesis. Her support, both emotionally and in managing our family, has enabled me to endure. To Thomas and Daniel, who never asked, during our many after school teas, why their dad couldn't be like all the other dads.

To Arturo Sánchez, supervisor of this research, who, in a distant past, convinced me that I should follow him to Edmonton to start this program and who has always actively supported my research, even if it was not always going in the same direction as his own academic pursuits. The freedom that he gave me to go down my own road has resulted in the thesis that lies before you.

On a more practical level, credit is due to the Department of Earth and Atmospheric Sciences at the University of Alberta, for providing me with an Academic Internship for several years and other forms of support. Other financial assistance was provided by the Sustainable Forest Management Network of Canada, and indirectly by the Sustainable Resources Development Branch of Alberta Environment.

The Fund for Support of International Development Assistance at the University of Alberta has financially supported my field work in Costa Rica.

Equipment for that field work was acquired with support from the Tinker Foundation.

The satellite imagery used in this study was acquired as part of the NASA's Earth Science Enterprise. The algorithms for the processing of these images into atmospheric products were developed by the MODIS Science Teams. The imagery was processed by the MODIS Adaptive Processing System (MODAPS) and Goddard Distributed Active Archive Center (DAAC), and are archived and distributed by the Goddard DAAC. In my opinion, the free provision of huge quantities of high quality satellite imagery to any interested person inside or outside of the United States is one of the great contributions of NASA to Mankind.

Long-term observation data of PAR at La Selva Biological Station were made available by the Organization for Tropical Studies (OTS).

Patrick Van Laake

April 2004

TABLE OF CONTENTS

Chapter 1	Introduction.....	1
A.	Focus on deforestation	2
B.	The PARcalc method.....	3
C.	Structure of the thesis.....	6
D.	Bibliography	6
Chapter 2	Focus on Deforestation: Zooming in on hot spots in highly fragmented ecosystems in Costa Rica	9
A.	Introduction.....	9
B.	Materials and methods	12
1.	Study area	12
2.	Methods.....	14
3.	Statistical procedures	16
C.	Results	19
1.	Siquirres.....	19
2.	Guápiles	21
3.	Talamanca.....	21
4.	Comparison between hot spots.....	22
5.	Biological corridors.....	24
D.	Discussion.....	26
1.	Advantages of hot spot analysis.....	26
2.	Implications of the study and need for future research	28

E.	Conclusions.....	30
F.	Bibliography	31
Chapter 3 Simplified atmospheric radiative transfer modelling for estimating		
	incident PAR using MODIS atmosphere products.....	35
A.	Introduction.....	35
B.	PAR Radiative Transfer.....	37
1.	Direct-beam irradiance.....	37
2.	Cloud top reflectance.....	39
3.	Diffuse irradiance	40
4.	Total surface-received PAR.....	41
C.	Computing PAR with MODIS	42
D.	Results	44
E.	Discussion.....	49
F.	Conclusion	52
G.	Bibliography	53
Chapter 4 Sensitivity, scale, and accuracy of the PARcalc method.....		
A.	Introduction.....	56
B.	PARcalc parameter sensitivity	59
1.	Ozone concentration.....	59
2.	Water content and aerosol concentration	59
3.	Cloud optical thickness and cloud top pressure.....	62
4.	Elevation.....	64
5.	Relative sensitivity of the parameters	65
C.	Topographic heterogeneity.....	68
D.	Discussion.....	74
1.	Parameter uncertainties	74
2.	Topographic heterogeneity and resolution of estimation.....	75
3.	Operational considerations.....	78

E.	Conclusion	78
F.	Bibliography	79
Chapter 5	Mapping PAR using MODIS atmosphere products	82
A.	Introduction.....	82
B.	Methods.....	83
1.	The PARcalc method.....	83
2.	Calculating PAR with MODIS imagery	83
3.	MODIS images.....	86
4.	Validation	86
C.	Results	88
1.	Comparison to field observations.....	89
2.	Monthly averaging	93
D.	Discussion.....	93
1.	Accuracy and sources of error	93
2.	Comparative performance.....	99
E.	Conclusion	101
F.	Bibliography	103
Chapter 6	Conclusions	106
A.	Focus on deforestation	106
B.	The PARcalc method.....	107
C.	Bibliography	109
Appendix A	Algorithmic structure of the PARcalc method	110

LIST OF TABLES

Table 2-1:	Fragmentation indices used in the analysis of the hot spots in the province of Limón, Costa Rica.....	18
Table 2-2:	Basic patch statistics for the province of Limón and selected deforestation hot spots in 1997.....	23
Table 2-3:	Composition of land cover in proposed GRUAS biological corridors inside selected deforestation hot spots in the province of Limón in 1997.....	26
Table 3-1:	MODIS atmospheric parameters used in calculating PAR.....	43
Table 3-2:	Locations in Costa Rica where PAR was measured.	44
Table 3-3:	Average error of incident PAR compared to measurements with a quantum sensor. <i>N</i> is the number of observations per location. Sampling is the period of time over which irradiance is averaged into a single recorded value.	45
Table 3-4:	Average error of incident PAR at two locations with spectrometer measurements. <i>N</i> is the number of observations per location.	48
Table 3-5:	Average error (%) of incident PAR compared to measurements with a quantum sensor, under different cloud conditions. The number of observations for each error is given in brackets below the error.	49
Table 4-1:	Default parameter values for the sensitivity analysis. These values are typical of tropical conditions. The skyview and exposition factors mimic the typical conditions under which a quantum sensor is deployed to measure PAR.	58
Table 4-2:	Symbology for the solar altitude angle used in the Figures in this Chapter.	58
Table 4-3:	Sensitivity $\Delta\text{PAR}/\beta$ of the PARcalc method to the Ångström turbidity coefficient β as a function of the solar altitude angle.....	61

Table 4-4: Parameter value intervals for the analysis of relative parameter sensitivity.....	66
Table 5-1: Errors in estimating daily integrated PAR at La Selva Biological Station and Santa Rosa National Park, October 2002 – January 2003.	90
Table 5-2: Monthly averaged daily PAR ($E\ m^{-2}\ day^{-1}$) measured at La Selva Biological Station and Santa Rosa National Park, and calculated with PARcalc, October 2002 – January 2003. The average of the N calculated values, is compared to the monthly average of the complete record of measurements....	94

LIST OF FIGURES

Figure 1-1: Location of the study sites referenced in this thesis. The grayed area along the Caribbean seaboard represents the Province of Limón where the deforestation hot spot study was performed. The three named locations are validation sites for the PARcalc method.....	2
Figure 2-1: The province of Limón (grayed) within Costa Rica, Central America.	13
Figure 2-2: Details of the deforestation contours. Solid contours depict the 10% deforestation isoline; dashed contours depict the 50% deforestation isoline. Dark gray represents forest cover, light gray other land cover, and black deforestation.....	16
Figure 2-3: Outline of the deforestation hot spots on the ternary image: A) Location of the hot spots within the province; B) Guápiles; C) Talamanca; D) Siquirres. Dark gray represents forest cover, light gray other land cover, and black deforestation.	20
Figure 2-4: Co-location of the Guápiles hot spot with a proposed GRUAS biological corridor. The Guápiles hot spot is outlined with the dashed line. The GRUAS area is indicated with the horizontal hash. The Tortuguero National Park is indicated with the slanted hash.	25
Figure 3-1: Graph of measured versus computed instantaneous PAR irradiance. Field campaign values at La Selva are indicated with ▲, Los Inocentes with ●, La Selva weather station data with +, and Santa Rosa data with □. A linear fit, constrained to pass through the origin at (0, 0), yields a correlation coefficient of 0.99, with an average error of 2.51%; N = 391.....	46

Figure 3-2: Absolute error of computed PAR versus measured PAR. Observations sampled at 1 minute (\blacktriangle and \bullet) show no correlation with irradiance, while observations sampled at 10 (\square) and 30 ($+$) minute intervals have an easily identified peak in the absolute error around $1000 \mu\text{E m}^{-2} \text{s}^{-1}$ which is due to changes in atmospheric conditions during the observation window. Symbols are identical to those in Figure 3-1.....	47
Figure 3-3: Comparison of measured PAR at 1 minute time-averaging, and 30 minute time-averaging. Data were recorded on 4 June 2002 at the La Selva location. The calculated PAR from MODIS data (9:57am) has an error of +1.04% compared to the 1 minute average and +2.52% compared to the 30 minute average.....	47
Figure 3-4: Graph of irradiance measured with a spectrometer (\bullet) versus computed irradiance in individual spectral bands (\blacksquare). The spectrometer has a band separation of $0.00158 \mu\text{m}$, while the computation uses bandwidths of $0.005 \mu\text{m}$ ($0.400 - 0.610 \mu\text{m}$) to $0.010 \mu\text{m}$ ($0.610 - 0.700 \mu\text{m}$). This data was recorded on 5 June 2002 at the La Selva location.....	48
Figure 4-1: Sensitivity $\Delta\text{PAR}/\text{O}_3$ of the PARcalc method to ozone absorption. Refer to Table 4-2 for symbology.....	60
Figure 4-2: Sensitivity $\Delta\text{PAR}/\beta$ of the PARcalc method to Ångström's turbidity coefficient β . Refer to Table 4-2 for symbology.....	61
Figure 4-3: Sensitivity $\Delta\text{PAR}/\tau$ of the PARcalc method to the cloud optical thickness τ . Refer to Table 4-2 for symbology.....	63
Figure 4-4: Relationship between the cloud optical thickness τ and the inverse of PAR. Refer to Table 4-2 for symbology.....	63
Figure 4-5: Sensitivity $\Delta\text{PAR}/P_c$ of the PARcalc method to the cloud top pressure P_c at a cloud optical thickness τ of 1.0 and an atmospheric water content w of 4.0 cm. Refer to Table 4-2 for symbology.....	64

Figure 4-6: Sensitivity $\Delta\text{PAR}/z$ of the PARcalc method to the elevation above mean sea level z . Refer to Table 4-2 for symbology.....	65
Figure 4-7: Relative sensitivity of the parameters in the estimation of PAR. The range of the parameters is given in Table 3. Solar altitude angles of (a) 30°; (b) 60° (preceding page); (c) 90° (this page).....	67-68
Figure 4-8: Northern flanks of the Cordillera Central in central Costa Rica used for the evaluation of the effects of topographic surface heterogeneity at 3 resolutions: 28.5 m (top left); 142.5 m (top right); 712.5 m (bottom). The 30 × 30 km area used for the evaluation is indicated with the black outline.....	70
Figure 4-9: Deviation of the cumulative distribution of the two lower resolution DEMs with respect to the native resolution DEM. The high frequency of the deviation at lower elevations is a result of the discrete elevation values.....	71
Figure 4-10: Distribution of slope classes for the three DEMs. At lower resolutions the slope is generally lower than at the native resolution of 28.5 m.....	72
Figure 4-11: Distribution of aspect classes for the three DEMs. At lower resolutions the aspect tends to the general direction of the slope in the area, which is to the north/north-east.....	72
Figure 4-12: Error surfaces of calculating PAR on the basis of the DEM at a resolution of 142.5 m (left) and 712.5m (right), relative to the DEM at the native resolution of 28.5 m. Light colours indicate an underestimation of PAR (up to $-165 \mu\text{E m}^{-2} \text{s}^{-1}$), dark colours an overestimation (up to $202 \mu\text{E m}^{-2} \text{s}^{-1}$), while gray tones indicate good correspondence between estimates. ...	73
Figure 4-13: Histogram of the distribution of errors in estimating PAR from DEMs at a resolution of 142.5 m (left) and 712.5 m (right), compared to the calculation of PAR from the DEM at a resolution of 28.5 m. The errors range from $-165 \mu\text{E m}^{-2} \text{s}^{-1}$ to $202 \mu\text{E m}^{-2} \text{s}^{-1}$. The magnitude of the bars is area in km^2	74

Figure 5-1: MODIS Terra and Aqua overpasses in relation to a typical progression of instantaneous irradiance from sunrise to sunset. About 84% of total irradiance occurs within 90 minutes of typical overpass times.	85
Figure 5-2: Location of La Selva Biological Station and Hacienda Los Inocentes in Costa Rica used to validate use of the PARcalc method with MODIS data. Contour lines are indicated at 500 meter intervals.....	87
Figure 5-3: Daily integrated PAR ($E\ m^{-2}\ day^{-1}$) in Costa Rica for julian days 5 (top left), 21 (bottom left), and 30 (bottom right) of 2003.	89
Figure 5-4: Scatterplot of daily irradiance ($E\ m^{-2}\ day^{-1}$) measured at La Selva Biological Station (\blacklozenge , $N = 61$) and Santa Rosa National Park (\blacktriangle , $N = 64$), and calculated with PARcalc, October 2002 - January 2003.	91
Figure 5-5: Comparison of high resolution PAR measurements ($\mu E\ m^{-2}\ s^{-1}$) (1 minute interval) to medium resolution measurements (30 minutes) at La Selva Biological Station, June 2002. The high frequency changes in PAR are caused by the alternating presence and absence of cloud cover.....	92
Figure 5-6: Average daily irradiance ($E\ m^{-2}\ day^{-1}$) for the month of January 2003, constructed from calculated PAR on a day-to-day basis. All available data was used (it was not restricted to a viewing angle of 45°). On average 13 daily PAR values were available for every land-based pixel. Orientation and legend are identical to those in Figure 5-3.....	95
Figure 5-7: Standard deviation of monthly averaged daily PAR ($E\ m^{-2}\ day^{-1}$) for the month of January 2003. Statistical support is the same as that in Figure 5-6. The standard deviation ranges from 0 (white) to 33.6 (black).....	96

LIST OF SYMBOLS

E_0	($W m^{-2} \mu m^{-1}$)	Monochromatic exoatmospheric solar irradiance.
F	(-)	Forward scatterance of diffuse radiation.
h	(degrees)	Hour angle of the Sun relative to local noon.
i	(degrees)	Angle between the incident radiation and the normal to the surface.
I_0	($W m^{-2} \mu m^{-1}$)	Monochromatic extraterrestrial incident radiation.
I_B	($W m^{-2} \mu m^{-1}$)	Monochromatic radiation receipt on a surface normal to the incident beam.
I_D	($W m^{-2} \mu m^{-1}$)	Monochromatic diffuse irradiance.
I_{PAR}	($E m^{-2} s^{-1}$)	Instantaneous PAR.
I_S	($W m^{-2} \mu m^{-1}$)	Total monochromatic surface irradiance.
k_{O_3}	(-)	Monochromatic absorption coefficient of ozone.
k_w	(-)	Monochromatic absorption coefficient of water vapour.
l	(cm)	Column atmospheric ozone concentration.
m_0	(-)	Relative atmospheric path to sea level.
m_p	(-)	Relative atmospheric path to surface pressure.
N	(-)	Julian day of the year.
PAR	($E m^{-2} day^{-1}$)	Daily integrated PAR.
P_z	(hPa)	Atmospheric pressure at the surface.

R_0	(-)	Cloud top reflectance coefficient.
T_0	(-)	Cloud transmittance coefficient.
V_D	(-)	Sky view factor.
w	(cm)	Column atmospheric water concentration.
z	(m)	Elevation above mean sea level.
α	(degrees)	Slope of the surface.
β	(-)	Ångström turbidity coefficient.
β_0	(-)	Cloud top backscatter coefficient.
δ	(degrees)	Solar declination angle.
ϕ	(degrees)	Latitude.
φ	(degrees)	Azimuth of the surface.
λ	(μm)	Wavelength of radiation.
θ	(degrees)	Solar zenith angle.
τ	(-)	Transmittance of the atmosphere.
τ_A	(-)	Atmospheric transmittance due to aerosol scattering.
τ_C	(-)	Cloud optical thickness.
τ_{OZ}	(-)	Atmospheric transmittance due to ozone absorption.
τ_R	(-)	Atmospheric transmittance due to Rayleigh scattering.
τ_W	(-)	Atmospheric transmittance due to water vapour absorption.
Ω	(-)	Solar geometry.
ω_0	(-)	Single scattering albedo.

Chapter 1

INTRODUCTION

Land cover changes in tropical environments have drawn considerable interest worldwide over the last 30 years for its implications at the local and global scale which mostly relate to the sustainability of new land uses on old forestland, climate change and biodiversity. Land managers have been plagued by a lack of adequate data to describe the current condition of the land-based resources and suitable tools to forecast their development sometime into the future, commensurate with forecasts of demographic development and plans for economic development (UNCED, 1993). In addition, the dynamics and the intrinsic value of the natural environment were not well understood. It is estimated, for instance, that more than 8,000 plant species are present in Costa Rica's forests, of which about 5,800 are catalogued. Many of these 8,000 species have not been studied, either to establish their physiological and environmental characteristics or their properties for human use (e.g. medicinal properties) (Hartshorn, 1983). As a result, the forest has not been regarded as a valuable resource, but rather as a repository of raw material waiting for conversion into something more tangible: timber and agricultural land.

The perception of the forest has since changed and considerably more (spatial) data has become available that, combined with increased knowledge of the forest ecosystem, now provides the possibility to describe the *state* of the forest in greater detail. However, the tools to model *change* in the forest still require further study as they are unable to incorporate the full body of knowledge of forest dynamics. This thesis deals with two aspects related to monitoring and modelling change in land cover, with application to Costa Rica. The first of these two aspects (Chapter 2) deals with the identification of areas at risk of land cover change. In

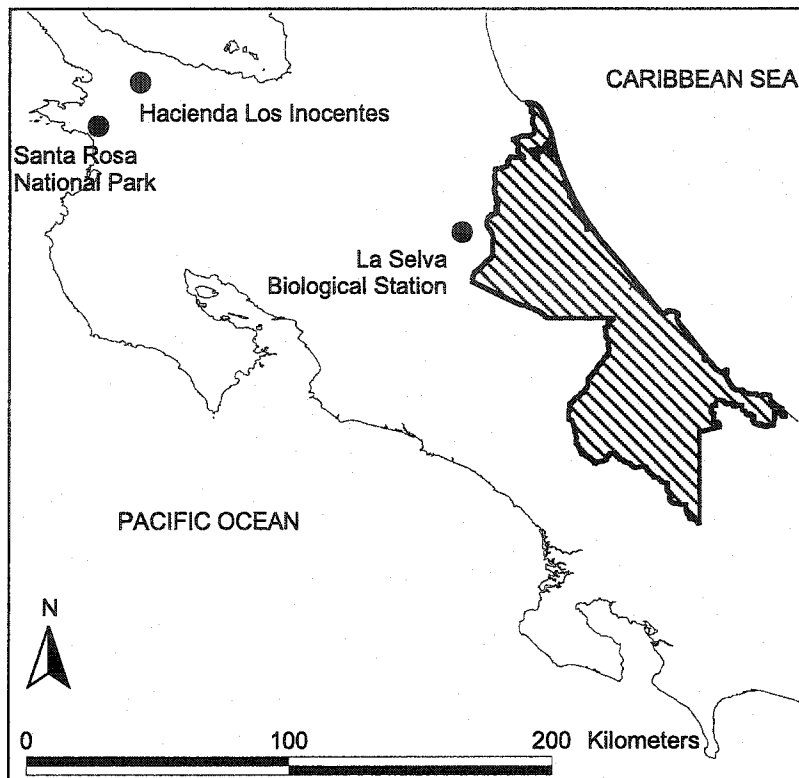


Figure 1-1: Location of the study sites referenced in this thesis. The grayed area along the Caribbean seaboard represents the Province of Limón where the deforestation hot spot study was performed. The three named locations are validation sites for the PARcalc method.

Chapters 3, 4, and 5 a model for the estimation of the terrestrial receipt of photosynthetically active radiation (PAR) is presented and applied to Costa Rica. PAR is an essential input for many models of plant growth.

A. Focus on deforestation

Land cover change – and then in particular deforestation – has been studied extensively using remotely sensed imagery. However, estimates of deforestation that are derived for arbitrarily defined regions (e.g., a single image, a country) provide little information that can be used for policy development, forest management or the

formulation of mitigation strategies. Without an indication of the drivers of deforestation the spatial pattern of deforestation provide nothing but an indication of where deforestation *took place*. When the spatial pattern can be placed into the context of why deforestation is occurring, it will be easier to predict where future deforestation *will take place*.

The use of such context has been applied in land cover change studies before (Allen and Barnes, 1985; Veldkamp and Fresco, 1996; Bawa and Dayandanan, 1997; Bouman et al., 1999), but rarely so in a spatially explicit manner and with the aim of predicting areas at high risk of deforestation in the near future. The method that is developed in Chapter 2 of this thesis combines a spatially explicit analysis with an analysis of what the likely socio-economic causes have been which led to the land conversion (Figure 1-1). This combination of “where” and “why” is very powerful in the development of policy governing land use, or management of land resources. Identifying specific areas at risk helps concentrate resources in those areas where they are likely to be most effective.

B. The PARcalc method

Increased knowledge of ecosystem component interaction and development has enabled the construction of models of system dynamics - e.g., vegetation growth, community development, and interaction between species - and the effects of disturbance - e.g. from human interference or catastrophic natural events (e.g. Harris, 1984; Swaine et al., 1987; Hartshorn, 1989; Overman et al., 1994; Bossel, 1996). These models are generally very detailed in the description of their core components, but they also tend to be more synoptic when it comes to the description of the larger environment in which the core components are to operate. For instance, in studies of plant growth and vegetation dynamics the physiology of photosynthesis may be very accurately described, but the lack of accurate data on solar irradiance in natural environments forces the model to rely on simulated data,

or data assembled from inferior sources (such as long-term climatological records of broad-band irradiance) (Bossel, 1996; Leigh, 1999; Running et al., 1999).

In the research that led to this thesis a physical model was developed with which an accurate estimate of PAR can be made from remotely sensed imagery from the MODIS sensor. This PARcalc model can estimate instantaneous PAR, coinciding with the local MODIS overpass, with an error ranging from 1.7% to 6.0% (Chapters 3 and 4). When instantaneous PAR is integrated over the day from two MODIS observations, from identical sensors aboard the Terra and Aqua satellite platforms, the error is between 5% and 8% (Chapter 5). This performance of the PARcalc method in combination with MODIS imagery is much better than any other practical method of estimating PAR over a large area that has been published in the scientific literature.

The importance of accurate estimates of PAR lies in the fact that PAR is an essential driver of all models of plant growth based on some representation of photosynthesis, which in its turn determines the amount of biomass in vegetation. In recent years the concern for the loss of natural habitat and biodiversity, as well as concern for global warming, have led to the development of a large number of models of vegetation dynamics (Penning de Vries, 1983; Bossel, 1996; Vandermeer, 1996). These models could potentially benefit from the increased accuracy with which PAR can now be estimated. Through the use of MODIS satellite imagery an estimate of PAR sensitive to local conditions can be made that will allow a more robust estimate of vegetation dynamics and thus total biomass contained in the forest. Such a spatialized estimate of biomass is important for at least three reasons:

1. Through the relationship between biomass and other important forest characteristics knowledge of the available biomass will improve the options to manage tropical forests to the extent that planned uses of the forest can

be assessed for their effect on available biomass and those related characteristics.

2. The spatialized estimate can be made sensitive to local disturbances in the forest, thus enabling the evaluation of land use changes in terms of the expected changes in biomass. Such information is critically important in forest policy development and management.
3. A robust estimate of biomass contained in the forest enables the reliable estimation of carbon stored in that biomass. Under the Kyoto Protocol of the Framework Convention on Climate Change countries can trade carbon emission rights, provided that the sequestering of carbon can be measured, monitored and verified - the so-called Clean Development Mechanism.

Such a spatialized estimate of biomass contained in the forest has traditionally been established using extrapolation of field observations (e.g. Helmer and Brown, 2000) or remote sensing (e.g. Fearnside, 1996; Lucas *et al.*, 2000a, 2000b). However, these studies do not consider the dynamics of the forest; an observation is made of the state of the forest at a certain point in time. Change may be inferred statistically by comparing multiple states (e.g. FAO, 1996), but this will reveal a regionalized trend rather than local dynamics. Such evidential change estimates are unlikely to yield reliable results when extrapolated into the future due to the highly non-linear dynamic interactions in the forest and they are mostly too insensitive to local conditions to be used for the evaluation of different land use scenarios. Process-based models of forest development on the other hand, are applicable over a larger parameter domain due to the consideration of physiological processes in the trees and community dynamics in the stand.

While the PARcalc method is strictly related to the terrestrial receipt of PAR, it is nonetheless a critical component in making more robust estimates of photosynthesis and thus vegetation dynamics and total biomass.

C. Structure of the thesis

In the next Chapter the analysis method for identifying areas at risk of land cover change is presented, with application to the Province of Limón, Costa Rica (Figure 1-1). This Chapter has been published in integral form in the journal *Agriculture, Ecosystems and Environment*.

In Chapter 3 the PARcalc method is developed. This method to calculate instantaneous PAR irradiance from MODIS observations is validated with observations made in Costa Rica at 3 locations in June 2002 (Figure 1-1). Chapter 4 contains a sensitivity analysis of the PARcalc method with hypothetical data. The combination of these Chapters has been published in the journal *Remote Sensing of Environment* as a single paper.

Chapter 5 presents a method to integrate PAR over the day from sunset to sunrise from pairs of MODIS observations from the Terra and Aqua satellite platforms. The resulting maps of daily PAR are validated against available field data from Costa Rica. This Chapter has been submitted for publication to the journal *Remote Sensing of Environment*.

Chapter 6 contains the synthesis and conclusions of this thesis.

D. Bibliography

Allen, J.C., & Barnes, D.F. (1985). The causes of deforestation in developing countries. *Ann. Assoc. Am. Geogr.*, 75,163-184.

Bawa, K.S., & Dayandanan, S. (1997). Socioeconomic factors and tropical deforestation. *Nature*, 386, 562-563.

Bossel, H. (1996). TREEDYN3 forest simulation model. *Ecological Modelling*, 90, 187-227.

- Bouman, B.A.M., Jansen, H.G.P., Schipper, R.A., Nieuwenhuyse, A., Hengsdijk, H., & Bouma, J. (1999). A framework for integrated biophysical and economic land use analysis at different scales. *Agric. Ecosys. Environ.*, 75, 55-73.
- FAO (1996). *Forest resources assessment 1990. Study of tropical forest cover and study of change processes*. Forestry Paper 130. Food and Agriculture Organization of the United Nations, Rome, Italy.
- Fearnside, P.M. (1996). Amazonian deforestation and global warming: carbon stocks in vegetation replacing Brazil's Amazon forest. *For. Ecol. and Mgmt.*, 80, 21-34.
- Harris, L.D. (1984). *The Fragmented Forest: Island biogeography theory and the preservation of biotic diversity*. The University of Chicago Press, Chicago, IL.
- Hartshorn, G.S. (1983). *Plants*. In: D.H. Janzen (ed.). *Costa Rican natural history*. The University of Chicago Press, Chicago, IL., pp. 118-350.
- Hartshorn, G.S. (1989). *Gap-phase dynamics and tropical tree species richness*. In: L.B. Holm-Nielsen, I.C. Nielsen and H. Balslev (eds.). *Tropical Forests: Botanical dynamics, speciation and diversity*. Academic Press, London, UK, pp. 65-73.
- Helmer, E.H., & Brown, S. (2000). *Gradient analysis of biomass in Costa Rica and a first estimate of countrywide emissions of greenhouse gases from biomass burning*. In: C.A.S. Hall, C. León Pérez and G. Leclerc. *Quantifying Sustainable Development. The future of tropical economies*. Academic Press, San Diego, CA, pp. 503-526.
- Leigh, E.G., Jr. (1999). *Tropical forest ecology: A view from Barro Colorado Island*. New York, NY: Oxford University Press.
- Lucas, R.M., Honzák, M., Curran, P.J., Foody, G.M. & Nguete, D.T. (2000). Characterizing tropical forest regeneration in Cameroon using NOAA AVHRR data. *Intl. J. of Remote Sensing*, 21, 2831-2854.

- Lucas, R.M., Honzák, M., Curran, P.J., Foody, G.M., Milne, R., Brown, T., & Amaral, S. (2000). Mapping the regional extent of tropical forest regeneration stages in the Brazilian Legal Amazon using NOAA AVHRR data. *Intl. J. of Remote Sensing*, 21, 2855-2881.
- Overman, J.P.M., Witte, H.J.L., & Saldarriaga, J.G. (1994). Evaluation of regression models for above-ground biomass determination in Amazon rainforest. *Journal of Tropical Ecology*, 10, 207-218.
- Penning De Vries, F.W.T. (1983). *Modeling of growth and production*. In: O.L. Lange, P.S. Nobel, C.B. Osmond & H. Ziegler (eds.). *Physiological Plant Ecology IV. Ecosystem processes: mineral cycling, productivity and Man's influence*. Springer-Verlag, Berlin, Germany.
- Running, S.W., Nemani, R., Glassy, J.M. & Thornton, P.E. (1999). *MODIS daily photosynthesis (PSN) and annual net primary production (NPP) product (MOD17). Algorithm theoretical basis document*. Version 3.0. Missoula, MT: University of Montana.
- Swaine, M.D., Lieberman, D., & Putz, F.E. (1987). The dynamics of tree populations in tropical forest: a review. *Journal of Tropical Ecology*, 3, 359-366.
- UNCED (United Nations Conference on Environment and Development) (1993). *Agenda 21, programme of action for sustainable development*. United Nations, New York.
- Vandermeer, J. (1996). Disturbance and neutral competition theory in rain forest dynamics. *Ecological Modelling*, 85, 99-111.
- Veldkamp, A., & Fresco, L.O. (1996). CLUE-CR: an integrated multi-scale model to simulate land use change scenarios in Costa Rica. *Ecol. Model.*, 91, 231-248.

Chapter 2

FOCUS ON DEFORESTATION: ZOOMING IN ON HOT SPOTS IN HIGHLY FRAGMENTED ECOSYSTEMS IN COSTA RICA[♦]

A. Introduction

Tropical deforestation and habitat fragmentation are increasingly recognized as being among the most important issues in global change research (Geist and Lambin, 2001). In many tropical countries forest is still being cut and replaced by agricultural fields or pastures at alarming rates (FAO, 2001). Typically, deforestation is assessed for some larger area where synoptic analysis or other evidence suggests conversion of natural forest cover to other land uses (Allen and Barnes, 1985; Singh, 1986; Sader and Joyce, 1988; Veldkamp et al., 1992). Study areas are often defined in terms of administrative regions or ecological zones, for which global statistics are derived. Both partition mechanisms have their merits for specific purposes, but they fall short of recognizing the spatial heterogeneity usually found in deforestation. Deforestation, particularly those kinds that are human-induced, tends to concentrate in certain areas, so-called deforestation hot spots, rather than being spread out evenly over an entire study area (Veldkamp et al., 1992).

In order to be useful in land cover change studies at the landscape level, deforestation has to be expressed as an 'instantaneous', localized process such that a relationship might be established between deforestation and its causes. The commonly used parameter of deforestation rate expressed for some larger area is

[♦] This Chapter has been published in integral form in *Agriculture, Ecosystems and Environment*, 2004, 102:3-15.

clearly not sufficient for land use change analysis, to the extent that it is insensitive to processes taking place at scales smaller than the reported area. In addition, it has been demonstrated that current approaches to estimate deforestation rates from remote sensing derived data sets produce underestimations (Puyravaud, 2003). It is important to indicate that Puyravaud (2003) does not question the different techniques used to generate remote sensing derived deforestation maps, but rather Puyravaud postulates how deforestation rates are estimated based on common algebraic techniques which tend to underestimate rates of change, and suggesting that an approach based on the Compound Interest Law may be more precise. This underestimation contributes to the current debate about the rate of tropical deforestation, a problem that reflects on the accurate estimation of hot spots.

To assess the local extent and impacts of deforestation, whether through illegal encroachment, controlled conversion or otherwise, a number of indicators has been developed that mostly revolve around the spatial organization of forest lands and other types of land cover and land use (Robinson et al., 1992; Hall et al., 1996; Fahrig, 1997). The indicators range from simple statistics – such as numbers of patches or forest blocks – to much more elaborate indicators that are related to the dispersal of plant and animal species as a function of land cover type extent and patch architecture (Harris, 1984; McGarigal and Marks, 1995; Cain et al., 1997). The indicators are often calculated for more or less arbitrarily chosen geographical areas relative to the drivers of deforestation, such as administrative units or ecological zones (Kerr et al., 2001). The first partition mechanism, the use of administrative units, makes sense from the perspective of policy development, planning and the evaluation of the effectiveness of conservation management. The second, usage of ecological zones, takes into consideration the natural delineation of plant and animal communities as a function of biotic and abiotic environmental conditioners (e.g. elevation, precipitation regime and biotemperature).

Recently much research into the drivers and consequences of tropical deforestation has been focused on modelling the behaviour of land managers faced with a multitude of biophysical, economical and cultural parameters and drivers at the landscape level (IGBP/HDP, 1995; Veldkamp and Fresco, 1996; Bouman et al., 1999; Pfaff et al., 2000; Sánchez-Azofeifa, 2000; Farrow and Winograd, 2001; Geist and Lambin, 2001; Schoorl and Veldkamp, 2001). A recurring issue found in these publications is the difficulty of finding sufficient data of adequate quality to support or validate the assumptions made in the models, making it difficult to establish a general cause/effect relationship to proximate the underlying causes of tropical deforestation (Bawa and Dayanadan, 1997; Veldkamp and Lambin, 2001). Achard et al. (1998) report the conclusions of an expert consultation on identifying hot spots in the pan-tropical moist forest domain. In that report a hot spot is subjectively defined as an area where deforestation took place recently, or where deforestation is expected in the near future, an assumption based on persistence (Sánchez-Azofeifa et al., 1998). The actual delineation of the hot spots is based on the knowledge of the experts and therefore subjective. As the authors acknowledge, the results should be taken as indicative only of areas of concern. It will be argued here that hot spot characterization based on subjective approaches should be used as an indicator at the (sub-) continental level only, for reasons of scale and methodology. Since the hot spot analysis reveals local patterns of change, a method to accurately detect and quantify hot spots of deforestation is necessary in order to support the modelling of land use/cover change.

In this Chapter a method is presented that identifies hot spots using an objective and reproducible approach. It will be demonstrated (1) how to identify the hot spots; (2) what the effects of separate analysis are on the magnitude of the indicators of deforestation; and (3) how the results could improve land use policy development and management through location-specific actions. The method is

applied to the province of Limón in Costa Rica, where commercial banana plantations have been the primary driver for deforestation.

B. Materials and methods

1. Study area

In Costa Rica several deforestation studies have been conducted in the last two decades providing conflicting information regarding the extent of forest cover and its deforestation rate. Sader and Joyce (1988) compared diverse maps of forest cover from five years between 1940 and 1983 to produce the first comprehensive nation-wide deforestation map. Their study concludes that by 1984 the country had only 17% of forest cover. This contrasted with Sánchez-Azofeifa et al. (2001) who demonstrated that, even with heavy cloud cover over a selected region and without considering the semi-arid Nicoya Peninsula in the north-west of Costa Rica, the country had a forest cover extent circa 30%. In 1998 the Tropical Science Center published a map of forest cover and deforestation, which was produced from Landsat TM 5 images from 1986 and 1997. These results indicate that once clouds are removed and the Nicoya Peninsula is considered, the total extent of forest cover was close to 45% of the national territory and that the total deforestation rate between 1986 and 1997 was less than 1% per year. In addition, the study reports the presence of three areas with high deforestation rates: the province of Limón, the Osa peninsula (southern Costa Rica), and in the north east of the country. A complete overview of deforestation studies in Costa Rica can be found in Sánchez-Azofeifa (2000).

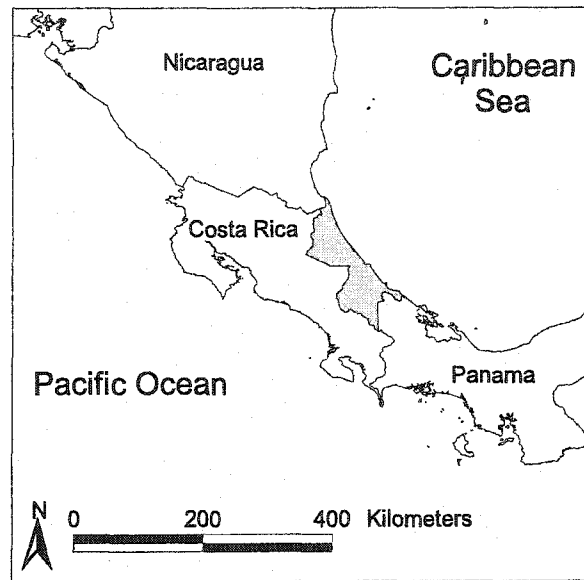


Figure 2-1: The province of Limón (grayed) within Costa Rica, Central America.

The province of Limón stretches along the full length of Costa Rica's Atlantic seaboard (Figure 2-1). Two of the most dynamic deforestation fronts (between 1986 and 1997) in Costa Rica are located within the province (Achard et al., 1998; Tropical Science Center, 1998). The southern third of the province is comprised of a narrow coastal zone, bordered to the southwest by the steep slopes of the Talamanca mountain range. An extensive alluvial plain, consisting of fertile deposits from the volcanic mountainous backbone of the country that is part of the Pan-American Andean geologic formation, forms the northern part of the province. The province has a humid to wet climate, with up to ten wet months (precipitation exceeding potential evapotranspiration) per year.

The construction of the railroad between the capital city San José and the Atlantic port city of Limón at the end of the 19th century established a corridor in the province along which the local economy developed. This development initially consisted of large-scale banana (Musa spp. L.) plantations. The banana plantations

have had a tremendous impact on the physical make-up of the Atlantic zone, as their establishment and operation are changing vegetation, topography and hydrology, to optimize the production environment. Although optimal to production, these changes also have impacts on the remaining natural environment through direct impacts related to banana production - including deforestation - and indirect impacts such as drainage, the isolation of ecotopes and the pollution of inland waters with agro-chemicals, synthetic fertilizer and sediment (Rosales et al., 1994; Castillo et al., 2000). Other large-scale land uses - albeit by large numbers of small to medium-sized farms - include cattle farming and the commercial production of palm heart (*Bactris gasipaes* Kunth) (Veldkamp et al., 1992; Huising et al., 1994; Hengsdijk et al., 1999).

2. Methods

For this Chapter a digital image was used that depicts the change in land cover between 1986 and 1997 in the province of Limón. The change image was produced from a set of Landsat 5 TM satellite images (path 15/row 53) that were clipped to the extent of the province, classified for major vegetation types and analyzed in conjunction to detect change. This process is completely described in Sánchez-Azofeifa et al. (2001). The classes in the change image have been reduced to produce a ternary "forest/deforestation/other land cover" image for the years the image was recorded. The minimum mapping unit used in this study was 3 ha.

In order to identify deforestation hot spots a number of preliminary steps had to be taken on the ternary image of the entire province. First, the patches of isolated forests in 1986 were removed. These patches are defined as areas where less than 25% of the land area within a one kilometer radius consisted of forest cover. This step was necessary to avoid reporting 100% deforestation in an area where a small patch of forest in 1986 was removed by 1997. Such small clearings would otherwise result in local 'spikes' in deforestation that are incidental rather

than structurally related to the major local land cover change processes. Thus about 25,000 ha of small and isolated forest cover were discarded from the 1986 forest cover class for the purpose of hot spot delineation. In the deforestation and patch statistics presented in the results these small patches of forest are included. Approximately 267,000 ha represents other land cover, mostly agriculture, and about 650,000 ha represents large patches of forest cover in 1986, which were used for hot spot delineation.

In a second step, the province was overlaid with a grid of 1 x 1 km cells. This cell size was chosen arbitrarily to group neighbouring pixels such that statistics could be derived from them, with each cell containing up to 900 pixels of the ternary image. The pixels of forest cover were assigned to their corresponding cell. Third, for each of the 9030 cells with some forest pixels the absolute deforestation rate from 1986 to 1997 was calculated and assigned to a point centered in the cell. (On the ternary image deforestation is defined as those areas that had forest land cover in 1986 and other land cover by 1997.) Absolute deforestation rate is here defined as:

$$\text{Deforestation Rate} = \text{forest} / (\text{forest} + \text{deforestation}) \times 100\%. \quad (2-1)$$

Finally, deforestation contours were drawn on the basis of these points (Figure 2-2). The hot spots are here defined as those areas with more than 25% deforestation between 1986 and 1997, plus a 5km wide buffer zone around them. The arbitrarily chosen 5km buffer represents the forest area that is most likely to become deforested as a result of the human activities taking place in the hot spots.

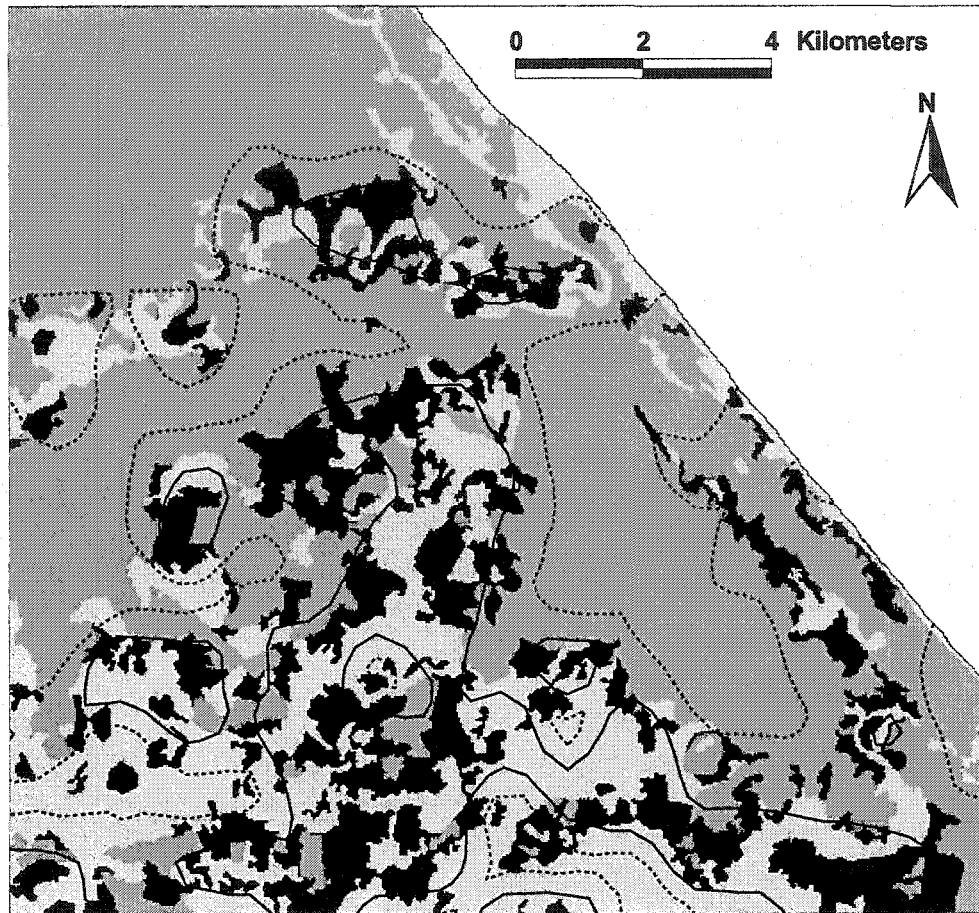


Figure 2-2: Details of the deforestation contours. Solid contours depict the 10% deforestation isoline; dashed contours depict the 50% deforestation isoline. Dark gray represents forest cover, light gray other land cover, and black deforestation.

3. Statistical procedures

Three hot spots were identified and basic areal and forest fragmentation statistics were derived for each of them, as well as for the remainder of the province and for the province as a whole. Forest fragmentation parameters were extracted

using the following landscape fragmentation statistics: largest patch index, average patch size, patch density, total core area, average core area per patch and total core area index. A full description of the mathematical formulae used to estimate these fragmentation indices can be found in McGarigal and Marks (1995). In addition, Table 2-1 briefly describes the fragmentation statistics used in this study.

Due to the separate analysis of the hot spots, the statistics overestimate forest fragmentation by not considering the forest which falls immediately outside of the hot spot, e.g. a forest patch which falls partially inside a hot spot is for that part included in the analysis of the hot spot, while the remainder is analyzed with the remainder of the province, disregarding the continuity across the imaginary borderline. This is not so much a concern when comparing hot spots that have comparable circumferences, as they all have similar effects. Furthermore, as stated before, the buffer area around the hot spots can be considered as being more vulnerable to deforestation than the forest farther away from current human activities.

Deforestation dynamics at each of the identified hot spots was cross-referenced against Costa Rica's new biological corridor proposal known as GRUAS. The GRUAS corridor represents an initiative aimed to identify and evaluate the feasibility of creating biological corridors that link the country's comprehensive national parks and biological corridor network. A complete description of the philosophy of GRUAS can be found in Sánchez-Azofeifa et al (2002).

Table 2-1: Fragmentation indices used in the analysis of the hot spots in the province of Limón, Costa Rica.

Metric	Description
Largest patch index	The size of the largest patch relative to the total area in that class.
Average patch size	Total area divided by number of patches in that class.
Patch density	Number of patches in that class per square kilometer.
Total core area	Forest patch interior area, where the core area is arbitrarily defined as the interior area of forest patches at least 100 meters from the edge of the patch. The purpose of using core area statistics is to demonstrate the effect of localized deforestation; they are not derived here for a specific bio-geographic scenario.
Average core area per patch	Total core area divided by the number of forest patches.
Total core area index	Total core area divided by total forest area.

C. Results

On the basis of the deforestation contours three hot spots were identified (Figure 2-3), each one having a different underlying dynamic or expression of deforestation: 1) Siquirres; 2) Guápiles; and 3) Talamanca. These names are drawn from the main city (Siquirres and Guápiles) or geographic feature (Talamanca Mountains) in their proximity. The Guápiles and Talamanca hot spots are formed by the convex hull of the buffer around a number of nearby contours of more than 25% deforestation. The Siquirres hot spot was manually digitized as a 5km buffer around a number of such contours, due to its irregular shape and the presence of the northern slopes of the Talamanca mountain range that form a natural barrier to the advancement of deforestation.

1. *Siquirres*

This area is dominated by commercial banana production. The area has been under cultivation for several decades. The plantations were designed and laid out at a time when the technology permitted only relatively small plantations with limited options of re-engineering the land (grading, drainage, transport, etc.). This led to a matrix of "small" clearings with interspersed natural areas. The current technology permits a much more intensive use of the land and between 1986 and 1997 a considerable part of the remaining forest patches interspersed between the plantations has been removed, yielding an open landscape with little opportunity for migrating animals or the exchange of plant genetic material (Hall et al., 1996). The rate at which these patches of remaining forest are removed stands at 44.8% deforestation between 1986 and 1997, which is 19.1% of the total land area in the hot spot. The process of forest patch removal is immediately clear from the spatial organization of the deforestation in the hot spot, where isolated forest patches inside

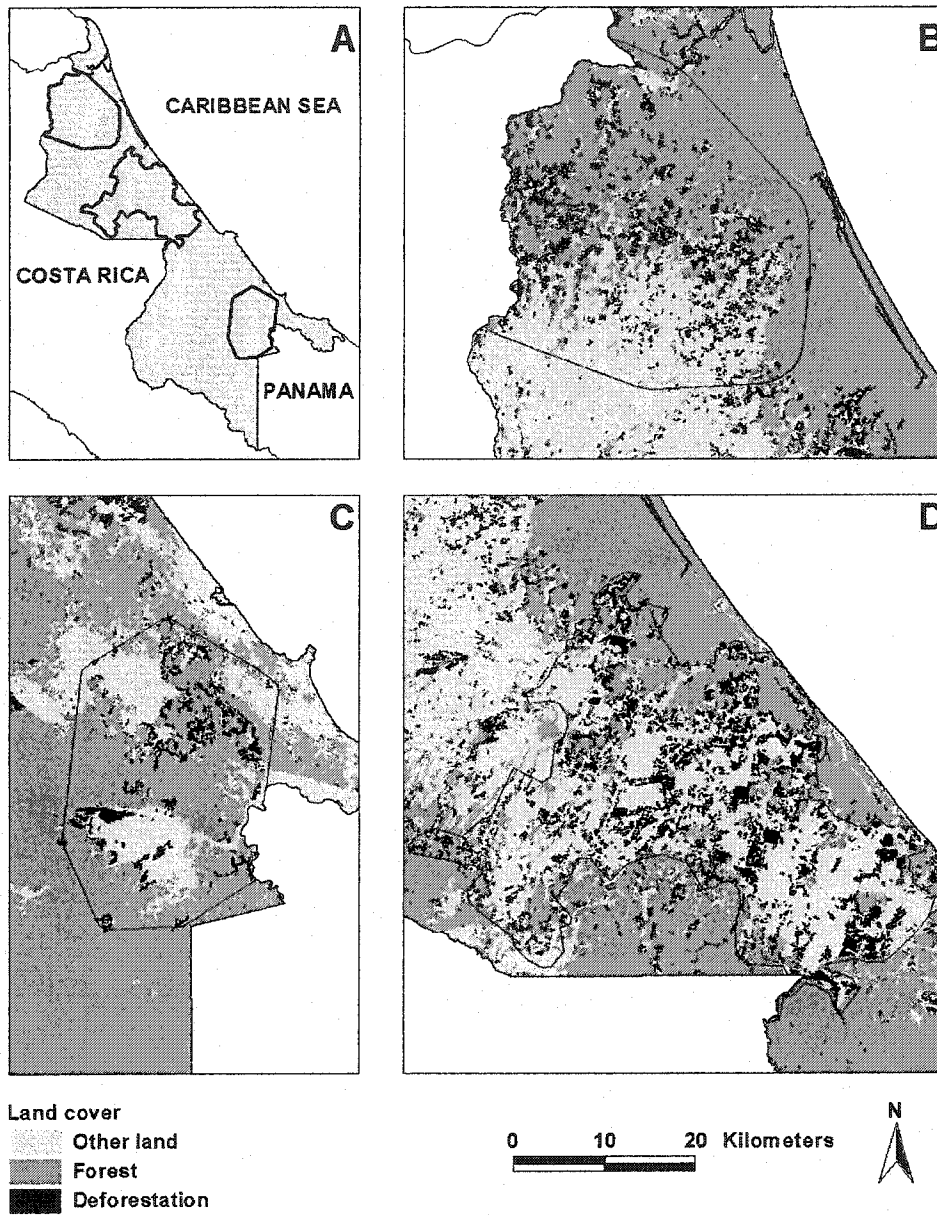


Figure 2-3: Outline of the deforestation hot spots on the ternary image:

A) Location of the hot spots within the province; B) Guápiles;

C) Talamanca; D) Siquirres. Dark gray represents forest cover,

light gray other land cover, and black deforestation.

the predominantly agricultural area are removed, yielding large uniform patches of other land (banana plantations) (Figure 2-3D). The deforestation patches are relatively large at an average of 25 ha, and with one of those patches for every 129 ha of hot spot area the density of deforestation is higher than anywhere else in the province. This expansion of banana cultivation in previously undisturbed areas is made possible by a change in technology, allowing areas of lesser agricultural capacity to be taken into production.

2. *Guápiles*

This hot spot is located immediately north of an area of commercial farming of mostly banana and palm heart that has been developed relatively recently. This more frontal deforestation trend is threatening the fragile aquatic environment formed by the confluence of several major rivers. The frontal nature of deforestation taking place in the Guápiles hot spot (Figure 2-3B) is immediately clear from the location of the deforestation patches and the high values of the largest patch index for both forest cover and other land use: 83.3% and 80.6%, respectively. The remaining patches of forest and other land cover are several orders of magnitude smaller. The deforestation rate of 17.8% is decidedly smaller than in the Siquirres hot spot, but it is still twice as high as the provincial average. More important is that the core area of forest (34.8%), which is essential for the maintenance of biological diversity (Harris, 1984), is well below the provincial average (54.9%) and almost completely contained in the largest patch of forest.

3. *Talamanca*

The steep flanks of the Talamanca mountain range dominate this remote area on the border with Panamá. The valleys are undergoing a rapid conversion into banana cultivation (Figure 2-3C). It has still considerable forest cover (57.3%, comparable to the average of 64.9% for the entire province), but the high

deforestation rate of 13.2% indicates that the area is undergoing rapid consolidation of an as-yet relatively dispersed cultivated land matrix. This is demonstrated by the small average size of other land cover of 88 ha, while the average patch of deforestation is 26 ha. The ratio of $(88+26)/88 = 1.30$, the growth rate of the other land class, contrasts sharply with the corresponding ratios of 1.12 and 1.15 for the Siquirres and Guápiles hot spots, respectively. This area is a prime candidate for remedial action, where appropriate planning could produce a matrix of different land uses that would allow both economic development of the area and a sustainable ecological superstructure.

4. *Comparison between hot spots*

Between 1986 and 1997 the province of Limón saw a total deforestation of 54,830 hectares, or 8.4% of the 1986 forest cover (Table 2-2). However, our analysis shows that the deforestation was mostly concentrated in the three hot spots, with the Siquirres hot spot showing a deforestation of 44.8%, which accounts for 40.7% of the total deforestation in the province. The hot spots show a higher patch density ($0.154 - 0.420 \text{ km}^{-2}$) and decidedly smaller average forest patch area (56 - 373 ha) than the entire province (0.153 km^{-2} , and 425 ha, respectively). All of the core area statistics for the hot spots indicate a higher degree of fragmentation (smaller proportion of total core area, smaller core area per forest patch, and smaller total core area index) than that of the entire province. When the hot spot statistics are compared to those parts of the province outside of the hot spot areas ("other" in Table 2-2) the differences are even more pronounced. For instance, in the Siquirres hot spot of the 27,552 ha of forest, only 12,887 ha are core area (46.8%), or at least 100 meter from the edge of the forest. When compared to the same statistics for the Talamanca hot spot, 35,049 ha of forest of which 25,515 ha are core area (72.8%), one can immediately appreciate that the fragmentation in the Siquirres hot spot is

Table 2-2: Basic patch statistics for the province of Limón and selected deforestation hot spots in 1997.

Indicator	Unit	Hot spots			Other	Province
		Talamanca	Guápiles	Siquirres		
Land area	(ha)	61 213	97 392	117 171	641 929	917 705
Forest	(ha)	35 049	49 156	27 552	484 098	595 855
	(%)	57.3	50.5	23.5	75.4	64.9
Deforestation	(ha)	5 353	10 635	22 331	16 511	54 830
(1986 - 1997)	(%)	13.2	17.8	44.8	2.6	8.4
Other land	(ha)	20 811	37 600	67 288	141 320	267 019
	(%)	34.0	38.6	57.4	22.0	29.1
Patch indicators						
Patches of forest		94	257	492	741	1 402
Largest patch index:	(%)					
Forest		53.7	83.3	4.6	36.5	40.8
Other land		14.9	80.6	51.3	3.9	17.9
Average patch size:	(ha)					
Forest		373	191	56	711	425
Deforestation		26	17	25	12	18
Other land		88	114	203	74	108
Patch density:	(km ⁻²)					
Forest		0.154	0.264	0.420	0.115	0.153
Deforestation		0.333	0.659	0.776	0.214	0.340
Other land		0.386	0.340	0.282	0.298	0.269
Core area indicators (forest patch interior area 100m from edge)						
Total core area	(ha)	25 515	33 916	12 887	427 458	504 638
	(%)	41.7	34.8	11.0	66.6	54.9
Average core area / patch	(ha)	271	132	26	577	360
Total core area index	(%)	72.8	69.0	46.8	88.3	84.7

very advanced. When the average core areas are considered for the two hot spots, 26 ha in Siquirres versus 271 ha in Talamanca, the contrast is even more pronounced.

The Siquirres hot spot has a very small core area for the remaining forest patches, making the deforestation in this area critical, as these patches might well function as biological corridors, stepping stones in the dissemination of plant genetic material and the migration of animals (Harris, 1984; Hall et al., 1996; Fahrig, 1997). The importance of such stepping-stones is accentuated by the fact that to the west of the Siquirres hot spot the landscape is composed of large agricultural enterprises, with little natural land cover. This agricultural landscape extends up to 60 km inland from the coast, thus forming a massive barrier between the natural areas to the north and south. In the Talamanca area this is much less of a concern, since the core areas are larger and the "steps" smaller.

5. *Biological corridors*

The hot spots have been cross-referenced with the areas identified in the biological corridor proposal known as GRUAS (Table 2-3). Each of the hot spots is partially co-located with a biological corridor. While in all three hot spots the deforestation is not preferentially taking place in the GRUAS areas (overall hot spot deforestation rate being higher than that in the overlapping GRUAS areas), the rate of deforestation is high enough to threaten the intended function as a biological corridor.

The encroachment of agricultural land on the biological corridors is particularly evident for the Guápiles hot spot, of which 37.2% coincides with a potential biological corridor, connecting the Tortuguero National Park on the Caribbean Sea with the biologically rich natural areas inland (Figure 2-4). Between 1986 and 1997 13.5% of the forest in the corridor has been converted to other land uses. The deforestation rates inside biological corridors for the Talamanca and

Siquirres hot spots are comparable, 10.6% and 19.3% respectively, but the GRUAS area in these hot spots is much smaller. Furthermore, the deforestation in the Guápiles hot spot is threatening to sever the connection between the coastal and inland areas, effectively isolating the Tortuguero National Park from other natural areas, and eliminating the feasibility of producing linkages between the Atlantic region and other biological reserves in the country.

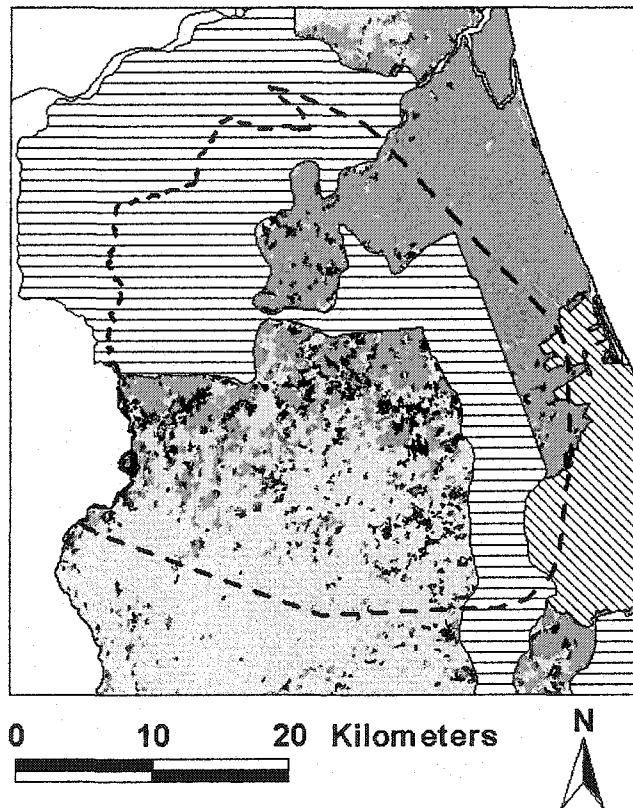


Figure 2-4: Co-location of the Guápiles hot spot with a proposed GRUAS biological corridor. The Guápiles hot spot is outlined with the dashed line. The GRUAS area is indicated with the horizontal hash. The Tortuguero National Park is indicated with the slanted hash.

Table 2-3: Composition of land cover in proposed GRUAS biological corridors inside selected deforestation hot spots in the province of Limón in 1997.

Indicator	Unit	Hot spots		
		Talamanca	Guápiles	Siquirres
Land area of hot spot	(ha)	61 213	97 392	117 171
<i>Land area under GRUAS proposal</i>	(ha)	9 478	36 208	10 609
	(%)	15.5	37.2	9.1
<i>Forest</i>	(ha)	7 752	23 789	4 708
	(%)	81.8	65.7	44.4
Deforestation (1986 - 1997)	(ha)	1 004	4 887	2 050
	(%)	10.6	13.5	19.3
<i>Other land</i>	(ha)	722	7 532	3 852
	(%)	7.6	20.8	36.3

D. Discussion

1. Advantages of hot spot analysis

The use of hot spots has clear advantages over analyzing deforestation for entire areas that have no inherent relationship to the causes of deforestation (e.g. administrative areas or ecological zones). Almost invariably large-scale deforestation is the result of some economic activity, which in turn is governed by a complex set of enabling factors such as infrastructure, population centers, tax incentives and global market prices for forest products or products raised on former forest land.

The complexity of the economic 'push-and-pull' on the local land manager is such that it cannot be easily modeled, even for small, well-defined areas such as the province of Limón in Costa Rica where a wealth of econometric data is available (Pfaff et al., 2000). On a continental or global scale such modelling is virtually impossible beyond very simplistic, deterministic models based on e.g. population density and major road networks (FAO, 1996; Gaston et al., 1998).

The study area analyzed here corresponds largely to the Sarapiquí hot spot identified by Achard et al. (1998). It does comprise the Guápiles and part of the Siquirres hot spots, but the Talamanca hot spot is not included. Also, the extent of the Sarapiquí hot spot has very little in common with the Guápiles and Siquirres hot spots, other than the natural barriers of the Talamanca mountains, the Caribbean coastline and the border with Nicaragua. Scale is but one reason for the generalized hot spot extent in the study of Achard (1998). The dependence on experts to *delineate* the hot spots necessarily leads to the observed generalizations, which yields maps that convey little more than the information describing the causes of the deforestation.

The granularity of the available information presented by Achard (1998) is such that it cannot be used but at the continental or global scale for an assessment of general risk areas. Furthermore, the identification of hot spots is (admittedly) subjective and dependent on the combined experience of the experts. The use of a repeatable and flexible approach, like the method presented above, yields more useful results because of its consistency (i.e. a dataset of uniform quality produces hot spots of uniform quality independent of terrain context or expert knowledge). The consistency offered by the presented method is essential in deforestation hot spot studies, as the hot spots are by definition dynamic and therefore requiring periodic reassessment to monitor their spread and/or to evaluate mitigating measures.

The overlap between deforestation hot spots and areas that are essential in the preservation of biodiversity is an indication of the vulnerability of biological corridors to land cover change processes. While more traditional statistical approaches can reveal deforestation and landscape fragmentation taking place inside biological corridors, the hot spot approach can identify those areas that are at risk of deforestation in the near future, allowing therefore for immediate conservation action. Such an outlook opens up possibilities to prevent land cover change, or implement policies mitigating its effects. In the case of the Guápiles hot spot, the Tortuguero National Park will become isolated from other natural areas unless deforestation is halted soon. In fact Sánchez-Azofeifa et al. (2002) have indicated that this corridor is part of the ones with least probability to contribute to national conservation efforts if deforestation processes are not controlled at the regional level. Even when the hot spot does not coincide with a biological corridor, important land cover change processes can be identified within the hot spots, providing additional information of the dynamics of land cover change in areas inside and outside of the proposed conservation area. In the Siquirres hot spot, for example, the observed removal of forest islands scattered over the landscape creates a barrier for the dispersal of genetic material and animal movement. This kind of information, relating land cover change and its drivers to effects on the ecological quality, can be instrumental in directing scarce resources to where they are most needed.

2. Implications of the study and need for future research

The presented approach to identify hot spots of deforestation has yet to be tested in more diverse situations (agriculturally, environmentally and socio-economically) and the parameters of the analysis have to be more thoroughly validated through further research. Specifically it would be desirable to test the method on larger areas with gradually changing ecological properties, and by using

different satellite imagery with different spatial resolutions (e.g. MODIS, AVHRR or SPOT VEGETATION).

There are limitations to the methodology proposed in this Chapter. In the analysis of the province of Limón some decisions have been made that affect the results. For instance, the minimum local forest cover for considering a particular forest patch in the analysis was specified. This threshold is necessary to filter out areas with observable but insignificant forest cover that would otherwise conceal real areas of interest. What constitutes significant forest cover is dependent on the application and the definition used by the map producers and requires further research. Further, the method discriminates on area within an arbitrarily placed grid (with reference to the location of interest) only. It does not consider adjacent land cover patches or shape-based parameters such as those related to edge analysis and core area, an issue that needs further research. In most situations this should not be a concern; only when the landscape is highly fragmented at a scale comparable to the resolution of the grid will this potentially bias the analysis, a problem that was not present in the Limón study area. A special case is where the land cover data set, which might well be derived from satellite imagery as was demonstrated here, has an inherent resolution (e.g. sensor spatial resolution, minimum mapping unit) that is close to the resolution of the grid (e.g. when using AVHRR or SPOT Vegetation imagery). In order to produce a sensible result the grid size should always be an order of magnitude greater than any such inherent resolution, in order to have a sufficiently large number of pixels upon which the statistical procedure will operate. Finally, the contouring process yields areas that are analytically correct, but they may not have any relevance for research, management or planning. As has been shown in this Chapter, the user can identify clusters of problem areas and group them in hot spots that do have relevance to

other factors, such as administrative units, socio-economic development, eco-regions, management capacity or ancillary data sets.

In the context of environmental protection and management, deforestation hot spots form an important tool in the identification of causes leading to deforestation. In the larger context of land use/cover change modeling, there are many other types of land cover conversions that together make up the land use dynamics of the region. The method here presented can be useful in better understanding the causes underlying land use/cover change and direct efforts to those areas where ecosystem functions are threatened, or where mitigation strategies might be most successful.

E. Conclusions

The current abundance of high-quality satellite imagery at different resolutions reduces the dependence on a-priori *models* (hypotheses) of land use/cover change and enable the *observation* of recent land cover change. Instead of testing hypotheses with available data, exhaustive data can now be used to develop hypotheses of the causes leading to actual land cover change. This can be considered as an implementation of "Focus 2: Land-Cover Dynamics - Direct Observation and Diagnostic Models" in the LUCC Science Plan (IGBP/HDP, 1995). The method here presented serves just this purpose: a large dataset is reduced to a small number of hot spots where deforestation is concentrated. Now that the hot spots have been localized, the drivers causing deforestation can be identified, or at least can efforts be concentrated in those areas where the drivers have a more pronounced effect.

A method has been presented to identify areas of high deforestation on the basis of satellite imagery and spatial analysis. These hot spots are identified using a localized analysis and they thus reflect local deforestation. Subsequently these hot spots might be linked to the drivers that have led to the deforestation. This linkage

between local causes and effects can lead to improved land use policies and management and it can be used to supplement land use change modelling at the landscape level.

F. Bibliography

- Achard, F., Eva, H., Glinni, A., Mayaux, P., Richards, T., & Stibig, H.J. (1998). *Identification of deforestation hot spot areas in the humid tropics*. TREES Publication Series B, Research report no. 4. Joint Research Centre, European Commission, Ispra, Italy.
- Allen, J.C., & Barnes, D.F. (1985). The causes of deforestation in developing countries. *Ann. Assoc. Am. Geogr.* 75,163-184.
- Bawa, K.S., & Dayandanan, S. (1997). Socioeconomic factors and tropical deforestation. *Nature*, 386, 562-563.
- Bouman, B.A.M., Jansen, H.G.P., Schipper, R.A., Nieuwenhuyse, A., Hengsdijk, H., & Bouma, J. (1999). A framework for integrated biophysical and economic land use analysis at different scales. *Agric. Ecosys. Environ.*, 75, 55-73.
- Cain, D.H., Riitters, K., & Orvis, K. (1997). A multi-scale analysis of landscape statistics. *Landscape Ecol.*, 12, 199-212.
- Castillo, L.E., Rüpert, C., & Solis, E. (2000). Pesticide residues in the aquatic environment of banana plantation areas in the north Atlantic zone of Costa Rica. *Environ. Toxic. Chem.*, 19, 1942-1950.
- FAO (1996). *Forest Resources Assessment 1990. Survey of tropical forest cover and study of change processes*. FAO Forestry Paper 130. Food and Agriculture Organization of the United Nations, Rome, Italy.

- FAO (2001). *FRA 2000 Summary Findings*. Food and Agriculture Organization of the United Nations, Rome, Italy. Online: <http://www.fao.org/forestry/fo/fra/index.jsp>.
- Fahrig, L. (1997). Relative effects of habitat loss and fragmentation on population extinction. *J. Wildlife Manage.*, 61, 603-610.
- Farrow, A., & Winograd, M. (2001). Land use modelling at the regional scale: an input to rural sustainability indicators for Central America. *Agric. Ecosys. Environ.*, 85, 249-268.
- Gaston, G., Brown, S., Lorenzini, M., & Singh, K.D. (1998). State and change in carbon pools in the forests of tropical Africa. *Global Change Biol.*, 4, 97-114.
- Geist, H.J., & Lambin, E.F. (2001). *What drives tropical deforestation? A meta-analysis of proximate and underlying causes of deforestation based on subnational case study evidence*. Lucc Report Series, 4. Lucc International Project Office, Louvain-la-Neuve, Belgium.
- Hall, P., Walker, S., & Bawa, K. (1996). Effect of forest fragmentation on genetic diversity and mating system in a tropical tree, *Pithecellobium elegans*. *Cons. Biol.*, 10, 1-13.
- Harris, L.D. (1984). *The Fragmented Forest. Island Biogeography Theory and the Preservation of Biotic Diversity*. The University of Chicago Press, Chicago, USA.
- Hengsdijk, H., Bouman, B.A.M., Nieuwenhuysse, A., & Jansen, H.G.P. (1999). Quantification of land use systems using technical coefficient generators: a case study for the Northern Atlantic zone of Costa Rica. *Agric. Syst.*, 61, 109-121
- Huising, E.J., Wielemaker, W.G., & Bouma, J. (1994). Evaluating land use at the sub-regional level in the Atlantic zone of Costa Rica, considering biophysical land potentials. *Soil Use and Manage.*, 10, 152-158.

- IGBP/HDP (1995). *Land-Use and Land-Cover Change Science/Research Plan*. IGBP Report 35. International Geosphere-Biosphere Programme, Stockholm.
- Kerr, S., Pfaff, A., Sánchez-Azofeifa, G.A., & Boscolo, M. (2001). *How can carbon sequestration in tropical forest be rewarded? Evidence from Costa Rica*. In: Panayotou, T. (Ed.). *Environment for Growth in Central America: Environmental Management for Sustainability and Competitiveness*. John F. Kennedy School of Government, Harvard University, pp. 371-408.
- McGarigal, K., & Marks, B.J. (1995). *FRAGSTATS: spatial pattern analysis program for quantifying landscape structure*. USDA For. Serv. Gen. Tech. Rep. PNW-351.
- Puyravaud, J. P. (2003). Standardizing the calculation of the annual rate of deforestation. *Forest Ecol. Manage.*, 177, 593-596.
- Pfaff, A.S.P., Kerr, S., Hughes, R.F., Liu, S., Sánchez-Azofeifa, G.A., Schimel, D., Tosi, J., & Watson, V. (2000). The Kyoto protocol & payments for tropical forest: An interdisciplinary method for estimating carbon-offset supply and increasing the feasibility of a carbon market under the CDM. *Ecol. Econ.*, 35, 203-221.
- Robinson, G.R., Holt, R.D., Gaines, M.S., Hamburg, S.P., Johnson, M.L., Fitch, H.S., & Martinko, E.A. (1992). Diverse and contrasting effects of habitat fragmentation. *Science*, 257, 524-526.
- Rosales, A., Maebe, P., & Sevenhuisen, R. (1994). Determinación de la pérdida de nutrientes y nematocida en las aguas de drenaje en un suelo bananero. *Agronomía Costarricense*, 18, 93-98.
- Sader, S.A., & Joyce, A.T. (1988). Deforestation rates and trends in Costa Rica, 1940 to 1983. *Biotropica*, 20, 11-19.
- Sánchez-Azofeifa, Daily, G.C., Pfaff, A.S.P., & Busch, C. (2003). Integrity and isolation of Costa Rica's national park and biological reserves: examining the dynamics of land-cover change. *Biol. Cons.*, 109, 123-135.

- Sánchez-Azofeifa, G.A., Harriss, R.C., & Skole, D.L. (2001). Deforestation in Costa Rica. A quantitative analysis using remote sensing imagery. *Biotropica*, 33, 378-384.
- Sánchez-Azofeifa, G.A. (2000). *Land use and cover change in Costa Rica: a geographic perspective*. In: Hall, C.A.S., León Pérez, C., Leclerc, G. (Eds.). *Quantifying Sustainable Development. The future of tropical economies*. Academic Press, San Diego, CA, pp. 473-501.
- Sánchez-Azofeifa, G.A., Skole, D.L., & Chomentowski, W. (1998). Sampling global deforestation databases: the role of persistence. *Mitigation and Adaptation Strategies for Global Change*, 2, 177-189.
- Schoorl, J.M., & Veldkamp, A. (2001). Linking land use and landscape process modelling: a case study for the Álora region (south Spain). *Agric. Ecosys. Environ.*, 85, 281-292.
- Singh, A. (1986). *Change Detection in the Tropical Forest Environment of Northeastern India using Landsat*. In: Eden, M., Parry, J. (Eds.). *Remote Sensing and Tropical Land Management*. John Wiley and Sons, London, UK, pp. 237-254.
- Tropical Science Center (1998). *Estudio de Cobertura Forestal Actual (1996/97) y de Cambio de Cobertura para el periodo entre 1986/87 y 1996/97 para Costa Rica*. Tropical Science Center, San Pedro, Costa Rica.
- Veldkamp, A., & Fresco, L.O. (1996). CLUE-CR: an integrated multi-scale model to simulate land use change scenarios in Costa Rica. *Ecol. Model.*, 91, 231-248.
- Veldkamp, A., Lambin, E.F. (2001). Predicting land-use change. *Agric. Ecosys. Environ.*, 85, 1-6.
- Veldkamp, E., Weitz, A.M., Staritsky, I.G., & Huising, E.J. (1992). Deforestation trends in the Atlantic Zone of Costa Rica: a case study. *Land Degrad. Rehab.*, 3, 71-84.

Chapter 3

SIMPLIFIED ATMOSPHERIC RADIATIVE TRANSFER MODELLING FOR ESTIMATING INCIDENT PAR USING MODIS ATMOSPHERE PRODUCTS[♦]

A. Introduction

The solar radiation receipt at the Earth's surface is an important parameter in models of ecosystem dynamics and climate change (Gates, 1980; Bossel, 1996; Leigh, 1999). Surface meteorological infrastructures around the world regularly measure the receipt of broadband radiation, albeit at reduced resolution in many areas. The advent of multispectral meteorological satellites since the launch of the TIROS-N platform in 1978 (e.g. GOES, METEOSAT) has led to the development of models of atmospheric attenuation of incident radiation that have allowed spatially exhaustive estimates of broadband shortwave irradiance (Gautier et al., 1980; Pinker and Laszlo, 1992; Dubayah and Loechel, 1997; Rossow and Schiffer, 1999).

The calculation of terrestrial radiation receipt from at-sensor radiances is not trivial, however. While the extraterrestrial radiation budget and its wavelength distribution are well known and relatively constant, the terrestrial reception is altered by a dynamically changing atmosphere. The most important atmospheric variable in this respect, and also the most dynamic, is water content and appearance (as vapour, liquid cloud or ice cloud). Radiation is attenuated via three processes: absorption (in the visible part of the spectrum mostly by water and ozone), Raleigh (molecular) scattering, and Mie (particle) scattering, which includes

[♦] This Chapter, in combination with a condensed version of Chapter 4, has been published in *Remote Sensing of Environment*, 2004, 91(1):98-113.

cloud top reflectance. The first two processes are strongly wavelength-dependent and since the vertical distribution of the main agents in these processes is not uniform, a complex set of equations arises that is often solved by applying empirical approximations (Gates, 1980).

For models of plant growth the radiation in the visible part of the spectrum (0.4 – 0.7 μm) is most important, as this is the range where absorption by chlorophyll takes place. The radiation in the visible part of the spectrum is commonly referred to as photosynthetically active radiation (PAR). Healthy vegetation has an absorption curve that is essentially similar between different species, which is due to the presence of chlorophyll in all green plant tissues (Gates, 1980). A proper assessment of PAR can thus be used to model photosynthesis in individual species, or over entire landscapes, something which is essential in, for instance, carbon budgeting models and global change studies (Bossel, 1996; Leigh, 1999).

In this Chapter a newly developed method is presented that explicitly incorporates atmospheric composition in the calculation of incident PAR, using data from MODIS atmosphere products. This method is a combination of clear sky irradiance equations given in Iqbal (1983) and the broadband cloud reflection algorithm given in Stephens et al. (1984). Incorporating the atmospheric composition into the method constitutes a significant increase in complexity compared to broadband empirical models, but it does allow for a spectrally explicit solution which is essential for biophysical modelling (Gates, 1980; Leigh, 1999). The method is a simplification of the general radiative transfer equations: in the visible part of the spectrum ozone and water vapour are the only gaseous components that absorb radiation, and the atmosphere is treated as a single layer in clear-sky conditions, or as a double layer in cloudy conditions (a layer above the cloud top, and a layer from the cloud top downwards). Surface reflectance is not included in

the presented method, although in applying this method to a particular vegetative surface reflectance from neighbouring areas may contribute significantly to the incident PAR through direct irradiance reflected of the surface and atmospheric scattering of surface reflected radiation; the application of a model of surface reflectance, such as that by Wenhan and Jupp (1993) or Castellu-Etchegorry et al. (1999), should then be considered.

The simplified, parameterized solution of the general radiative transfer equations here employed imply a “standard” atmosphere, particularly with regard to the relative proportion of the different gases (excluding water vapour and ozone) that make up the atmosphere. While more advanced formulations exist that explicitly calculate the contribution of the individual gases to the attenuation of radiation in the atmosphere, such as MODTRAN and HITRAN (Berk et al., 1998; Rothman et al., 1998), the simpler approach was preferred because of the lack of data on the amounts of those gases in the atmosphere.

Calculations made with the method were validated with high temporal resolution field observations made at several sites in Costa Rica during June 2002, and with data from two permanent observation stations in Costa Rica made over a longer period of time at reduced temporal resolution.

B. PAR Radiative Transfer

1. Direct-beam irradiance

The attenuation of the monochromatic direct-beam radiation I_B in the atmosphere is usually expressed in terms of the transmittance τ , such that

$$I_B = I_0 \tau \quad (3-1)$$

where I_0 is the monochromatic extraterrestrial incident radiation ($\text{W m}^{-2} \mu\text{m}^{-1}$), τ is the dimensionless wavelength dependent transmittance of the atmosphere, and I_B is

the monochromatic radiation receipt on a surface normal to the incident beam ($W m^{-2} \mu m^{-1}$). I_0 varies slightly throughout the year because of the eccentric path of the earth around the sun:

$$I_0 = E_0 (1 + 0.0344 \cos(360 N / 365)) \quad (3-2)$$

where E_0 is the monochromatic exoatmospheric solar irradiance ($W m^{-2} \mu m^{-1}$), and N is the day number (for January 1, $N=1$).

The transmittance τ can be decomposed into a number of transmittances specific to some attenuation process taking place in the atmosphere:

$$\tau = \tau_R \tau_{OZ} \tau_W \tau_A \quad (3-3)$$

where the subscripts refer to the wavelength dependent processes of Rayleigh scattering (R), ozone (OZ) and water vapour absorption (W), and aerosol (A) scattering, respectively. These transmittances are dependent on the concentration of the attenuating element in the atmosphere and on the relative optical mass m_0 to mean sea level of the path of the direct beam relative to the atmospherical depth in the zenith direction (Iqbal, 1983),

$$\tau_R = \exp[-0.008735 \lambda^{-4.08} m_P] \quad (3-4)$$

$$\tau_{OZ} = \exp[-k_{OZ} l m_0] \quad (3-5)$$

$$\tau_W = \exp[-0.2385 k_W w m_0 / (1 + 20.07 k_W w m_0)^{0.45}] \quad (3-6)$$

$$\tau_A = \exp[-\beta \lambda^{-1.3} m_P] \quad (3-7)$$

where λ (μm) is the wavelength of the monochromatic direct beam, l (cm) and w (cm) refer to the abundance of ozone and water, respectively, β is the Ångström turbidity coefficient (Ångström, 1929), k_{OZ} and k_W are the wavelength dependent monochromatic absorption coefficients of ozone and water vapour, respectively, and m_P is the relative optical mass corrected for local pressure. m_P relates to m_0 via the

local atmospheric pressure P_z (hPa), or, assuming a hydrostatic equilibrium in the atmosphere, to the local elevation above mean sea level z (m),

$$m_0 = 1 / \cos\theta \quad , \theta \leq 60^\circ \quad (3-8a)$$

$$m_0 = 1 / (\cos\theta + 0.15 (93.885 - \theta) - 1.253) \quad , \theta > 60^\circ \quad (3-8b)$$

$$m_P = m_0 P_z / 1013.25 \quad (3-9a)$$

$$m_P = m_0 \exp[-0.0001184 z] \quad (3-9b)$$

where θ is the zenith angle (degrees) of the sun.

2. Cloud top reflectance

The top of any cloud cover can reflect a considerable portion of incident radiation back into space (Stephens et al., 1984),

$$R_\theta = (\beta_\theta \tau_c / \cos\theta) / (1 + \beta_\theta \tau_c / \cos\theta) \quad (3-10)$$

$$T_\theta = 1 - R_\theta \quad (3-11)$$

where τ_c is the optical thickness of the cloud, β_θ is the backscattered fraction of incident radiation as a function of the solar zenith angle, R_θ is the reflected radiation and T_θ is the transmittance. Values for β_θ are linearly interpolated from data given in Stephens et al. (1984). This formulation assumes that no absorption is taking place in the cloud. It applies to broadband radiation below 0.7 μm , which covers the entire PAR spectrum. The backscattered fraction of incident radiation β_θ is calculated using the two-stream delta-Eddington approach of multiple scattering.

In the presence of clouds the monochromatic direct-beam and diffuse irradiance is first computed for the atmosphere above the clouds, i.e. m_P is calculated to the level of the cloud top pressure, and the atmospheric water content is assumed to be contained entirely below the cloud top. The scattered radiation above the cloud top originating from Rayleigh and aerosol scattering interacting with

the cloud is included by averaging β_θ over the incidence angle θ for the scattered radiation, which assumes an isotropic distribution of the scattered radiation. The radiation transmitted through the clouds is then used to compute the attenuation in the lower part of the atmosphere. In this approach to compute irradiance in the presence of clouds two assumptions are made: 1) All ozone absorption is assumed to occur above any clouds (Pinker and Laszlo, 1992); and 2) Cloud cover is homogeneous, plane-parallel, and temporally stationary. The error introduced by this latter assumption can be large, depending on the cloud type and the degree of coverage throughout the pixel. A method to account for geometrical effects of cloud reflection using MODIS data has recently been developed (Várnai and Marshak, 2002), but the retrieval of accurate estimates of these 3D effects can only be made at high solar zenith angles, when irradiance is low. Inversely, irradiance is highest when the solar altitude angle is small, and then the geometrical effects of non-plane-parallel cloud cover are minimal.

3. Diffuse irradiance

The fraction $1 - \tau$ of the direct beam radiation that is scattered by the atmosphere (below the clouds, if present) is available as diffuse radiation. Of the Rayleigh scattered radiation half is scattered towards the surface, while the other half is scattered into space. The aerosol-scattered radiation is commonly approximated using the single scattering albedo ω_0 and the forward scatterance F . ω_0 is determined using the aerosol type given in the MODIS Aerosol product (Kaufman and Tanré, 1998). The forward scatterance is dependent on the zenith angle of the sun; equation (3-12) given here is developed from data given in Iqbal (1983). Under the assumption of single scattering and disregarding surface-reflected radiation, the monochromatic diffuse irradiance I_D ($\text{W m}^{-2} \mu\text{m}^{-1}$) can be readily calculated:

$$F = 0.9302 \cos\theta^{0.2556} \quad (3-12)$$

$$I_D = I_0 \cos\theta \tau_{OZ} \tau_W ([0.5 \tau_A (1 - \tau_R)] + [F \omega_0 \tau_R (1 - \tau_A)]) \quad (3-13)$$

where the first term in square brackets refers to the diffuse radiation originating from Rayleigh direct-beam scattering, and the second term to aerosol direct-beam scattering.

4. Total surface-received PAR

Direct-beam and diffuse irradiance are both dependent on the zenith angle of the sun, which changes in a seasonal cycle and daily from sunrise to solar noon to sunset, and on the orientation of the surface. On an arbitrarily tilted surface of slope α and azimuth ϕ at latitude ϕ , the angle i between the incident radiation and the normal to the surface is expressed as

$$\cos i = \sin\delta (\sin\phi \cos\alpha - \cos\phi \sin\alpha \cos\phi) \quad (3-14)$$

$$+ \cos\delta \cosh (\cos\phi \cos\alpha + \sin\phi \sin\alpha \cos\phi) + \cos\delta \sin\alpha \sin\phi \sinh$$

$$\delta = 23.45 \sin(360 (284 + N) / 365) \quad (3-15)$$

where δ is the declination angle of the sun on day N , and h is the angle of the local hour relative to solar noon. Depending on terrain properties and solar geometry the surface may be in the shadow of nearby topographic features; $\cos i$ is then assigned a value of 0, i.e. no direct-beam irradiance.

Diffuse radiation is assumed to be isotropically distributed in the atmosphere, i.e. the sky is uniformly bright. Depending on the slope α and nearby topography, only a fraction of the hemisphere might be visible, which is referred to as the sky-view factor V_D . V_D is calculated analogous to Dozier and Frew (1990), but the maximum horizontal range is here limited by the turbidity of the atmosphere which, for computational simplicity, is set to a corresponding visibility of 23 km, i.e.

a clear atmosphere. (This simplification makes V_D time-invariant, it is dependent only on terrain properties.)

The total monochromatic surface irradiance I_s ($W m^{-2} \mu m^{-1}$) on an arbitrarily tilted surface is now the sum of the direct-beam irradiance corrected for the position of the sun relative to the normal of the surface, and the diffuse irradiance corrected for the sky-view factor,

$$I_s = I_B \cos i + I_D V_D. \quad (3-16)$$

Instantaneous PAR can be calculated by discretizing the spectral continuum of 0.4 – 0.7 μm in small wavelength intervals of the exoatmospheric irradiance E_o . Instantaneous PAR is typically expressed as a photon flux density ($E m^{-2} s^{-1}$) and is calculated by summing I_s over the discrete wavelength intervals and conversion of radiant power to photon flux density:

$$I_{PAR} = 8.360 \sum (I_s \lambda \Delta\lambda) \quad (3-17)$$

yielding a singular measure of instantaneous irradiance of PAR on an arbitrarily tilted surface under actual atmospheric conditions. Daily irradiance can be obtained by time integration of instantaneous irradiance.

C. Computing PAR with MODIS

The Moderate Resolution Imaging Spectroradiometer (MODIS) was launched in December 1999 aboard the Terra platform operated by NASA. It has 36 bands from the visible to the infrared regions of the spectrum, with a spatial resolution ranging from 250 m to 1 km and a revisit time of one day for most locations on Earth. The MODIS sensor is supported by a scientific program with the aim of producing high quality, calibrated physical parameters of the Earth's surface and the atmosphere. All of the atmospheric parameters are currently declared validated from the start of the data stream in February 2000. All the atmospheric parameters

Table 3-1: MODIS atmospheric parameters used in calculating PAR.

Parameter	Product	Resolution
Ångström turbidity coefficient	MOD04	10km
Atmospheric water content	MOD05	1km
Cloud optical thickness	MOD06	1km
Cloud top pressure	MOD06	5km
Total atmospheric ozone	MOD07	5km

required for computing PAR are produced under the MODIS program, but PAR itself is not. In Table 3-1 an overview is given of the MODIS parameters used in the calculation of PAR.

The PAR algorithm is coded in the Pascal programming language for use on computers running the Windows or Linux operating systems. The so-called PARcalc program ingests the available MODIS products as 5 minute swath images and reads out the physical parameters from the image pixel closest to the ground observation points. No correction of any kind (geometric, temporal) is applied to the data. The only other inputs the PARcalc program requires are the location and altitude of the ground observation points. The program outputs the computed instantaneous irradiance at the specified location.

In June 2002 incident PAR was measured during a field campaign, where two locations at different elevations and in different ecological regions were visited. PAR was measured with a LI-COR Li190 quantum sensor (LI-COR, Inc., Lincoln, NE) over a 1 minute sampling interval, coinciding with the satellite overpass. Simultaneous measurements were made with an ASD FieldSpec HandHeld spectrometer (Analytical Spectral Devices, Inc., Boulder, CO), fitted with remote cosine receptor optics, to measure the spectral composition of the incident

Table 3-2: Locations in Costa Rica where PAR was measured.

Location	Longitude	Latitude	Elevation	Environment
La Selva	W83° 59'	N10° 26'	34 m	Humid lowland, forested
Los Inocentes	W85° 30'	N11° 02'	307 m	Transitional wet/dry, rangeland
Santa Rosa	W85° 37'	N10° 50'	290 m	Dry forest

radiation. Incident PAR was also collected from two permanent observation stations, one between January 2002 and March 2003 and the other between October 2002 and January 2003 (Table 3-2). These permanent stations both use a LI-COR Li190 quantum sensor to measure PAR, but they use longer sampling intervals (10 to 30 minutes). The La Selva location has a permanent observation station and it was also visited during the field campaign, such that a comparison could be made between observations using a larger sampling interval (30 minutes) around the overpass and “instantaneous” measurements.

D. Results

During the field campaign in Costa Rica 14 measurements of PAR were made with the quantum sensor that coincided with a MODIS overpass at two locations. An additional 377 observations were taken from the two permanent observation stations. The average absolute error of the calculated PAR from the measured PAR ranges from 1.5% to 2.7% (Table 3-3 and Figure 3-1), which is comparable to the typical uncertainty of the measurement of the sensors used (LI-COR, 1996). The error is biased towards lower calculated values with respect to the measured values.

The error is most prominent in the center of the range of irradiance, reaching over 5% for some observations, while the extremes of the range have decidedly lower errors at 1~3% (Figure 3-2). This trend is most obvious for the set of data that has been averaged over the longest period of time (La Selva permanent observation

Table 3-3: Average error of incident PAR compared to measurements with a quantum sensor. *N* is the number of observations per location. Sampling is the period of time over which irradiance is averaged into a single recorded value.

Location	N	Sampling	Av. error
Field campaign:			
La Selva	6	1 min.	1.52%
Los Inocentes	8	1 min.	1.71%
Permanent stations:			
Santa Rosa	108	10 min.	2.09%
La Selva	269	30 min.	2.73%

station, averaged over 30 minutes), while it is absent from the data of the field campaign which is averaged over 1 minute. This effect can be attributed to the presence of multiple "extreme" conditions (clear sky, cloudy sky; i.e. cumulus-type broken cloud cover) within a single observation period of the PAR measurement, leading to averaged values, while the MODIS sensor records the reflected radiation instantaneously, picking up either one of the "extremes" (Figure 3-3). This effect has a larger probability of occurrence when a larger time-averaging window is used, which is the underlying cause of the difference in the reported average errors for the different sets of observations (Table 3-3).

Thirteen measurements were made with the spectrometer that coincided with a MODIS overpass. The spectral data shows a good correspondence between observed and computed irradiance in small spectral bands (Figure 3-4), with a total error (over the PAR wavelength range) comparable to that obtained with the quantum sensor (Table 3-4).

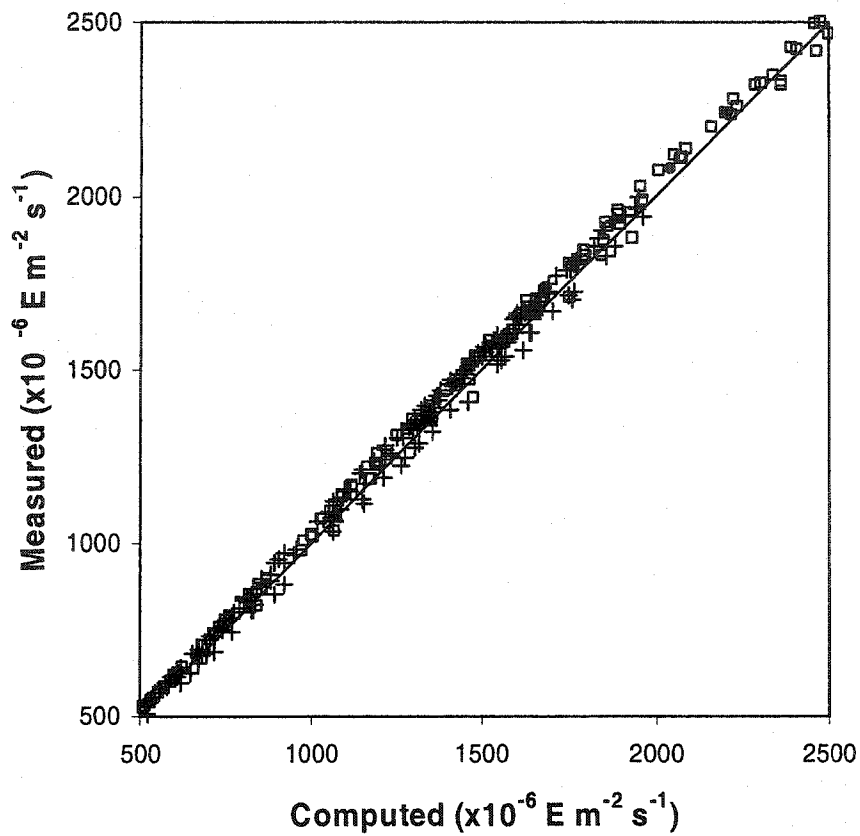


Figure 3-1: Graph of measured versus computed instantaneous PAR irradiance. Field campaign values at La Selva are indicated with \blacktriangle , Los Inocentes with \bullet , La Selva weather station data with $+$, and Santa Rosa data with \square . A linear fit, constrained to pass through the origin at (0, 0), yields a correlation coefficient of 0.99, with an average error of 2.51%; $N = 391$.

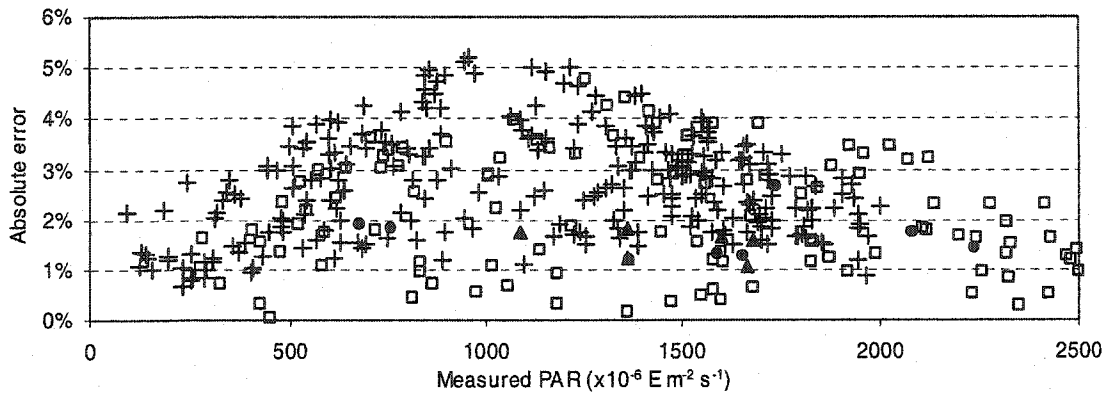


Figure 3-2: Absolute error of computed PAR versus measured PAR.

Observations sampled at 1 minute (\blacktriangle and \bullet) show no correlation with irradiance, while observations sampled at 10 (\square) and 30 ($+$) minute intervals have an easily identified peak in the absolute error around $1000 \mu\text{E m}^{-2} \text{s}^{-1}$ which is due to changes in atmospheric conditions during the observation window. Symbols are identical to those in Figure 3-1.

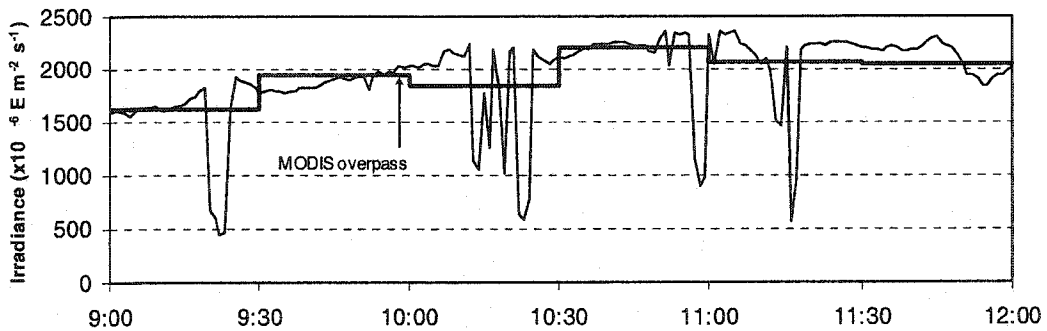


Figure 3-3: Comparison of measured PAR at 1 minute time-averaging, and 30 minute time-averaging. Data were recorded on 4 June 2002 at the La Selva location. The calculated PAR from MODIS data (9:57am) has an error of +1.04% compared to the 1 minute average and +2.52% compared to the 30 minute average.

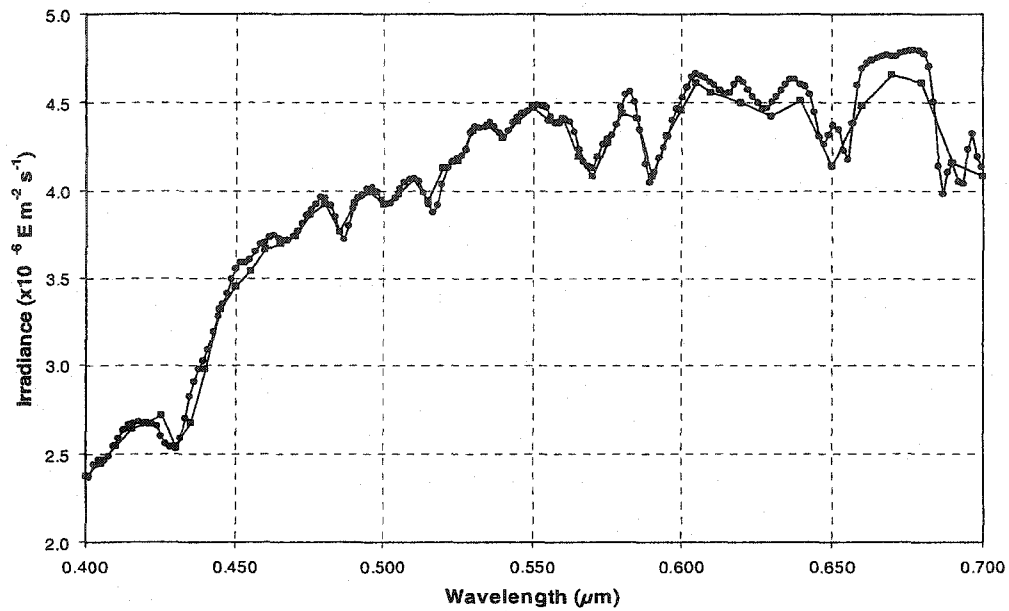


Figure 3-4: Graph of irradiance measured with a spectrometer (●) versus computed irradiance in individual spectral bands (■). The spectrometer has a band separation of 0.00158 μm , while the computation uses bandwidths of 0.005 μm (0.400 – 0.610 μm) to 0.010 μm (0.610 – 0.700 μm). This data was recorded on 5 June 2002 at the La Selva location.

Table 3-4: Average error of incident PAR at two locations with spectrometer measurements. *N* is the number of observations per location.

Location	N	Av. error
La Selva	6	1.52%
Los Inocentes	7	1.74%

Table 3-5: Average error (%) of incident PAR compared to measurements with a quantum sensor, under different cloud conditions. The number of observations for each error is given in brackets below the error.

Location	1 < τ_c	1 < τ_c < 5	$\tau_c > 5$
Santa Rosa	1.56%	1.85%	3.86%
	(42)	(47)	(19)
La Selva	1.40%	2.66%	4.19%
	(99)	(76)	(94)

When the error is stratified according to the cloud optical thickness for the two permanent observation stations (Table 3-5), it becomes immediately clear that the estimation of PAR is more accurate in clear sky conditions than under cloudy conditions. This is partially due to the difficulty of extracting atmospheric parameters from MODIS imagery (Kaufman and Tanré, 1998), and partially to the simplifications in the PARcalc algorithm, which suffers from the increase atmospheric complexity under cloudy conditions. It is interesting to note that under clear conditions the error is lower at the La Selva location, even when the temporal observation window is larger than at Santa Rosa. This may be due to salt crystals blown in from the nearby Pacific Ocean and from the higher amount of dust in this dry climate, compared to the inland, densely vegetated environment of the La Selva location.

E. Discussion

The objective of this study was to develop a method for the calculation of incident photosynthetic active radiation. The method has been demonstrated to produce accurate results for instantaneous PAR when used with MODIS data. The

average absolute error of 1.5% to 2.7% in the calculation of instantaneous PAR compares well to the typical uncertainty in the measurement of PAR using quantum sensors, which is around 3% for the LI-COR Li190. The observed error is in part related to the spatial resolution of the MODIS data, where a point observation made in the field is compared to a computed value based on the spatially averaged data as observed at the sensor. In MODIS the aerosol load is reported at a resolution of 10 km, and while its effect on longer wavelengths is more important than, for instance, Rayleigh scattering, the lower accuracy found at longer wavelengths can not be explained by spatial accuracy alone (Figure 3-4). The simplifications in the radiative transfer equations are likely to play a role as well. The assumptions of plane-parallel atmospheric layers and homogeneity in the field-of-view and within the layers are not very realistic under most atmospheric conditions, particularly not in the case of broken cumulus type cloud cover that is prevalent in the humid tropics. Multiple scattering of incident radiation is not considered for the cloud-free atmosphere; for the cloudy atmosphere it is implicitly used in the cloud top backscattered fraction. However, the overall accuracy obtained with the method relative to the measured data does suggest that the model as such might be accurate enough to be applied in biophysical models of photosynthesis and vegetation growth, at scales comparable to the spatial resolution of the MODIS data (~10 km).

MODIS atmospheric data is unrivalled in spatial resolution, but the temporal resolution is not adequate to produce daily integrated PAR, something which is important in biophysical studies of vegetation dynamics. With data from the second MODIS instrument on the Aqua platform becoming available this situation is much improved, but the short temporal scales of many atmospheric processes in the tropics (particularly cloud cover) could still cause problems for integration and averaging. The method presented in this paper is not restricted to the use of MODIS data, however. A much higher temporal resolution can be attained by using data

from operational meteorological satellites, but the lack of validated methods to derive more complex atmospheric parameters, such as cloud optical thickness and aerosol load, at the original high resolution provides a dilemma between choosing for high temporal resolution at reduced spatial resolution, or high spatial resolution at reduced temporal resolution, as with MODIS data. The International Satellite Cloud Climatology Project (ISCCP), for instance, produces physical cloud parameters, including cloud optical thickness, from imagery from operational meteorological satellites, but at a spatial resolution of 30 km and a reduced temporal resolution of 3 hours (Rossow and Schiffer, 1999). In many circumstances, the 30 km spatial resolution introduces generalizations of surface heterogeneity that have a profound effect on irradiance, something which is most prevalent in mountainous regions.

PAR irradiance computed with a physical model from high resolution satellite imagery has important advantages over approaches typically used to date. In the absence of better data PAR is usually estimated to be 40% - 50% of total broadband irradiance, as measured with a pyranometer (Leigh, 1999). This approximation is also used in the calculation of Net Primary Productivity (NPP) for the MODIS Land Product (MOD17), where a value of 45% is used (Running et al., 1999). The approximation does not account for the underlying physics of atmospheric attenuation and the wavelength dependency of attenuation mechanisms. It is therefore also insensitive to time-of-day effects related to increasing atmospheric path lengths early and late in the day, and to the different composition of irradiance under cloudy conditions. The presented model, on the other hand, has the flexibility to incorporate individual mechanisms in the computation of incident PAR, and to present the result separately as direct and diffuse components or as irradiance in individual spectral bands (Figure 3-4). This latter feature has the potential to improve the estimation of photosynthesis, and

thus derived parameters such as NPP, by combining PAR in separate wavelength intervals with the selective absorption rate of chlorophyll, which takes place preferentially in the blue and red wavelength regions.

F. Conclusion

A method has been demonstrated to derive instantaneous PAR from MODIS imagery at high spatial resolution. Despite the difficulty of capturing the full spatial and temporal atmospheric dynamics, the presented model has some characteristics that make its use attractive. First, it allows for the computation of spectrally disaggregated PAR irradiance, which is important in models of vegetation dynamics, because absorption is not uniform in the PAR spectrum and the growth response curve is not linear with increasing irradiance (Gates, 1980). Second, the method is based on the physical properties of attenuation processes in the atmosphere, making the method applicable over a large range of conditions. The low frequency of MODIS observations relative to the dynamics of the atmosphere, particularly in unstable environments such as the tropics, restricts the use of the presented method to the calculation of instantaneous PAR, rather than daily integrated PAR which has a larger potential in current biophysical models of photosynthesis and vegetation dynamics.

Although the accuracy of the presented method is high relative to the accuracy of the validation measurements, there are certain aspects of the model that may require enhancement to sustain that high accuracy over a wider range of atmospheric conditions. An important assumption in the calculation of direct and diffuse irradiance is the linearity and independence of the different attenuation processes taking place in the atmosphere. Scattering was assumed to occur before absorption. While such a separation between processes is hard to avoid, the vertical stratification of the atmospheric profile in the Atmospheric Profile product (MOD07) makes a physically more accurate model, such as those used in MODTRAN and

HITRAN, possible. It is not applied here, though, as the gains in precision might not be justified given the approximations applied in the radiative transfer computation of the PARcalc method itself.

The daily MODIS Terra overpass in Costa Rica occurs sometime between 9:15am and 11:05am, local time. Given the strong within-day variations in cloud cover in tropical countries the observed value can not be used to estimate daily integrated irradiance. Here the observation is used to compute instantaneous irradiance I_{PAR} . When MODIS Aqua data becomes validated a similar value can be derived for afternoon irradiance. Significant improvements might be achieved when data sets with higher temporal resolution are used, such as data from the geostationary weather satellites (e.g. GOES, METEOSAT, ERS). The increased spectral resolution of the new generation of these satellites (e.g. 12 channels on the new METEOSAT Second Generation, GOES-R Advanced Baseline Imager) is particularly promising, as this allows for a more accurate extraction of physical atmospheric parameters at the full spatial and temporal resolution of the sensor.

G. Bibliography

- Ångström, A. (1929). On the atmospheric transmission of sun radiation and on dust in the air. *Geografische Annalen*, 2, 156-166.
- Berk, A., Bernstein, L.S., Anderson, G.P., Acharya, P.K., Robertson, D.C., Chetwynd, J.H., & Adler-Golden, S.M. (1998) MODTRAN Cloud and Multiple Scattering Upgrades with Application to AVIRIS. *Remote Sensing of Environment*, 65, 367-375.
- Bossel, H. (1996). TREEDYN3 forest simulation model. *Ecological Modelling*, 90, 187-227.

- Dozier, J., & Frew, J. (1990) Rapid calculation of terrain parameters for radiation modeling from digital elevation data. *IEEE Transactions on Geoscience and Remote Sensing*, 28, 5, 963-969.
- Dubayah, R., & Loechel, S. (1997). Modeling topographic solar radiation using GOES data. *Journal of Applied Meteorology*, 36, 141-154.
- Gastellu-Etchegorry, J.P., Guillevic, P., Zagolski, F., Demarez, V., Trichon, V., Deering, D., & Leroy, M. (1999). Modeling BRF and radiation regime of boreal and tropical forests: I. BRF. *Remote Sensing of Environment*, 68, 281-316.
- Gates, D.M. (1980). *Biophysical ecology*. New York, NY: Springer-Verlag.
- Gautier, C., Diak, G. & Masse, S. (1980). A simple physical model to estimate incident solar radiation at the surface from GOES satellite data. *Journal of Applied Meteorology*, 19, 1005-1012.
- Iqbal, M. (1983). *An introduction to solar radiation*. (pp. 107-152). Toronto: Academic Press Canada.
- Kaufman, Y.J., & Tanré, D. (1998). *Algorithm for remote sensing of tropospheric aerosols from MODIS. Algorithm theoretical basis document*. Revised October 26, 1998. Greenbelt, MD: NASA Goddard Space Flight Center.
- Leigh, E.G., Jr. (1999). *Tropical forest ecology: A view from Barro Colorado Island*. New York, NY: Oxford University Press.
- LI-COR (1996). Calibration procedures for LI-COR spectroradiometers, radiation sensors & lamps. LI-COR Biosciences, Application note #109. Lincoln, NE: LI-COR, Inc.
- Pinker, R.T., & Laszlo, I. (1992). Modeling surface solar irradiance for satellite applications on a global scale. *Journal of Applied Meteorology*, 31, 194-211.

- Rossow, W.B., & Schiffer, R.A. (1999). Advances in Understanding Clouds from ISCCP. *Bulletin of the American Meteorological Society*, 80, 2261-2287.
- Rothman, L.S., Rinsland, C.P., Goldman, A., Massie, S.T., Edwards, D.P., Flaud, J.-M., Perrin, A., Camy-Peyret, C., Dana, V., Mandin, J.-Y., Schroeder, J., McCann, A., Gamache, R.R., Wattson, R.B., Yoshino, K., Chance, K.V., Jucks, K.W., Brown, L.R., Nemtchinov, V., & Varanasi, P. (1998). The HITRAN molecular spectroscopic database and HAWKS (HITRAN Atmospheric workstation): 1996 edition. *Journal of Quantitative Spectroscopic Radiative Transfer*, 60, 665-710.
- Running, S.W., Nemani, R., Glassy, J.M. & Thornton, P.E. (1999). *MODIS daily photosynthesis (PSN) and annual net primary production (NPP) product (MOD17). Algorithm theoretical basis document. Version 3.0.* Missoula, MT: University of Montana.
- Stephens, G.L., Ackerman, S., & Smith, E.A. (1984). A shortwave parameterization revised to improve cloud absorption. *Journal of the Atmospheric Sciences*, 41, 687-690.
- Várnai, T., & Marshak, A. (2002). Observations of three-dimensional radiative effects that influence MODIS cloud optical thickness retrievals. *Journal of the Atmospheric Sciences*, 59, 1607-1618.
- Wenhan, Q., & Jupp, D.L.B. (1993). An analytical and computationally efficient reflectance model for leaf canopies. *Agricultural and Forest Meteorology*, 66, 31-64.

Chapter 4

SENSITIVITY, SCALE, AND ACCURACY OF THE PARCALC METHOD[♦]

A. Introduction

The PARcalc method can estimate instantaneous photosynthetically active radiation (PAR) from MODIS satellite imagery with an absolute error ranging from 2% to 6% compared to field observations (Figure 3-2). In order to use the PARcalc method to construct spatially exhaustive maps of PAR from MODIS satellite imagery, thus without resorting to geostatistical interpolation of sparse field observations, it is imperative to analyze the behaviour of the PARcalc method with respect to the (extreme) values that the atmospheric parameters can assume. This analysis will assist in evaluating at least three operational considerations: 1) which image pixels to reject for calculation because the (combination of) atmospheric parameters are not reliable; 2) establish confidence intervals on the calculated estimates of PAR; and 3) determine an appropriate resolution (pixel size) of the products generated with the PARcalc method.

In this Chapter an analysis is made of the impact of uncertainties in the magnitude of atmospheric parameters in the estimation of PAR using the PARcalc method. The analysis addresses two key issues:

- The sensitivity of the PARcalc method to uncertainties in the parameters used by the method. This involves assessing the effect of parameter fluctuations on the estimations, by making a sensitivity analysis of

[♦] A condensed version of this Chapter, in combination with the complete Chapter 3, has been published in *Remote Sensing of Environment*, 2004, 91(1):98-113.

individual parameters used in the PARcalc method. (Rayleigh scattering is dependent only on the atmospheric path length, which in turn depends on the solar altitude and the surface elevation. Since an exact solution is known for calculating solar altitude, and the surface elevation is typically known to a high degree of accuracy, Rayleigh scattering is not considered in the sensitivity analysis.)

- The impact of topographic heterogeneity on the estimations. In mountainous areas there can be substantial relief within the field-of-view of a single pixel in the satellite imagery. Both the elevation and the surface slope and orientation impact on the estimation of PAR irradiance. The assessment of the effects of topographic heterogeneity is essential in establishing scales at which PAR irradiance can reliably be mapped. The surface parameters relate to the elevation z (m) of the surface, for the determination of atmospheric path lengths, the exposition factor $\cos i$, for the determination of the contribution of direct beam radiation to the total irradiance, and the sky-view factor V_D , for the determination of the contribution of diffuse irradiance to the total irradiance.

In this Chapter each of these parameters is analyzed to establish the sensitivity of the PARcalc method to fluctuations in its values. Most parameters are analyzed in isolation, with other parameter values being held constant while the target parameter slowly varies in magnitude, but certain parameters require secondary parameters to vary in conjunction (e.g. cloud optical thickness and atmospheric water content). The default parameter values are typical for tropical conditions (Table 4-1). Table 4-2 lists the symbology used in the Figures that illustrate the sensitivity of the individual parameters.

Table 4-1: Default parameter values for the sensitivity analysis. These values are typical of tropical conditions. The skyview and exposition factors mimic the typical conditions under which a quantum sensor is deployed to measure PAR.

Parameter	Clear sky	Cloudy sky
Elevation	0 m	0 m
Sky view factor	1.0	1.0
Exposition factor	1.0	1.0
Ozone concentration	250 DU	250 DU
Turbidity coefficient	0.4	0.4
Water content	4.0 cm	4.0/5.6/8.4 cm
Cloud optical thickness	-	1/10/50
Cloud top pressure	-	700 mbar

Table 4-2: Symbology for the solar altitude angle used in the Figures in this Chapter.

Solar altitude angle	Symbol
15°	△
30°	■
45°	◇
60°	▲
75°	□
90°	◆

For notional brevity, sensitivity is indicated as " $\Delta\text{PAR}/\text{parameter}$ ", where "PAR" represents instantaneous PAR irradiance in $\mu\text{E m}^{-2} \text{s}^{-1}$ and the parameter being expressed in its particular physical unit. For example, $\Delta\text{PAR}/w$ should be interpreted as the slope of the sensitivity curve plotting PAR as the dependent variable against the primary variable of atmospheric water content.

B. PARcalc parameter sensitivity

1. Ozone concentration

The presence of high-altitude atmospheric ozone is well-known for its absorption of ultraviolet radiation, which is harmful to most living materials. However, ozone also absorbs appreciable amounts of radiation in the PAR spectrum (Leckner, 1978). The effect of absorption by ozone on the overall PAR estimate is not very pronounced; the nearly perfect linear relationship has a maximum slope of $-0.118 \Delta\text{PAR}/\text{l}$ (with ozone expressed in DU) at the maximum solar altitude of 90° . At a solar altitude angle of 15° the slope is reduced to its minimum of $-0.059 \Delta\text{PAR}/\text{l}$ (Figure 4-1).

2. Water content and aerosol concentration

The presence of water and aerosols (dust, smoke, smog) in the atmosphere form complex interactions that are difficult to model analytically. Water may be present as a pure vapour, coagulated into tiny liquid droplets, as ice crystals, or, under the right conditions of temperature and concentration, as clouds. Nitrous and sulfurous gases (NO_x and SO_2) absorb water molecules, forming smog that consists of particles comparable in size to smoke particles and fine dust. While there are formulations to calculate attenuation of radiation due to particular aerosols (Rothman et al., 1998), the interaction between aerosols is not yet fully understood

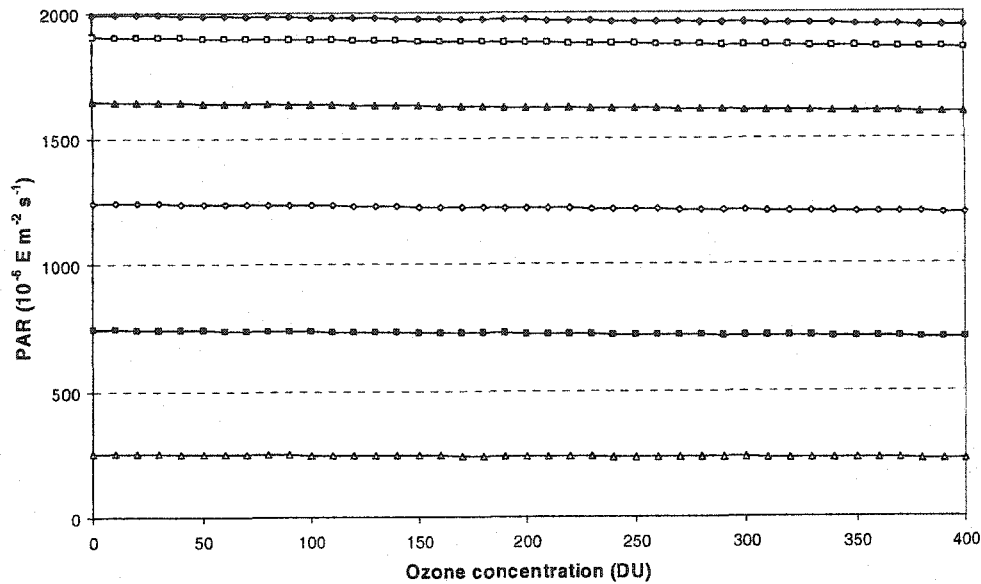


Figure 4-1: Sensitivity $\Delta\text{PAR}/\text{O}_3$ of the PARcalc method to ozone absorption. Refer to Table 4-2 for symbology.

and there are no data sources that provide sufficient information to simulate the effect of aerosols on attenuation for any particular location at any given time.

The Ångström turbidity formula (Ångström, 1929), expressed as the atmospheric transmittance coefficient in Equation 3-7, treats all scattering by aerosols and water as a single process. This is representative of the interactions between water vapour and airborne particulate matter. While it is attractive in its simplicity, it does not perform well when the cloud optical thickness is high (i.e. opaque clouds). The PARcalc method compensates for this by only considering aerosol scattering under the cloud top, that is, after cloud top reflection has been accounted for, but it is only a partial address of the problem. The PARcalc method is moderately sensitive to the turbidity coefficient β , particularly at lower values of β and at lower solar altitudes (longer atmospheric path length m_p in Equation 3-7) (Table 4-3, Figure 4-2).

Table 4-3: Sensitivity $\Delta\text{PAR}/\beta$ of the PARcalc method to the Ångström turbidity coefficient β as a function of the solar altitude angle.

Solar altitude angle	$\beta = (0.0...0.2)$	$\beta = (0.2...0.4)$	$\beta = (0.4...1.0)$
15°	-1016	-191	-13.9
30°	-1157	-469	-98.3
45°	-1067	-558	-174
60°	-960	-563	-212
75°	-887	-549	-226
90°	-862	-514	-229

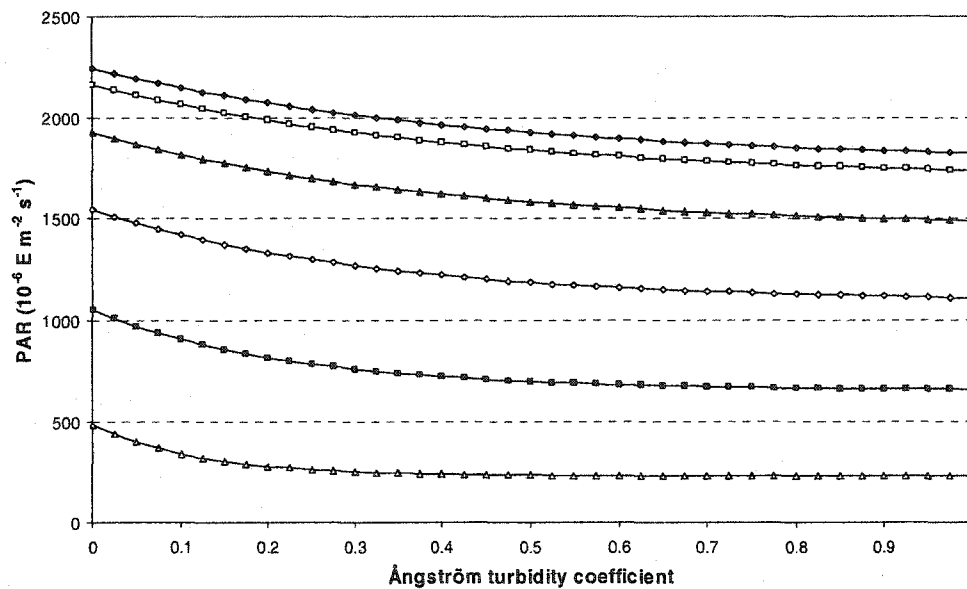


Figure 4-2: Sensitivity $\Delta\text{PAR}/\beta$ of the PARcalc method to Ångström's turbidity coefficient β . Refer to Table 4-2 for symbology.

Atmospheric water also absorbs radiation above 0.69 μm . Because this is on the high end of the PAR spectrum, the PARcalc method is virtually insensitive to water vapour absorption, although the absorption is appreciable at 0.69 μm and 0.70 μm .

3. *Cloud optical thickness and cloud top pressure*

Cloud optical thickness τ is a complex property which indicates the opacity of clouds to incident radiation. Since it is obvious that elevated levels of cloud optical thickness require greater amounts of water in the atmosphere, for the sensitivity analysis this latter parameter is increased along with the cloud optical thickness, increasing linearly from the default 4.0 cm at a cloud optical thickness of 0.0, to 8.4 cm at a cloud optical thickness of 50.0. This relationship between water content and cloud optical thickness was derived by a random sampling of a total of 20,462 pixels from 12 MODIS images over Costa Rica recorded in June 2002, yielding a correlation coefficient of 0.81.

The PARcalc method is highly sensitive to cloud optical thickness, particularly at lower levels of τ (Figure 4-3). At higher levels of τ , above a cloud optical thickness of approximately 10, τ is inversely proportional to PAR (Figure 4-4).

The cloud top pressure P_c (mbar) has a moderate influence on the estimation. This is because the cloud top altitude is used to vertically distribute water vapour and aerosols in the atmosphere and to estimate the amount of Rayleigh scattered radiation that is radiated out to space. The average (over the solar altitude angle) sensitivity $\Delta\text{PAR}/P_c$ ranges from 0.162 for a cloud optical thickness of 1.0 (Figure 4-5), to 0.089 for a cloud optical thickness of 10.0, to 0.030 for a cloud optical thickness of 50.0.

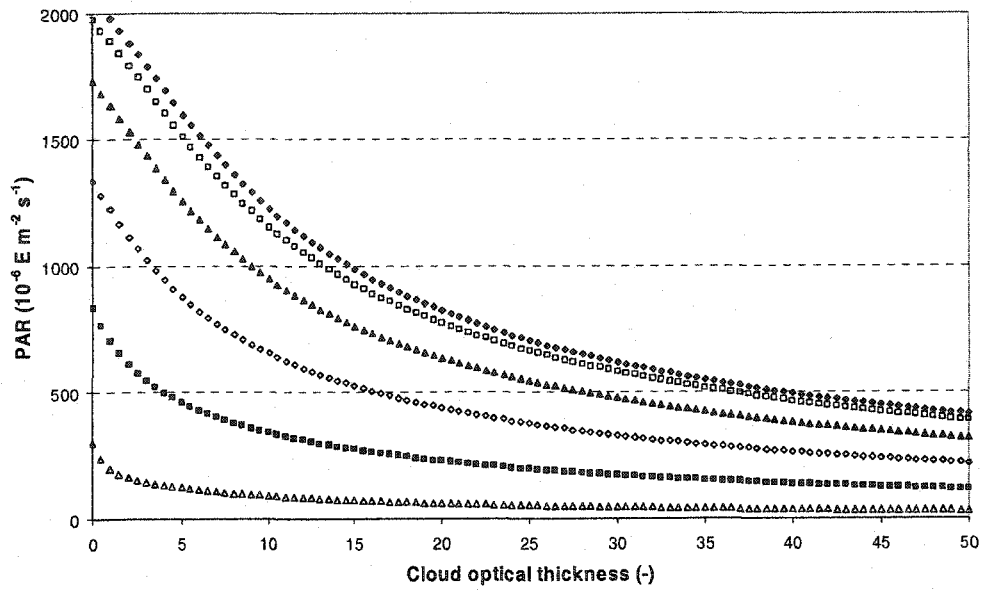


Figure 4-3: Sensitivity $\Delta\text{PAR}/\tau$ of the PARcalc method to the cloud optical thickness τ . Refer to Table 4-2 for symbology.

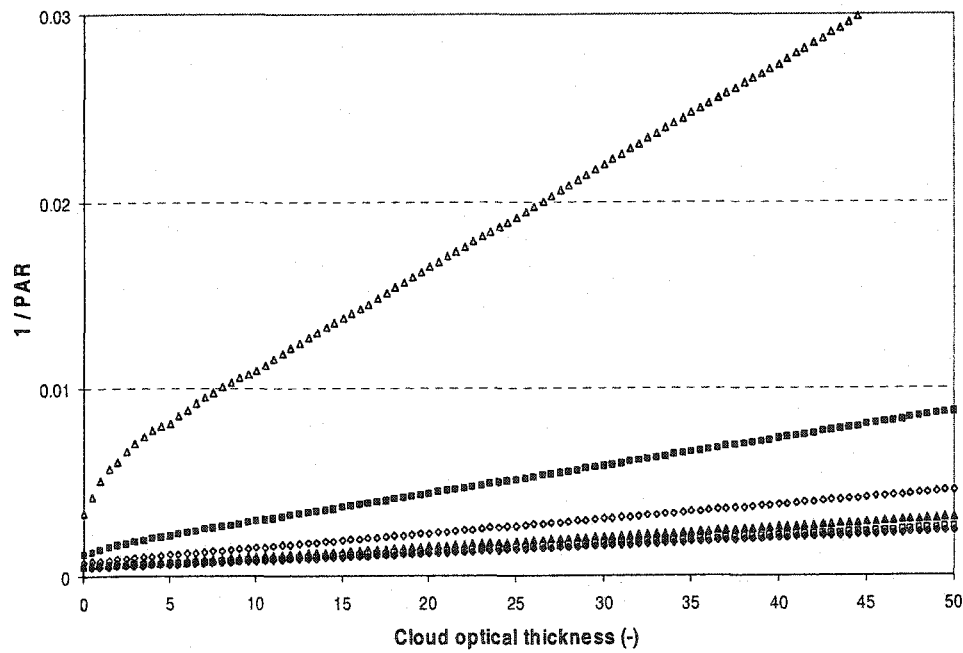


Figure 4-4: Relationship between the cloud optical thickness τ and the inverse of PAR. Refer to Table 4-2 for symbology.

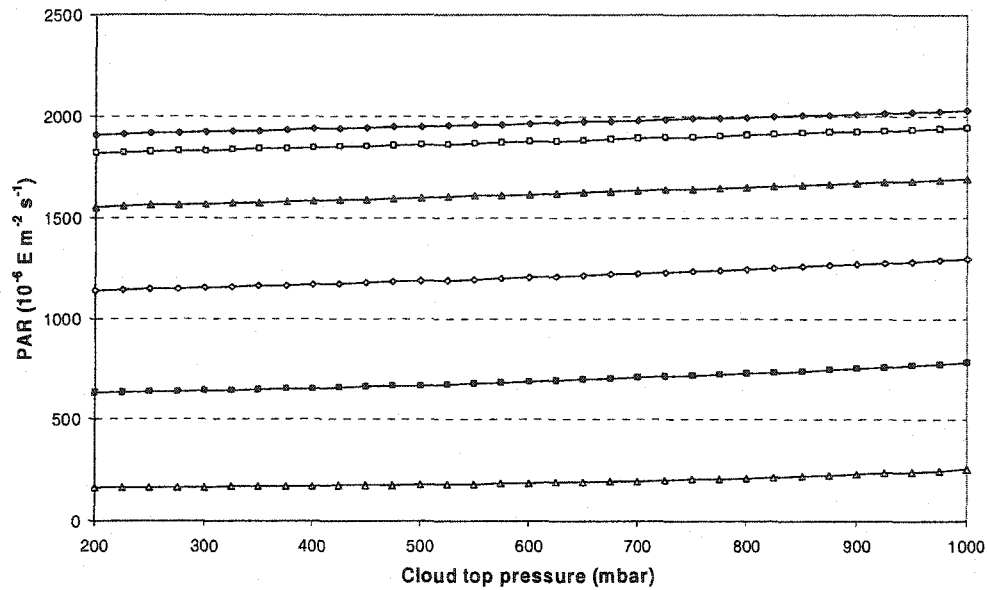


Figure 4-5: Sensitivity $\Delta\text{PAR}/P_c$ of the PARcalc method to the cloud top pressure P_c at a cloud optical thickness τ of 1.0 and an atmospheric water content w of 4.0 cm. Refer to Table 4-2 for symbology.

4. Elevation

Of the surface parameters elevation, exposition factor, and sky view factor only the first is evaluated here. The exposition factor and the sky view factor are purely geometrical constructs that have no bearing on the attenuation process, and thus the sensitivity of the PARcalc method, although they do impact on the calculation of total incident PAR at a given location, which is treated in later on.

The elevation above mean sea level indirectly affects atmospheric transmittance by shortening the actual atmospheric path length m_p with increasing elevation. This directly impacts the transmittances due to Rayleigh scattering τ_R , and aerosol scattering τ_A . There is a linear dependency between elevation and incident PAR, with a sensitivity $\Delta\text{PAR}/z$ of 0.035 for solar altitude angles over 45° , falling to 0.015 for a solar altitude angle of 15° (Figure 4-6). The linear dependency

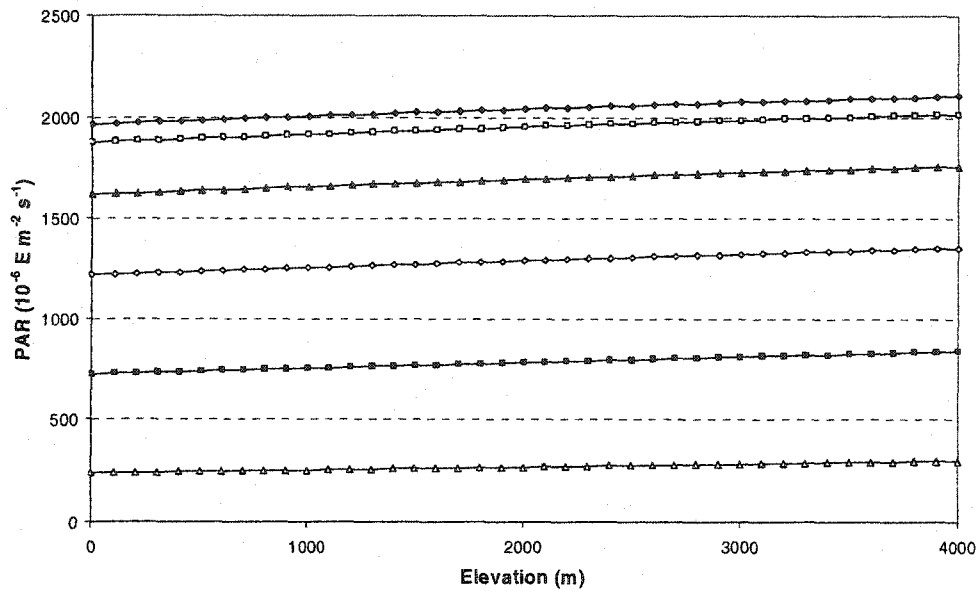


Figure 4-6: Sensitivity $\Delta\text{PAR}/z$ of the PARcalc method to the elevation above mean sea level z . Refer to Table 4-2 for symbology.

between elevation and incident PAR may appear surprising given the exponential decline in atmospheric pressure with increasing elevation. However, aerosols are assumed to have a constant concentration independent of atmospheric pressure, and their contribution to attenuation becomes larger relative to Rayleigh scattering as the atmospheric pressure falls with increasing elevation, effectively creating a quasi-linear relationship.

5. Relative sensitivity of the parameters

Comparing the sensitivity of individual parameters is not straightforward because the physical units are different. However, knowing the sensitivity of every parameter relative to the others is an important indication of the quality of the source data that is required in order to extract meaningful estimations from the PARcalc method. This is particularly important where data with different levels of

Table 4-4: Parameter value intervals for the analysis of relative parameter sensitivity.

Parameter	Interval
Ozone concentration	250 ± 25 DU
Turbidity coefficient	0.4 ± 0.1
Water content	4.0 ± 0.4 cm
Cloud optical thickness	5.0 ± 1.5
Cloud top pressure	700 ± 100 mbar
Elevation	1000 ± 100 m

support (spatial resolution, temporal resolution, measurement technique, etc) are combined, as will often be the case.

In this section, the reference atmospheres (Table 4-1) are used to analyze the effects of individual parameter uncertainties on the estimation, by establishing a confidence interval for each parameter (Table 4-4) and plotting them in a single graph for several solar altitude angles (Figure 4-7). The confidence intervals are typical, though conservative, for use with imagery from meteorological satellites (Guillory et al., 1993; Rossow and Garder, 1993; King et al., 1997; Kaufman and Tanré, 1998; Suggs et al., 1998). For these simulations the standard elevation is set to 1000 m, and the cloudy atmosphere has a cloud optical thickness τ of 5.0 with a corresponding atmospheric water content w of 4.8 cm.

In Figure 4-7 cloud optical thickness clearly stands out as the most sensitive parameter, and its sensitivity is consistently high, independent of the solar altitude angle, which is not the case with the other parameters. Ozone, on the other hand is the least sensitive. The PARcalc method is moderately sensitive to the other five

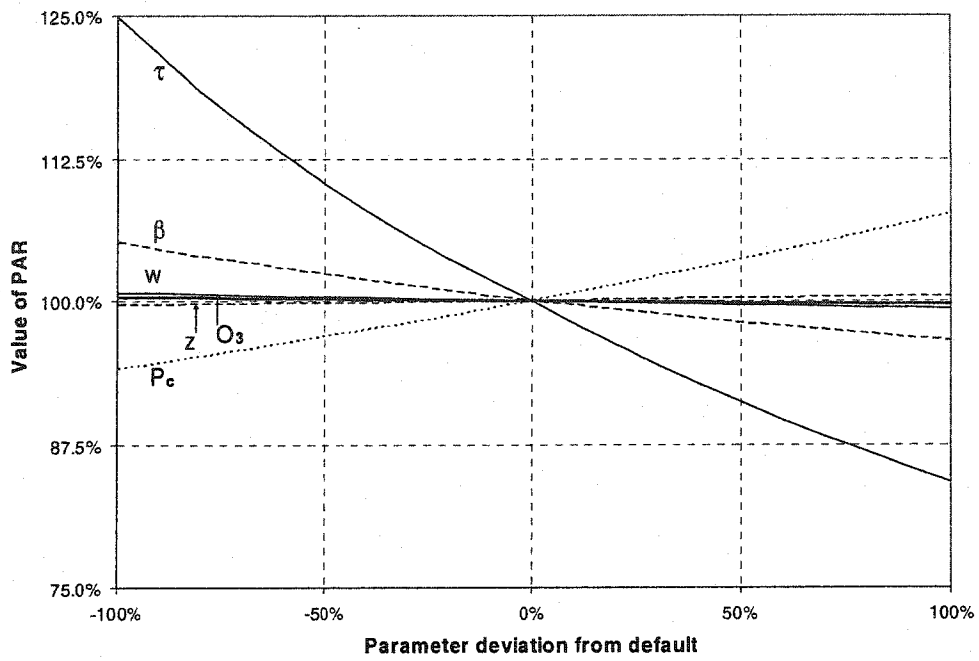


Figure 4-7a: Solar altitude angle of 30°.

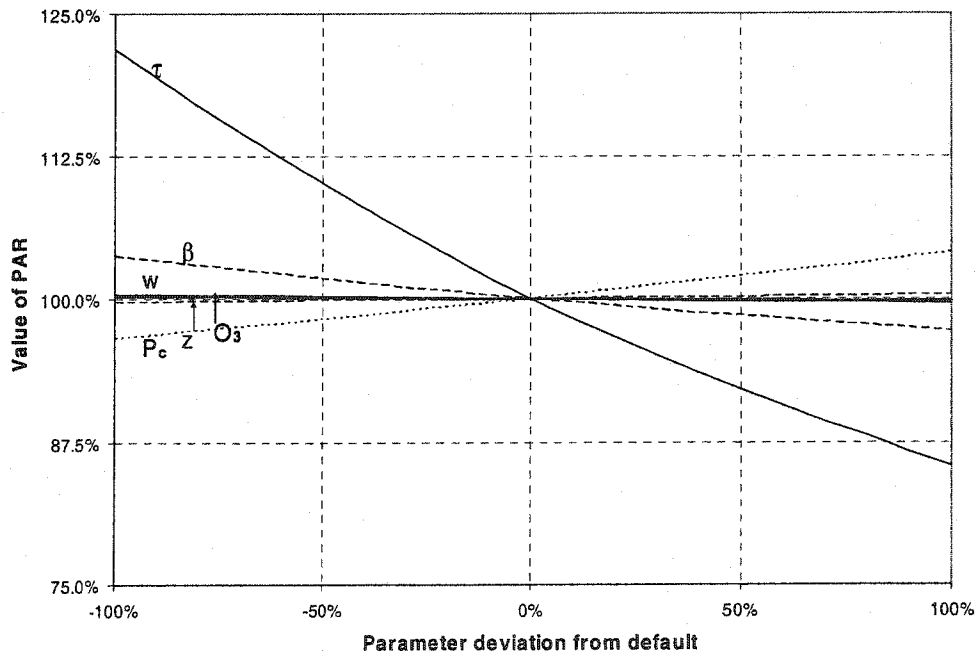


Figure 4-7b: Solar altitude angle of 60°.

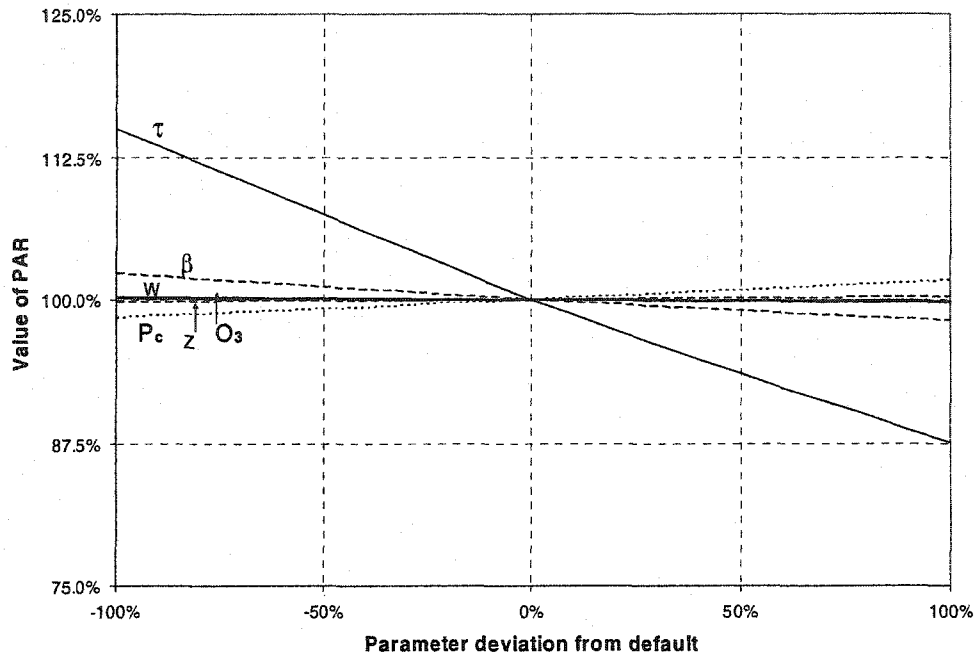


Figure 4-7: Relative sensitivity of the parameters in the estimation of PAR. The range of the parameters is given in Table 3. Solar altitude angles of (a) 30°; (b) 60° (preceding page); (c) 90° (this page).

parameters, but only so at low solar altitude angles. At high solar altitude angles (Figure 4-7c) the only parameter of concern is cloud optical thickness.

C. Topographic heterogeneity

For application in vegetation dynamics PAR normally needs to be estimated for a larger area. Typically, the topographical surface is represented as a Digital Elevation Model (DEM), and many algorithms have been developed to analyze DEMs, including extracting the PARcalc surface parameters exposition factor $\cos i$ and sky-view factor V_D . (Horn, 1981; Iqbal, 1983; Dozier and Frew, 1990; Corripio, 2003). However, abstraction of natural topography into a DEM inevitably leads to simplification of the naturally occurring surface (Bolstad and Stowe, 1984;

Burrough and McDonnell, 1998), with respect to the surface parameters the PARcalc method uses in its estimation of PAR.

The effect of the simplification of topography can be quite dramatic, particularly with regards to the exposition factor $\cos i$. In the extreme case, which may actually occur quite frequently, analysis of the DEM will yield an exposition factor of 1.0 (surface oriented perpendicular to the direct-beam radiation), while parts of the DEM pixel are shadowed by surrounding terrain so their specific exposition factor should have a value of 0.0. Given that in a cloud-free sky direct-beam radiation makes up about 80% of total PAR, the irradiance could locally be overestimated by a factor of 5. This effect is most pronounced when the daily maximum solar altitude angle, at the time of day when the irradiance is highest, is comparable to the average slope of the surface. It is thus a major concern when estimating incident radiation in highly dissected terrain at higher latitudes, invalidating straightforward but simplistic approaches such as those by Kumar et al. (1997) and Corripio (2003). In the tropics this condition is less severe, because at the time of maximum irradiance the solar altitude angle is so large (i.e. with the Sun close to zenith) that topographic shadowing is not very common. Earlier and later in the day the effect does occur, but the lower level of irradiance makes the contribution of any estimation error less important to the daily integrated PAR irradiance. Similar effects, but with a less dramatic impact, can be observed in the determination of the other surface parameters elevation z and sky-view factor V_D .

In this section an analysis is made of the impact of simplifying topographical surface heterogeneity on the estimation of PAR using the PARcalc method. For this analysis a high resolution DEM is used at its native resolution of 28.5 meter, and at reduced resolutions of 142.5 meter and 712.5 meter. (These reductions are integer multiples of the native resolution, thus no interpolation was required to obtain the lower resolution DEMs; the values were simply averaged from the higher resolution

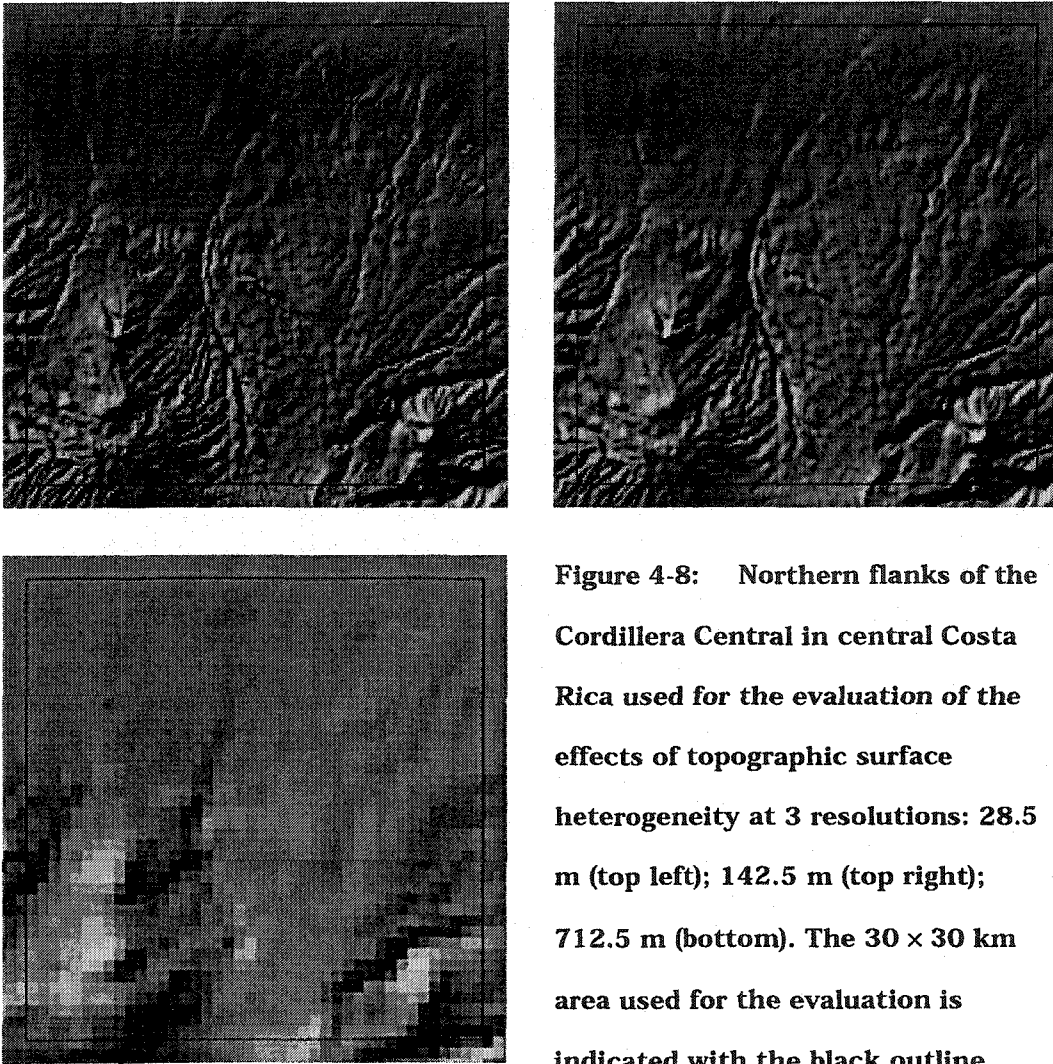


Figure 4-8: Northern flanks of the Cordillera Central in central Costa Rica used for the evaluation of the effects of topographic surface heterogeneity at 3 resolutions: 28.5 m (top left); 142.5 m (top right); 712.5 m (bottom). The 30 × 30 km area used for the evaluation is indicated with the black outline.

DEM.) An area of 30 × 30 km in mountainous terrain in Costa Rica is extracted from the DEMs (Figure 4-8); this area roughly corresponds to the spatial resolution of the cloud parameters published by the International Satellite Cloud Climatology Project (ISCCP) (Rossow et al., 1996). The topography in the southern half of the area is dominated by the volcanoes crowning the Central Cordillera, reaching a maximum altitude of 2,703 meter, and sloping down in a northerly direction towards the plains of the Huetar, to a minimum altitude of 32 meter.

The cumulative distribution graphs of elevation are essentially the same for all three resolutions, with the lower resolution DEMs suffering a relatively minor

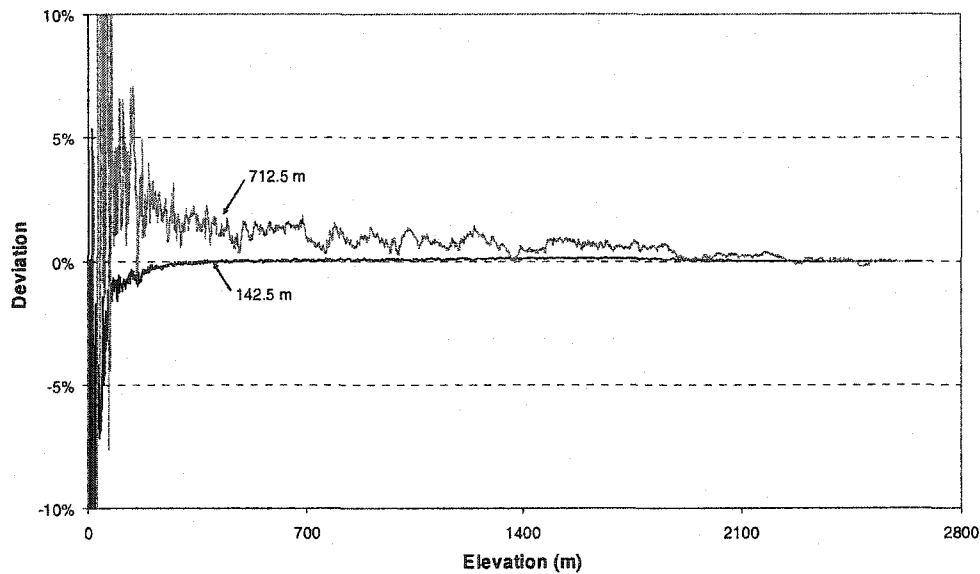


Figure 4-9: Deviation of the cumulative distribution of the two lower resolution DEMs with respect to the native resolution DEM. The high frequency of the deviation at lower elevations is a result of the discrete elevation values.

degradation of accuracy (Figure 4-9). The derivative parameters slope and aspect, on the other hand, suffer quite obviously from the reduction in resolution (Figures 4-10 and 4-11). At lower resolutions, the slope tends to be lower, which is an effect of the averaging of neighbouring pixels (Horn, 1981; Bolstad and Stowe, 1984). The aspect values tend to the overall direction of the slope, which is towards the N-NE. Since slope and aspect values combined define the normal vector to the surface, there is thus a negative impact on the exposition factor $\cos i$, which is defined as the cosine of the angle between the normal to the surface and the angle towards the Sun.

The sky view factor V_D displays a scale-related degradation similar to that of the exposition factor, being defined in the same topographical terms of slope and aspect as the exposition factor. However, since the sky view factor affects the

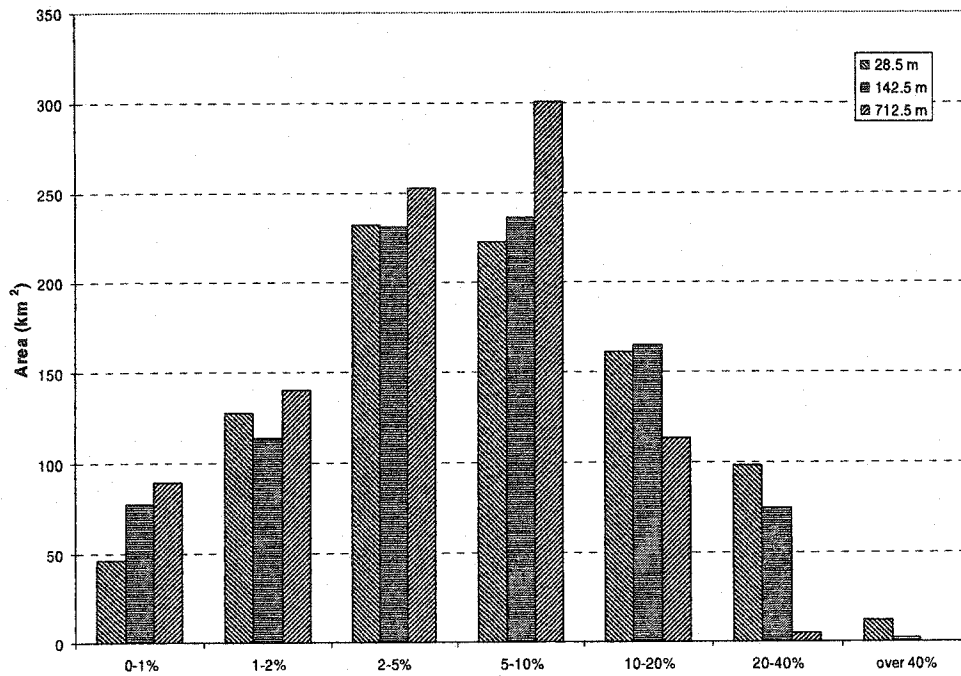


Figure 4-10: Distribution of slope classes for the three DEMs. At lower resolutions the slope is generally lower than at the native resolution of 28.5 m.

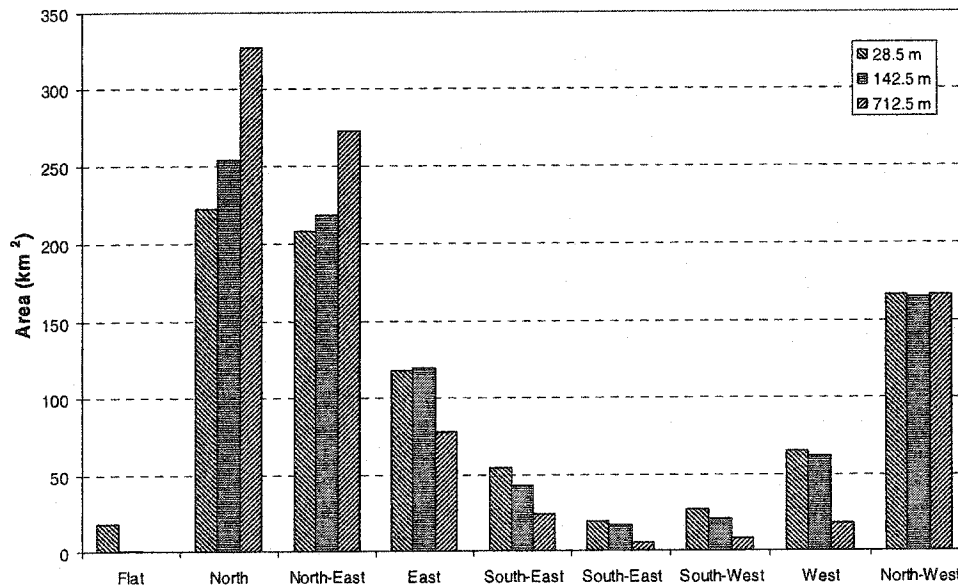


Figure 4-11: Distribution of aspect classes for the three DEMs. At lower resolutions the aspect tends to the general direction of the slope in the area, which is to the north/north-east.

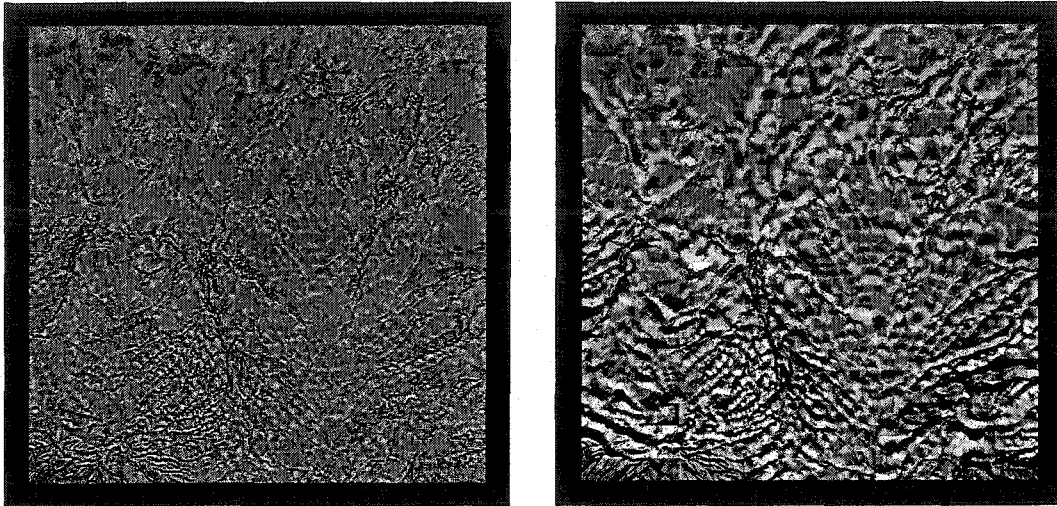


Figure 4-12: Error surfaces of calculating PAR on the basis of the DEM at a resolution of 142.5 m (left) and 712.5m (right), relative to the DEM at the native resolution of 28.5 m. Light colours indicate an underestimation of PAR (up to $-165 \mu\text{E m}^{-2} \text{s}^{-1}$), dark colours an overestimation (up to $202 \mu\text{E m}^{-2} \text{s}^{-1}$), while gray tones indicate good correspondence between estimates.

usually lower diffuse radiation component its effect is typically less, unless under conditions of prolonged thick cloud cover. The sky view factor and exposition factor are necessary to compute PAR in natural topography, and their errors propagate into the results. Figure 4-12 shows error surfaces for PAR, comparing the estimation of PAR at the reduced resolutions of 142.5 m and 712.5 m to the estimation at the fine resolution of 28.5 m, using the standard atmospheric parameter values (Table 4-1). While the range of errors is very comparable in both error surfaces, ranging from -165 to $202 \mu\text{E m}^{-2} \text{s}^{-1}$, the distribution of error is much broader in the error surface of the 712.5 m DEM than that of the 142.5 m DEM (Figure 4-13).

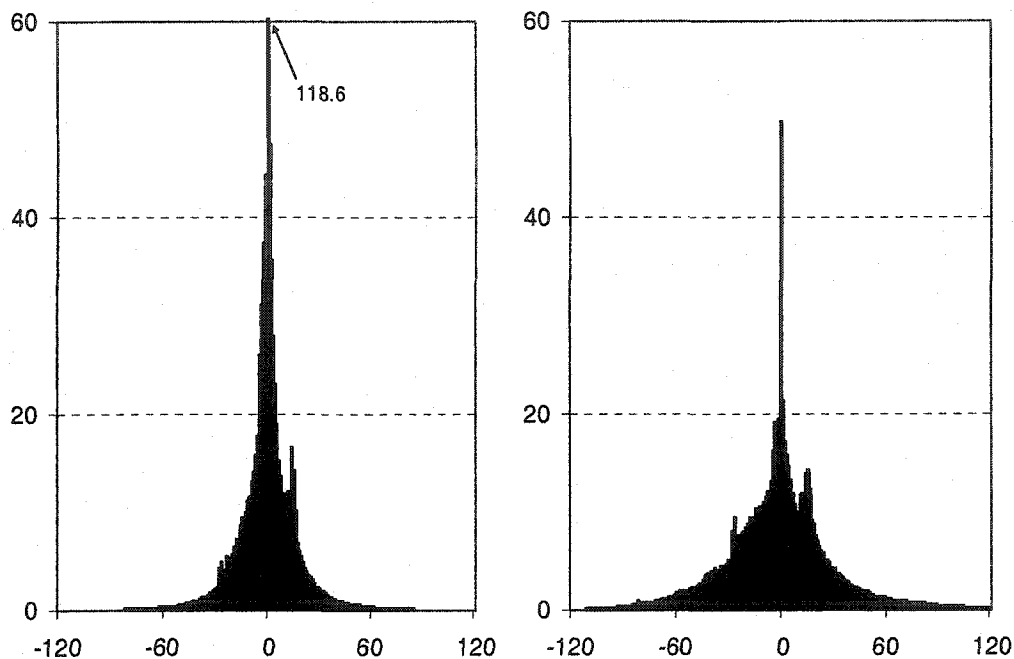


Figure 4-13: Histogram of the distribution of errors in estimating PAR from DEMs at a resolution of 142.5 m (left) and 712.5 m (right), compared to the calculation of PAR from the DEM at a resolution of 28.5 m. The errors range from $-165 \mu\text{E m}^{-2} \text{ s}^{-1}$ to $202 \mu\text{E m}^{-2} \text{ s}^{-1}$. The magnitude of the bars is area in km^2 .

D. Discussion

1. Parameter uncertainties

Having an accurate idea of the effect of uncertainties in the values of individual parameters in the calculation of PAR is essential in various ways. First, it allows for the establishment of confidence intervals on the estimates. Such information can be helpful in the statistical analysis of estimates from large volumes of observations, or in the (spatial) interpolation of sparse data over time or space. Second, it provides guidance in the establishment of accuracy or resolution when

parameters with disparate (spatial, temporal) support are being used in the estimation of PAR, which is the case with all current data sets suitable for use with the PARcalc method.

The cloud parameters cloud optical thickness τ_c and cloud top pressure P_c are the most sensitive parameters in the estimation of PAR (Figure 4-7), over the range of values tested (Table 4-4). Fortunately, high quality cloud parameters are available from the MODIS sensors at the native sensor resolution of 1 km. Aerosol parameters have a moderate impact on the estimation of PAR, particularly at lower concentrations, but unfortunately there are no data sets to match the spatial resolution of the cloud parameters. MODIS reports the Ångström turbidity coefficient at a spatial resolution of 10 km, which is the only readily available source of atmospheric aerosols. The remaining parameters all have a low impact on the estimation of PAR, each introducing an error of up to 3% in the estimate at the extreme of the tested intervals.

2. Topographic heterogeneity and resolution of estimation

The surface parameters elevation z , exposition factor $\cos i$, and sky-view factor V_D can usually be calculated at spatial resolutions much higher than the atmospheric parameters, and since they are defined in terms of the local topography they are time-invariant and they thus do not require interpolation at the temporal scale.

Typically, high resolution data is averaged to match the resolution of the parameter with the lowest resolution. This ensures that no spurious effects of low resolution data are introduced in the result and the (implied) quality of the result is comparable to the quality of the input data. In the case of the estimation of PAR, however, such an approach is undesirable for two reasons:

- The physical processes do not have the same spatial and temporal frequency. The concentration of ozone, for example, varies slightly throughout the year, showing very low spatial and temporal dynamics, particularly so in the tropics. Combined with the low sensitivity of the estimation to ozone concentration it would make little sense to dimension the output resolution on this parameter. Cloud optical thickness, on the other hand, fluctuates wildly over time and space, and its spatial and temporal resolution must be taken as a maximum that the output can reliably attain.
- Certain applications favour resolution over accuracy. The typical spatial resolution at which input parameters for the estimation of PAR are available might not be sufficient for certain applications. For instance, in mountainous regions the exposition of an inclined surface (a high spatial frequency parameter, see Figure 4-12) has a far greater impact on irradiance than, say, the atmospheric turbidity (Figure 4-7). Computing PAR over a DEM resampled to match the spatial resolution of the atmospheric resolution would yield results that are not representative of the local irradiance over most of the surface, and it would likely not even give an accurate average due to the non-linear nature of the PARcalc method.

There are no straightforward answers to the question of the optimal scale to represent PARcalc estimates. This depends both on the quality of the input data, the characteristics of the terrain, and on the application of the estimates to a particular problem. MODIS data, for instance, typically but not always has a higher degree of accuracy in its atmospheric parameters than assumed here in the sensitivity analysis (Table 4-4). However, when certain assumptions are made about the atmospheric parameters and the way that the results need to be interpreted a workable solution can be defined.

The first assumption is that atmospheric phenomena express themselves at scales that are larger than a few kilometers, and that their properties vary slowly in the spatial dimension. This assumption is not generally true for broken cloud cover and near geophysical boundaries (e.g. land/sea). Fortunately, the cloud parameters are provided at a relatively large scale (1 km) in the MODIS Atmospheric products. For aerosols the assumption is only applicable for naturally occurring particulates (e.g. airborne salt from the oceans, dust over deserts, and high humidity in the tropics), while anthropogenic aerosols (e.g. urban and industrial smog, smoke from fires) are more localized. However, anthropogenic aerosols tend to occur in high concentrations, where the PARcalc method is less sensitive to the aerosol load.

The second assumption is that the pixel of an image of an atmospheric parameter is homogenous with respect to the value of that parameter; i.e. that the value is averaged from conditions throughout the field-of-view of the pixel and that the average is reasonably representative of all of those conditions. For the MODIS sensor, where the lower resolution atmospheric parameters are aggregate values based on a statistical analysis of pixels at the resolution of approximately 1 km of the sensor arrays, this appears to be a reasonable assumption. For data from the meteorological satellites, at a comparable spatial resolution as MODIS, the data is typically averaged over a larger area in order to derive atmospheric parameters, such as cloud optical thickness, as is the case with the 30 km resolution ISCCP data set (Rossow et al., 1996).

Using these two assumptions a scale must be chosen at which the PARcalc method estimates irradiance. One can decouple the atmospheric path calculations from the topographical parameters. In this case the direct beam and diffuse irradiance I_B and I_D (Equations 3-1 and 3-13) are calculated first at a reduced resolution, after which these are applied at the higher resolution of the topographical parameters exposition factor $\cos i$ (Equation 3-14), and sky-view factor

V_D to compute total irradiance (Equation 3-16). The assumption of homogeneity within pixels at a lower resolution is required in this procedure, but it should be obvious that the assumption is no more than that, and acutely so in the case of cloud cover, and that such arithmetically correct estimates must be interpreted as being approximate. In applications where the irradiance is not required at the high resolution of the DEM the results can be aggregated at a suitable lower scale, along with a statistical description of the variability within the area, based on the high resolution topography.

3. *Operational considerations*

The low sensitivity of the PARcalc method to parameter accuracy at high solar altitude angles is beneficial for attaining high accuracy estimates of incident PAR. Typically about 85% of total daily irradiance is received between two hours before and two hours after local solar noon. With the Sun high in the sky, there is little atmosphere to traverse and consequently relatively little interaction with atmospheric constituents (air molecules, ozone, water, aerosols). Applying MODIS data to the PARcalc method is also benefited by this characteristic of low sensitivity during high irradiance, since the sun-synchronous orbit of the satellites gives a late morning overpass of the Terra platform and an early afternoon overpass of the Aqua platform. If atmospheric conditions are stable enough to allow interpolation of the key parameters of the two observations, something which is often assumed in Earth observation, then the crucial portion of the day accounting for the largest part of daily irradiance can be estimated at the high spatial resolution provided by the MODIS sensor.

E. Conclusion

In this Chapter the sensitivity of the individual parameters used in the estimation of incident PAR has been established. Given the wide disparity in the

quality and the spatial and temporal support of the parameters, it is hard to establish the accuracy of estimates made with the PARcalc method, as well as the spatial resolution at which these estimates can be reliably represented. From the sensitivity analysis it is clear, though, that the cloud parameters should be the overriding factor in determining accuracy and resolution. Assuming homogeneity at the level of the pixel of the parameters at lower resolution, and for which the PARcalc method is less sensitive, one can then establish confidence intervals suitable to the specific application for which the PARcalc method is used.

F. Bibliography

- Ångström, A. (1929). On the atmospheric transmission of sun radiation and on dust in the air. *Geografische Annalen*, 2, 156-166.
- Bolstad, P.V., & Stowe, T. (1984). An evaluation of DEM accuracy: elevation, slope, and aspect. *Photogrammetric Engineering and Remote Sensing*, 60, 1327-1332.
- Burrough, P.A., & McDonnell, R.A. (1998). *Principles of geographical information systems*. New York, NY: Oxford University Press.
- Corripio, J.G. (2003). Vectorial algebra algorithms for calculating terrain parameters from DEMs and solar radiation modelling in mountainous terrain. *International Journal of Geographical Information Science*, 17, 1-23.
- Dozier, J., & Frew, J. (1990) Rapid calculation of terrain parameters for radiation modeling from digital elevation data. *IEEE Transactions on Geoscience and Remote Sensing*, 28, 5, 963-969.
- Guillory, A.R., Jedlovec, G.J., & Fuelberg, H.E. (1993) A technique for deriving column-integrated water content using VAS split-window data. *Journal of Applied Meteorology*, 32, 1226-1241.

- Horn, B.K.P. (1981). Hill shading and the reflectance map. *Proceedings of the IEEE*, 69, 14-47.
- Iqbal, M. (1983). *An introduction to solar radiation*. (pp. 107-152). Toronto: Academic Press Canada.
- Kaufman, Y.J., & Tanré, D. (1998). *Algorithm for remote sensing of tropospheric aerosols from MODIS. Algorithm theoretical basis document*. Revised October 26, 1998. Greenbelt, MD: NASA Goddard Space Flight Center.
- King, M.D., Tsay, S.C., Platnick, S.E., Wang, M., & Liou, K.N. (1997) *Cloud retrieval algorithms for MODIS: optical thickness, effective particle radius, and thermodynamic phase. MODIS algorithm theoretical basis document no. ATBD-MOD-05. MOD06-Cloud product*. 23 December 1997, version 5. Greenbelt, MD: NASA Goddard Space Flight Center.
- Kumar, L., Skidmore, A.K., & Knowles, E. (1997). Modelling topographic variation in solar radiation in a GIS environment. *International Journal of Geographical Information Science*, 11, 475-497.
- Leckner, B. (1978) The spectral distribution of solar radiation at the Earth's surface – elements of model. *Solar Energy*, 20, 143-150.
- Rossow, W.B., & Garder, L.C. (1993) Validation of ISCCP cloud detections. *Journal of Climate*, 6, 2370-2393.
- Rossow, W.B., Walker, A.W., Beuschel, D.E., & Roiter, M.D. (1996) *Documentation of new cloud datasets*. Science Systems and Application Inc. at NASA Goddard Institute for Space Studies.

Rothman, L.S., Rinsland, C.P., Goldman, A., Massie, S.T., Edwards, D.P., Flaud, J.-M., Perrin, A., Camy-Peyret, C., Dana, V., Mandin, J.-Y., Schroeder, J., McCann, A., Gamache, R.R., Wattson, R.B., Yoshino, K., Chance, K.V., Jucks, K.W., Brown, L.R., Nemtchinov, V., & Varanasi, P. (1998). The HITRAN molecular spectroscopic database and HAWKS (HITRAN Atmospheric workstation): 1996 edition. *Journal of Quantitative Spectroscopic Radiative Transfer*, 60, 665-710.

Suggs, R.J., Jedlovec, G.J., & Guillory, A.R. (1998) Retrieval of geophysical parameters from GOES: evaluation of a split-window technique. *Journal of applied meteorology*, 37, 1205-1227.

Chapter 5

MAPPING PAR USING MODIS ATMOSPHERE PRODUCTS[♦]

A. Introduction

Solar radiation in the range from 400 to 700nm is commonly referred to as Photosynthetically Active Radiation (PAR), being that part of the electromagnetic spectrum which is absorbed by chlorophyll and applied to power the photosynthetic processes in green plant tissues (Gates, 1980). Despite its potential application in vegetation modelling and crop forecasting (Chazdon and Fetcher, 1984; Ostertag, 1998), PAR is not typically measured by weather stations. Using satellite remote sensing, PAR is often estimated from the reflected shortwave radiation as a fraction, ranging from 0.40 to 0.50, of the total shortwave radiation (Gautier *et al.*, 1980; Dubayah and Loechel, 1997; Running *et al.*, 1999). While this approach is straightforward, it does not account for the actual atmospheric composition at the time the observation was made and the estimate will be affected by atmospheric water content, aerosol concentration and solar geometry, to name a few of the environmental factors. Furthermore, this approach assumes that the reflected radiation is the difference of the total incident PAR and the absorbed PAR by the vegetation, which assumes that healthy vegetation is in place to absorb the incident PAR (Choudhury, 2001) and that PAR radiation does not interact with other surface materials.

In Chapter 3 of this thesis a method is presented based on actual atmospheric composition and physics which does not suffer from estimation errors

[♦] This Chapter has been submitted to the journal Remote Sensing of Environment.

and assumptions on surface material. This method, PARcalc, was shown to accurately calculate incident PAR using data from the Moderate Resolution Imaging Spectroradiometer (MODIS), Atmosphere products MOD04 - MOD07. There are two observations per day for most locations on Earth, from the identical MODIS sensors on the Terra and Aqua satellite platforms. Daily atmospheric dynamics can be so large that PAR can not be integrated to a daily value from just two observations. However, the timing of the two observations is such that a reasonably accurate estimate can be derived for many locations on Earth. In this paper the PARcalc method is applied to pairs of MODIS Terra and Aqua scenes, with the objective of mapping daily integrated PAR for Costa Rica.

B. Methods

1. The PARcalc method

In the PARcalc method, instantaneous PAR is calculated as a function of solar irradiance E_0 ($W m^{-2} s^{-1}$), local elevation z (m), atmospheric parameters related to transmittance τ in the spectrum from 400 to 700nm, and the solar geometry Ω relative to the surface:

$$PAR = f (E_0, z, \tau, \Omega). \quad (5-1)$$

The calculation of the transmittance τ requires data on the composition of the atmosphere at the times the satellite observations were made. The required parameters are the amount of atmospheric water, cloud cover, the density of aerosols, the amount of ozone, and the vertical distribution of cloud cover.

2. Calculating PAR with MODIS imagery

All of the atmospheric parameters required by the PARcalc method are readily available from the MODIS Atmosphere products MOD04 - MOD07. Geolocation data, surface elevation, and sensor viewing geometry are taken from the

geolocation product MOD03 at the native resolution of 1 km. The most sensitive parameter, cloud optical thickness, is available at a resolution of 1 km, as well as total atmospheric water content and all MOD03 parameters. Total column ozone and cloud top pressure are available at 5 km resolution, and the aerosol parameters are available at 10 km resolution. Given the high sensitivity of the PARcalc method to cloud optical thickness, relative to the sensitivity to the other parameters (Chapter 4), PAR is here calculated at a resolution of 1 km. This approach of combining MODIS data at different resolutions is applied in the calculation of surface reflectance as well (Vermote & Vermeulen, 1999).

The Terra and Aqua satellite platforms have nominal Equator crossings of 10:30AM on the descending node, and 1:30PM on the ascending node, respectively. They are thus spaced (almost) symmetrically around the local solar noon in areas close to the Equator (Figure 5-1). Having a morning and an afternoon observation is important when applying integrating radiation from sunrise to sunset, because often the weather has distinct patterns in the morning and in the afternoon. This is particularly prevalent in the humid tropics, where mornings tend to be dry and afternoons overcast and rainy (Sanford et al., 1994), but similar patterns can be found in temperate zones as well.

Daily integrated PAR is obtained by calculating instantaneous PAR from astronomical sunrise to sunset in 30 minute intervals. The MODIS Terra observation is assumed to be representative of early morning atmospheric conditions, while the MODIS Aqua observation is used for the late afternoon atmosphere. The atmospheric condition during the crucial midday part, when irradiance is highest, is linearly interpolated from the parameters of the two observations. When either of the two observations did not report any of the least

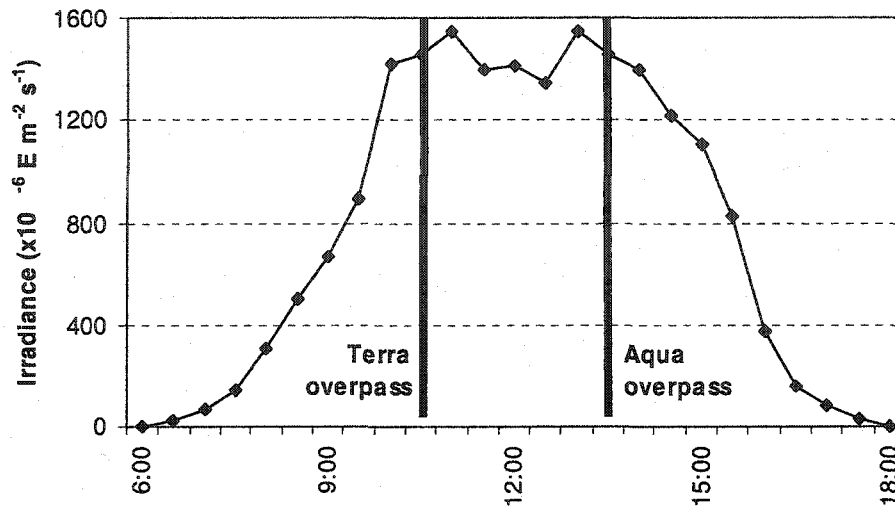


Figure 5-1: MODIS Terra and Aqua overpasses in relation to a typical progression of instantaneous irradiance from sunrise to sunset. About 84% of total irradiance occurs within 90 minutes of typical overpass times.

sensitive parameters (aerosol properties, ozone concentration, or total atmospheric water content), these values were held constant for the day from the other observation. This affected primarily the aerosol properties, which tend to have large gaps in the images due to their complex retrieval from at-sensor radiance.

Many agricultural and environmental applications require averaged PAR at time-scales of months or even over a complete growing season (Bossel, 1996; Leigh, 1999). Integration of daily PAR to longer periods is very straightforward once the MODIS imagery is registered to a local coordinate system (as opposed to the orbital reference system of data in the image swaths). This integration is very informative because it provides an estimate of variability over temporal and spatial scales. Here, the daily integrated PAR values are summarized on a monthly basis.

3. *MODIS images*

With the launch of the second MODIS instrument on board the Aqua satellite platform on 24 June 2002 two daily images became available for most locations on Earth. Starting in August 2002 the data stream was designated validated and daily integrated PAR can be derived from the Terra and Aqua observations. In this paper all data in the period October 2002 to January 2003 for Costa Rica are analyzed.

Of all the observations during the months of October 2002 – January 2003, 44 days had complete coverage of Costa Rica from both Terra and Aqua platforms, with both sensors having a sensor viewing angle of no more than 45° (in the across-track direction). Another 65 days had complete or partial coverage from both sensors, where at least one of the sensors had a viewing angle of more than 45° . Limiting the sensor viewing geometry to 45° filters out those pixels at the edges of the swath that suffer from greatly reduced resolution of the pixel footprint and the “bowtie” effect. This does of course reduce the number of available observations, but the quality of the observations will be higher. Both days with “good” data (viewing angle less than 45°) and those with “bad” data (viewing angle $> 45^\circ$) were used to calculate PAR, but their results were analyzed separately.

4. *Validation*

As a brief validation experiment, the daily integrated PAR as calculated with the method above were compared to field measurements made in Costa Rica. At La Selva Biological Station, in the humid north-east of Costa Rica, systematic measurements of PAR have been made since 1992. At Santa Rosa National Park, in the dry north-west of Costa Rica, measurements were taken from October 2002 onwards. These two sites represent different meteorological regimes, the former being humid and with significant cloud cover year round, while the latter has

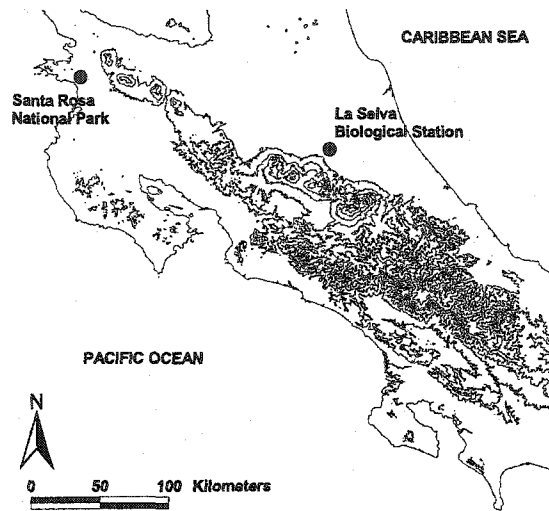


Figure 5-2: Location of La Selva Biological Station and Hacienda Los Inocentes in Costa Rica used to validate use of the PARcalc method with MODIS data. Contour lines are indicated at 500 meter intervals.

strongly defined wet and dry seasons. See Figure 5-2 for a map of both sites used in the validation.

At the meteorological station of La Selva Biological Station (10°26'N, 83°59'W) PAR is measured daily from sunrise to sunset using a LI-COR LI-190SZ quantum sensor and reported as average irradiation in 30 minute intervals. Further information and the data we used here can be found on OTS (2004). The La Selva Biological Station lies at an altitude of 34 m above sea level at the western fringe of the Caribbean coastal plains, with a strong influence of the Caribbean Sea on the local weather (Sanford et al., 1994).

At Santa Rosa National Park (10°50'N, 85°37'W) PAR was measured at an altitude of 290 m above sea level using a LI-COR LI-190SZ quantum sensor as well, but reported as average irradiation in 10 minute intervals. The Santa Rosa National Park forms the southern limit of the Central American semi-arid region. October

and November are wet months, while December and January are dry months, with strong winds coming from the Pacific Ocean.

These two sites have also been used to validate the PARcalc method in Chapter 3, where instantaneous PAR was derived from the MODIS sensor aboard the Terra satellite with average errors ranging from 2.1% to 2.7%.

C. Results

In Figure 5-3 the daily integrated PAR irradiance for julian days 5, 21, and 30 are mapped (5, 21, and 30 January 2003). Julian day 5 is a typical example of a day with large gaps in the data mainly due to missing data on aerosol properties. Julian day 21 clearly shows the sunny western part of the country, with high irradiance values, while the eastern half of the country is overcast. Julian day 30 is mostly overcast, with the exception of the extreme north-west.

None of the maps show substantial correlation with elevation, as one might intuitively expect, because the irradiance is mostly determined by cloud cover (Chapter 4) and the cloud cover in Costa Rica is largely influenced by the major weather systems on the Pacific Ocean and the Caribbean Sea, rather than by local orographic effects (Sanford et al., 1994). Areas with lower irradiance had a pattern of speckles, which are indicative of broken cloud cover. This pattern is revealed because cloud properties are reported at high resolution (1 km). Areas with high irradiance, on the other hand, had more blocky patterns because here the spatial stratification of differences in irradiance is largely dominated by aerosol properties, which are reported at 10 km resolution.

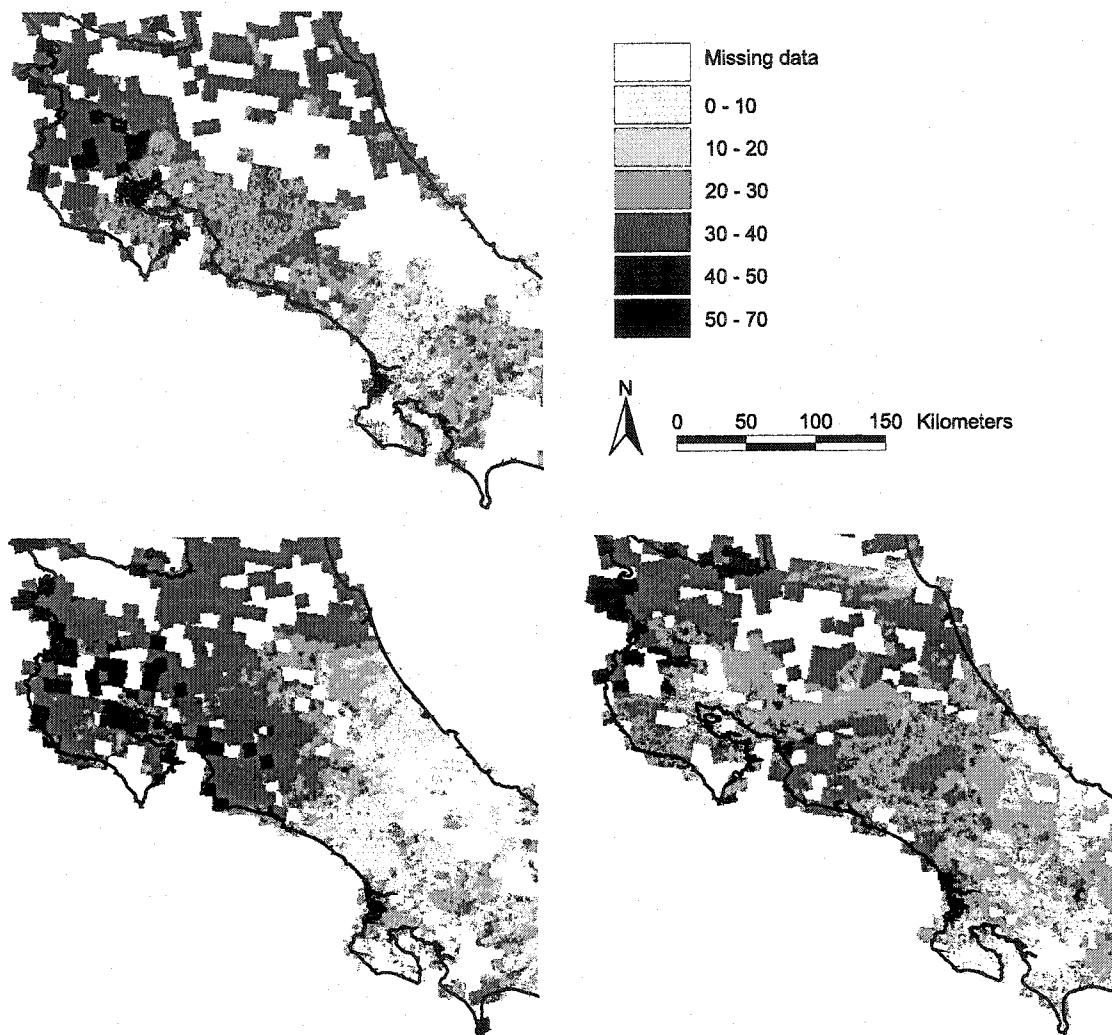


Figure 5-3: Daily integrated PAR ($E\ m^{-2}\ day^{-1}$) in Costa Rica for Julian days 5 (top left), 21 (bottom left), and 30 (bottom right) of 2003.

1. Comparison to field observations

Of the 109 days between October 2002 and January 2003 that were analyzed, 44 had images with a low sensor viewing angle, while 65 images had a viewing angle higher than 45° for at least part of the country. Of those images, not all reported a full set of atmospheric properties for the La Selva or Santa Rosa locations for which field observations were available, so PAR could not be calculated.

Table 5-1: Errors in estimating daily integrated PAR at La Selva Biological Station and Santa Rosa National Park, October 2002 – January 2003.

Location	Month	View angle <45°		View angle >45°	
		N	Av. Error	N	Av. Error
Santa Rosa	October 2002	9	6.2%	7	7.6%
	November 2002	8	5.8%	6	7.5%
	December 2002	11	5.1%	8	6.9%
	January 2003	8	5.2%	7	6.4%
	Overall	36	5.6%	28	7.1%
La Selva	October 2002	7	6.1%	8	7.4%
	November 2002	9	6.1%	5	8.1%
	December 2002	10	5.8%	7	7.6%
	January 2003	9	5.5%	6	7.1%
	Overall	35	5.9%	26	7.5%
Both locations		71	5.7%	54	7.3%

Table 5-1 shows the results of comparing the calculated daily integrated PAR to the measured values at both locations, both for images with low (<45°) and high (>45°) sensor viewing angle.

The errors for the daily integrated PAR are considerably higher than that for the instantaneous PAR reported in Chapter 3. The increased error is mostly due to the interpolation and extrapolation of atmospheric conditions from the instantaneous observation by the MODIS sensors during their overpass. The average errors still compare reasonably well to the typical error associated with quantum sensors, which is in the order of 3% (LI-COR, 1996). However, on a day-to-day basis the error in the calculated values can be much larger. The scatterplot in

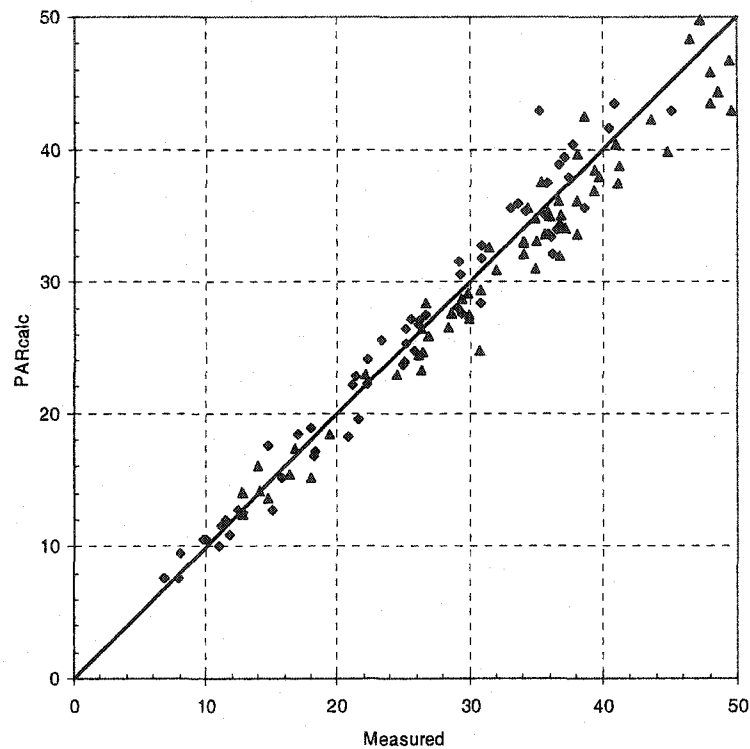


Figure 5-4: Scatterplot of daily irradiance ($E \text{ m}^{-2} \text{ day}^{-1}$) measured at La Selva Biological Station (\blacklozenge , $N = 61$) and Santa Rosa National Park (\blacktriangle , $N = 64$), and calculated with PARcalc, October 2002 – January 2003.

Figure 5-4 shows the correspondence between measured and calculated PAR for the 64 observations at Santa Rosa and the 61 observations at La Selva. The largest recorded discrepancy was 21.4% (on 22 December, at the La Selva location). Much of this error can be attributed to high frequency changes in (particularly) cloud cover (Figure 5-5). This sensitivity of the PARcalc method was already discussed Chapter 3 (see for instance Figure 3-3).

The data with lower sensor viewing angles consistently had lower errors than the data with higher viewing angles. This can be explained from the larger uncertainties in retrieving atmospheric parameters at higher slant angles, when the

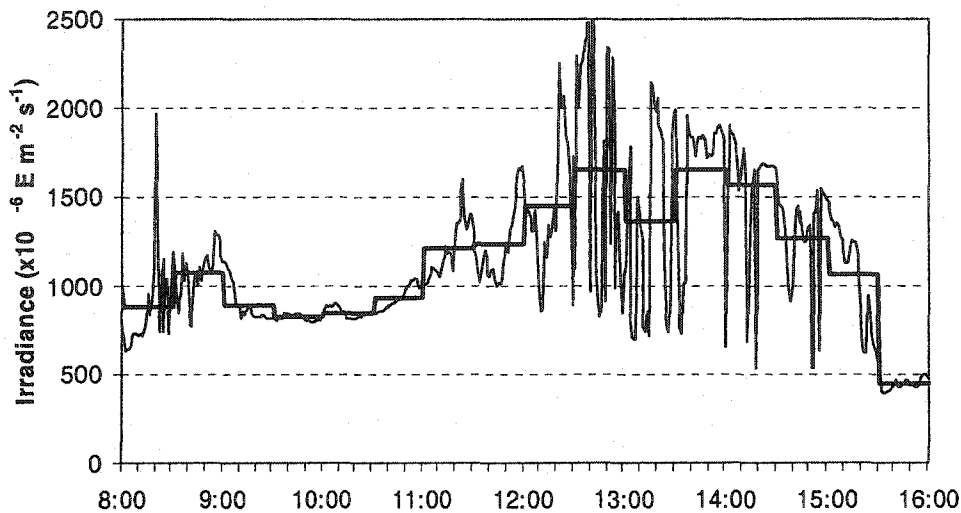


Figure 5-5: Comparison of high resolution PAR measurements ($\mu\text{E m}^{-2} \text{s}^{-1}$) (1 minute interval) to medium resolution measurements (30 minutes) at La Selva Biological Station, June 2002. The high frequency changes in PAR are caused by the alternating presence and absence of cloud cover.

radiation reaching the sensor has to traverse a larger atmospheric path, which results in increased scattering and “pollution” with radiation scattered onto the sensor from locations other than the footprint of the pixel (Kaufman & Tanré, 1998; Vermote & Vermeulen, 1999). The increased error is easily distinguished (Table 5-1), but is not so much larger that calculations made with atmospheric data collected at higher sensor viewing angles should be discarded outright. Considering that only about 30% of all days have data at low viewing angles (at near-equatorial latitudes, such as in Costa Rica), for certain applications it might be beneficial to have more actual data at a lower average accuracy than to have to use scarce data at higher accuracy. The larger number of calculated irradiances will better capture the variability of the radiation regime, which could be beneficial to, for instance, models of plant growth.

Calculations at the Santa Rosa location are consistently more accurate than those at the La Selva location. A similar trend can be observed going from the wet month of October to the much drier month of January. The discrete nature of many types of cloud cover (Figure 5-5) is at least partially due to this inaccuracy. As with the data at higher sensor viewing angle though, the differences are too small for many practical applications to be of major concern.

2. Monthly averaging

When the daily PAR calculations are integrated to monthly averages, a complete map of average daily PAR can be constructed without (most of the) areas with missing data due to uncertainties in the retrieval of atmospheric parameters (Figure 5-6 and Table 5-2). The average also smoothes out the sometimes large errors in the estimation of daily PAR from a single pair of MODIS images. Temporal averaging has the added advantage that statistics can be derived to characterize the variability in the data; Figure 5-7 shows the standard deviation of the monthly average data for the month of January. With little more than a year of data available from the MODIS sensor on the Aqua platform it is now possible to average over multiple years of data and thus produce data with a wider statistical support.

D. Discussion

1. Accuracy and sources of error

The error of 5-8% in the calculation of daily integrated PAR over a period of a few months compares well to the typical uncertainty in the measurement of PAR using quantum sensors, which is around 3% for the Li-Cor LI190-SZ. However, on individual days the error can be much larger (Figure 5-4). These large errors can be related to the temporal and spatial resolution in the data.

Table 5-2: Errors in estimating monthly integrated PAR at La Selva Biological Station and Santa Rosa National Park, October 2002 - January 2003.

Location	Month	View angle <45°		All angles	
		N	Abs. Error	N	Abs. Error
Santa Rosa	October 2002	9	5.2%	16	4.6%
	November 2002	8	5.3%	14	4.8%
	December 2002	11	5.8%	19	5.3%
	January 2003	8	4.8%	15	4.8%
	Overall	36	5.3%	64	4.9%
La Selva	October 2002	7	5.6%	15	4.8%
	November 2002	9	5.5%	14	5.3%
	December 2002	10	5.0%	17	5.0%
	January 2003	9	5.1%	15	4.8%
	Overall	35	5.3%	61	5.0%
Both locations		71	5.3%	125	4.9%

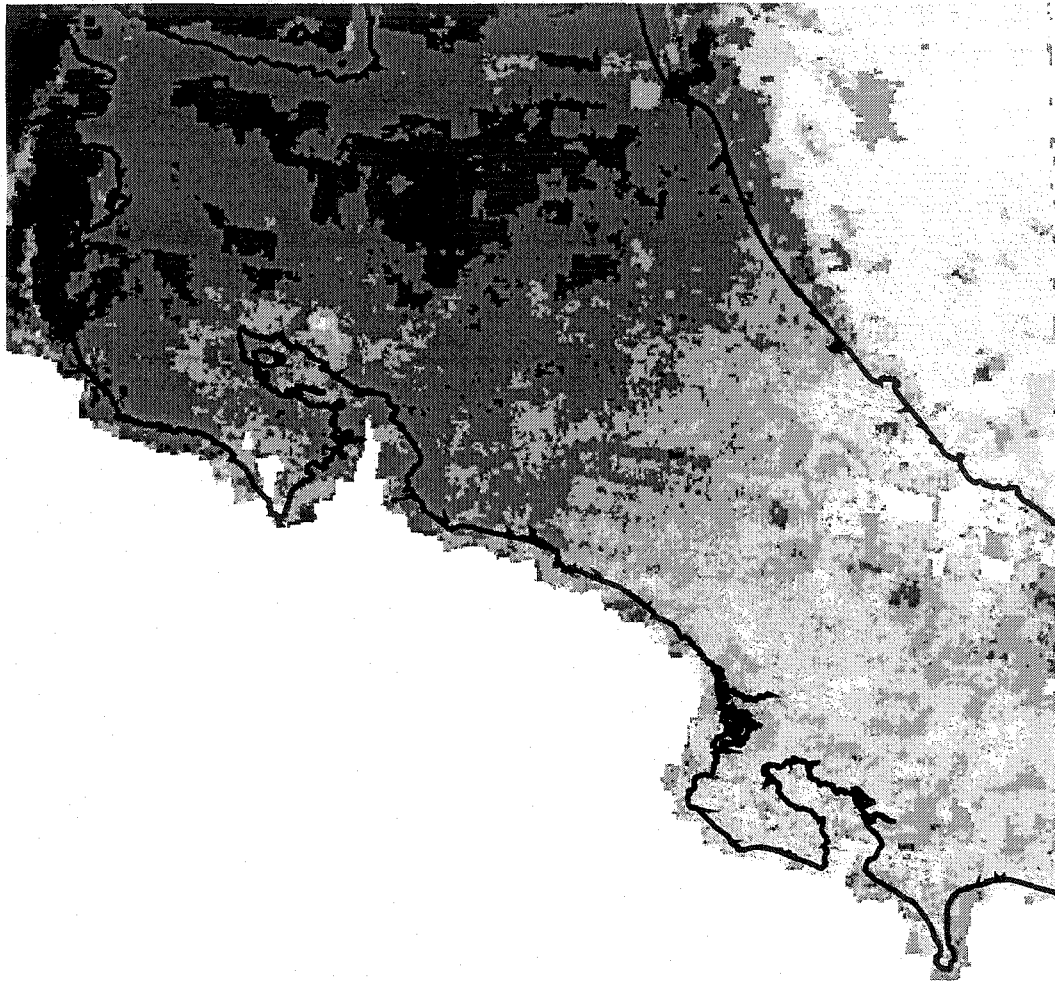


Figure 5-6: Average daily irradiance ($E \text{ m}^{-2} \text{ day}^{-1}$) for the month of January 2003, constructed from calculated PAR on a day-to-day basis. All available data was used (it was not restricted to a viewing angle of 45°). On average 13 daily PAR values were available for every land-based pixel. Orientation and legend are identical to those in Figure 5-3.

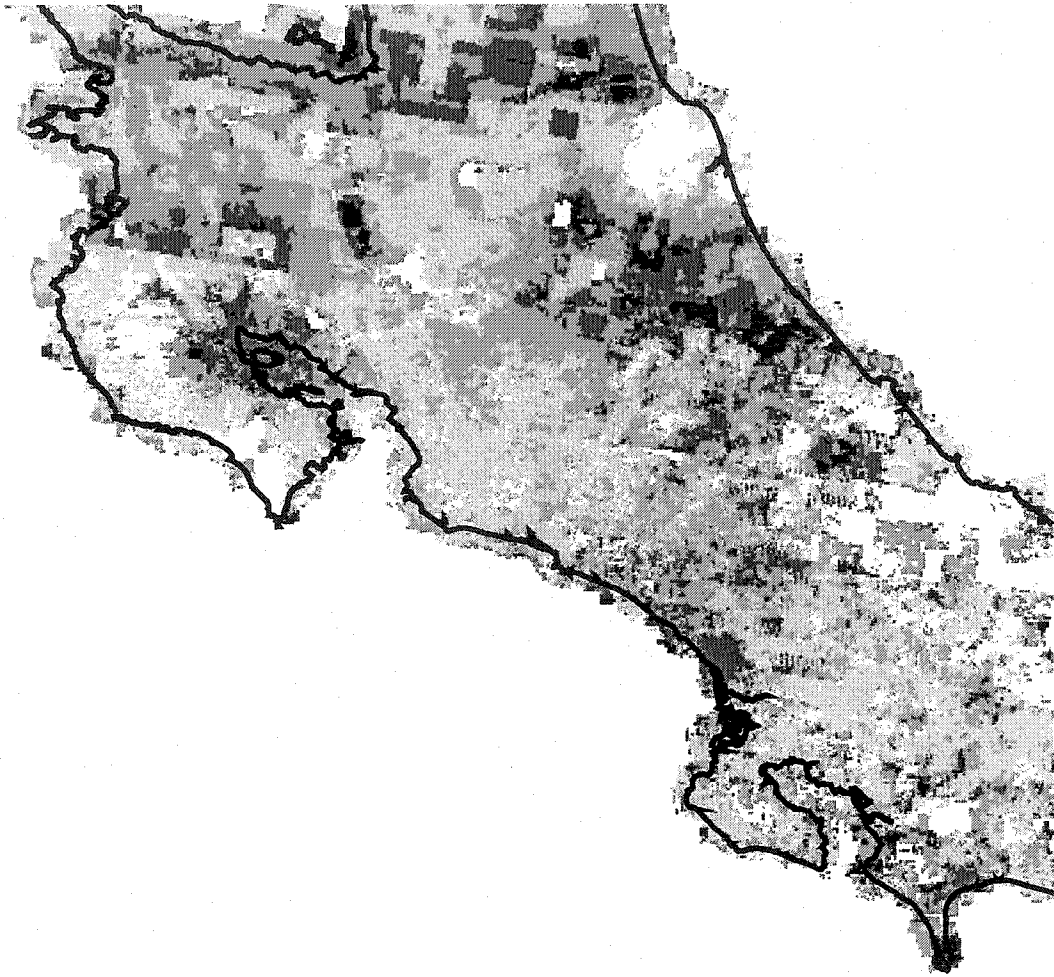


Figure 5-7: Standard deviation of monthly averaged daily PAR ($E\ m^{-2}\ day^{-1}$) for the month of January 2003. Statistical support is the same as that in Figure 5-6. The standard deviation ranges from 0 (white) to 33.6 (black).

An evident source of error is the heterogeneity of the topography and the surface material within the pixel. At a scale of 1 kilometer, at which cloud optical thickness and total column atmospheric water are expressed, this heterogeneity is likely to play a minor role, except in very steep or dissected terrain. However, at scales of 5 kilometer (ozone concentration, cloud top pressure) and 10 kilometer (aerosol properties) the within-pixel differences in topography and surface material can be dramatic. Calculation of PAR under cloud-free conditions is likely to suffer most from such heterogeneity, since the dominant atmospheric property in that calculation is the aerosol load. This is evidenced by the checkerboard pattern in the areas of high irradiance, where the pattern corresponds to the spatial resolution of the MODIS Aerosol product MOD04 (Figure 5-3).

Another source of error is the low temporal resolution of the MODIS observations. In Chapter 3 we reported noticeable differences when measured PAR was averaged over a period of 10 to 30 minutes. In Figure 5-5 a comparison is made between ground-based PAR measurements at 1 minute and 30 minute intervals. As can be seen, even at a 30 minute interval a quantum sensor is incapable of reproducing the sharp edges between sunny and cloudy periods. Although over a longer period of time these deviations tend to cancel out, this smoothing trend is of concern when the method is applied to simulate photosynthesis at the leaf level, because the saturation that takes place at high levels of irradiance can not be realistically reproduced. The two daily MODIS observations are instantaneous and there is thus an element of chance involved in the accurate calculation of PAR based on MODIS observations. This error is of course more prominent in areas of high atmospheric dynamics. Time-averaging of observations can help reduce these errors (Figure 5-6 and Figure 5-7), as is done with the observation of meteorological parameters that have a stochastic element, such as precipitation and wind speed and direction, but the available record of MODIS Aqua data is currently too short to

allow for a statistically rigorous approach comparable to that for other meteorological parameters.

The PARcalc method is a simplification of current radiative transfer models to the degree that the atmosphere is treated as being composed of one (clear sky) or two (cloudy sky) plane-parallel layers. Given the high accuracy of the calculation of instantaneous PAR from MODIS imagery, with an error in the order of 2%, (Chapter 3) these simplifications are acceptable, and even the relatively high accuracy of daily integrated PAR retrieved from pairs of MODIS images should be sufficient for many practical applications, such as models of plant growth or the estimation of NPP (Gates, 1980; Bossel, 1996; Leigh, 1999; Running et al., 1999; Choudhury, 2001).

There are a number of characteristics of MODIS data that influence the most appropriate use of PARcalc estimates of daily PAR in practical applications:

- There are two daily observations on most but not all days, and about half of the days with data are recorded at high viewing angles of the sensor, which negatively impacts on the accuracy of the retrieval of physical parameters.
- Aerosol properties are recorded at a resolution of 10 kilometer, which impacts the calculation of PAR under cloud-free conditions.
- There are sometimes large areas of missing data in MODIS images, due to the inability to extract physical properties of the atmosphere with sufficient accuracy.

Based on these conditions it is advisable not to use individual calculations of PAR from a single pair of MODIS images, but rather to aggregate data over a larger temporal domain (Figure 5-6). Apart from countering the issues identified above, this also allows for the calculation of local statistics (Figure 5-7) that help in establishing the uncertainty or confidence intervals of the PAR data, which in turn can be used in assessing the accuracy of, for instance, models of vegetation growth.

It is interesting to note that including the data calculated from MODIS observations at higher viewing angles in the averaging actually improves the correspondence between the calculated and the observed monthly average (Table 5-2). This appears to be contrary to the results in Table 5-1, where the observations taken at low viewing angles gave better results than those at high viewing angles. However, adding these observations of lower accuracy dampens outlying values due to "uncharacteristic" weather (i.e. an overcast day in the dry season), and it increases the statistical support for the averaging.

2. Comparative performance

Comparing the presented method to other approaches of computing incident PAR is not straightforward as the characteristics of the presented approach (spectral disaggregation, actual atmospheric composition, spatially and temporally explicit) are not included in most other methods. Nevertheless, the PARcalc method is here compared to three approximate methods commonly employed in vegetation studies, a field where the PARcalc method may be very useful. Only a brief description of these methods is given here; full treatment of the methods is provided in the original publications.

The first of these methods uses solar geometry and local topography in combination with a standard atmosphere (developed for the continental United States) (Kumar et al., 1997; Corripio, 2003). This method is spatially and temporally sensitive, but it lacks any information on the state of the atmosphere, which is assumed to be cloud-free and to hold 0.35cm of ozone and 2.0cm of precipitable water. This method is comparable to the PARcalc method, with the notable differences being the empirical relationships used to compute atmospheric transmittance and the broad-band treatment of incident radiation. Kumar et al. (1997) indicate that its primary application would be in the detection of spatial variability in incident radiation, but its assumption of a clear sky results in a very

approximate balance between direct and diffuse irradiation which directly relates to spatial variability in total incident radiation. In locations with considerable cloud cover, which includes essentially all areas of interest to agriculture and forestry, this method is not likely to be accurate.

The second alternative approach here evaluated uses annual trends combined with local observation of total yearly irradiance. This method is presented by Bossel (1996) as part of the TREEDYN3 forest simulation model, but similar approaches are typically employed where local observations are not available. This method uses the total annual radiation receipt in combination with the seasonal cycle of the Sun and the fraction of cloudy days to compute daily irradiance. The method is computationally efficient, but lacks spatial and temporal sensitivity: slope and orientation of the surface, elevation, and seasonality of cloud cover are not considered, and it would be hard to create spatial representations of PAR irradiance. Furthermore, this method relies on measured total radiation, typically from a meteorological observation station, which may be far away. The amount of PAR is assumed to be a portion of total radiation, and it can only be considered correct in magnitude, rather than in actual value.

The third method is based on the remotely sensed radiation balance of the Earth. Several methods have been developed to extract the radiation budget from the Earth (Gautier et al., 1980; Pinker & Laszlo, 1992; Rossow & Garder, 1993; Dubayah & Loechel, 1997; Rossow & Schiffer, 1999), mostly from operational meteorological satellites such as GOES and METEOSAT, but also from the polar-orbiting AVHRR. These methods are attractive, because the radiation budget can be derived at a medium resolution (typically 1 - 4 km), and at a high temporal resolution of 30 minutes to 3 hours. However, there is no accurate method to estimate the amount of PAR in the total radiation balance. Typically, a fraction of 0.4 to 0.5 of total radiation is used (Leigh, 1997; Running et al., 1999), but any

value should be considered approximate. This broad-band method is spatially and temporally explicit (to the scale of the imagery), but it lacks the spectral properties of the PARcalc method.

The most obvious feature in the methods of Kumar and Bossel is the absence of temporal sensitivity. Both methods show a smooth sinusoidal trend which originates in the solar geometry. The sequence of dry and wet seasons is not represented. In Bossel's method there is a linear dependence on the solar declination angle; in Kumar's method the dependence is indirect through the optical air mass. Kumar's method consistently overestimates PAR due to its unrealistically low atmospheric water content and disregard of cloud top reflection. Since this method builds upon empirical relationships developed for a standard atmosphere, there is no mechanism to incorporate actual atmospheric conditions. Bossel's method distributes the actual total annual radiation receipt according to a simple sinusoidal function of the solar zenith angle. In Costa Rica however, as in many other places, the actual distribution is largely dominated by cloud cover (Sanford et al., 1994). This leads to periods of overestimation and underestimation. Further, Bossel's method is completely insensitive to the topography of the terrain and it would be difficult to extrapolate the results over large areas. The broad-band radiation budget derived from remote sensing performs much better both in the temporal and in the spatial domain. However, the radiation balance is only a proxy indicator of actual PAR irradiance.

E. Conclusion

The PARcalc method was applied to pairs of MODIS Terra and Aqua images to produce maps of daily integrated PAR for Costa Rica. Compared to field observations made simultaneously, the daily integrated PAR values had average errors in the order of 5 - 8%, with individual estimation errors as high as 21%, but

monthly averages showed much better correspondence with observations, yielding averaged absolute errors of around 5%.

Compared to alternative methods of estimating daily PAR, the PARcalc method is unique in considering actual atmospheric conditions, twice a day, as well as the topography of the land, and calculating PAR at medium spectral resolution (5 - 10 nm). This makes the PARcalc method particularly suitable for mapping PAR from satellite imagery, something which is virtually impossible with other methods of estimating irradiance, and applying it to studies of vegetation growth and dynamics.

With the spatial resolution of MODIS data, ranging from 1 km for the sensitive cloud optical thickness and total atmospheric water column, to 5 km for ozone concentration and cloud top pressure, to 10 km for aerosol properties, moderately detailed maps of PAR can be produced for regional studies. There are at most two observations of atmospheric conditions per day, which is sufficient to capture the major diurnal atmospheric dynamics in many places on Earth, but not the higher frequency events such as appearance and clearing of cloud cover. It is therefore advisable not to use images of a single day as an accurate estimate of PAR; one should rather rely on temporally aggregated data.

While the combination of pairs of images from MODIS Terra and Aqua sensors yields good estimates of PAR, the use of multi-spectral imagery at higher temporal resolution will enable the extraction of daily integrated PAR with higher accuracy, by being better able to capture changes in the atmospheric state (Figures 5-1 and 5-5). This would be particularly beneficial to plant growth models, as these are typically sensitive to saturation at high levels of irradiance. If the physical atmospheric parameters that the PARcalc method uses can be extracted at the full spatial and temporal resolution of the sensors, the emerging new generation of multispectral meteorological satellites (e.g. METEOSAT Second Generation, GOES-R

Advanced Baseline Imager) holds great promise for the accurate estimation of PAR from remotely sensed imagery.

F. Bibliography

- Bossel, H. (1996). TREEDYN3 forest simulation model. *Ecological Modelling*, 90, 187-227.
- Chazdon, R.L., & Fetcher, N. (1984). Photosynthetic light environments in a lowland tropical rain forest in Costa Rica. *Journal of Ecology*, 72, 553-564.
- Choudhury, B.J. (2001). Estimating gross photosynthesis using satellite and ancillary data: Approach and preliminary results. *Remote Sensing of Environment*, 75, 1-21.
- Corripio, J.G. (2003). Vectorial algebra algorithms for calculating terrain parameters from DEMs and solar radiation modelling in mountainous terrain. *International Journal of Geographical Information Science*, 17, 1-23.
- Dubayah, R., & Loechel, S. (1997). Modeling topographic solar radiation using GOES data. *Journal of Applied Meteorology*, 36, 141-154.
- Gates, D.M. (1980). *Biophysical ecology*. New York, NY: Springer-Verlag.
- Gautier, C., Diak, G. & Masse, S. (1980). A simple physical model to estimate incident solar radiation at the surface from GOES satellite data. *Journal of Applied Meteorology*, 19, 1005-1012.
- Kaufman, Y.J., & Tanré, D. (1998). *Algorithm for remote sensing of tropospheric aerosol from MODIS. Algorithm theoretical basis document*. Greenbelt, MD: NASA Goddard Space Flight Center.
- Kumar, L., Skidmore, A.K. & Knowles, E. (1997). Modelling topographic variation in solar radiation in a GIS environment. *International Journal of Geographical Information Science*, 11, 475-497.

- Leigh, E.G., Jr. (1999). *Tropical forest ecology: A view from Barro Colorado Island*. New York, NY: Oxford University Press.
- LI-COR (1996). Calibration procedures for LI-COR spectroradiometers, radiation sensors & lamps. LI-COR Biosciences, Application note #109. Lincoln, NE: LI-COR, Inc.
- Ostertag, R. (1998). Belowground effects of canopy gaps in a tropical wet forest. *Ecology*, 79, 1294-1304.
- OTS (Organization for Tropical Studies) (2004). La Selva Meteorological data. Online: http://www.ots.ac.cr/rdmcnfs/datasets/meteoro/ls_met/.
- Pinker, R.T., & Laszlo, I. (1992). Modeling surface solar irradiance for satellite applications on a global scale. *Journal of Applied Meteorology*, 31, 194-211.
- Rossow, W.B., & Garder, L.C. (1993). Validation of ISCCP cloud detections. *Journal of Climate*, 6, 2370-2393.
- Rossow, W.B., & Schiffer, R.A. (1999). Advances in Understanding Clouds from ISCCP. *Bulletin of the American Meteorological Society*, 80, 2261-2287.
- Running, S.W., Nemani, R., Glassy, J.M. & Thornton, P.E. (1999). *MODIS daily photosynthesis (PSN) and annual net primary production (NPP) product (MOD17). Algorithm theoretical basis document*. Version 3.0. Missoula, MT: University of Montana.
- Sanford, R.L., Jr., Paaby, P., Luvall, J.C., & Phillips, E. (1994). Climate, geomorphology and aquatic systems. In: L.A. McDade, K.S. Bawa, H.A. Hespenheide and G.S. Hartshorn (Eds.), *La Selva: Ecology and natural history of a neotropical rain forest*. Chicago, IL: The University of Chicago Press.

Vermote, E.F., & Vermeulen, A. (1999). *Atmospheric correction algorithm: spectral reflectances (MOD09). Algorithm theoretical basis document. Version 4.0.* MD: University of Maryland.

Chapter 6

CONCLUSIONS

This thesis dealt with two conceptually disparate subjects – focusing in on where change in the landscape is taking place, and providing detailed PAR base data for biophysical models – but they are nevertheless both required in constructing advanced models of natural systems such that more accurate analyses can be made in a spatially exhaustive manner.

A. Focus on deforestation

The spatial analysis presented in Chapter 2 enables a user to identify those areas that are at risk of land cover change in the near future, based on an analysis of recent land cover change and the causes of that change. Given the typically scarce resources of land management agencies, the ability to concentrate on certain areas rather than on an expansive land base can mean the difference between proactive management or enforcement and responsive action after the damage has been done.

Apart from using the method as an indicator tool, it can also be used to assess the vulnerability of special areas, such as national parks or biological corridors, for land cover changes either in those areas themselves, or in their vicinity. Since the method indicates potential future land cover changes, mitigation strategies can be developed in time to protect those sensitive areas.

The method also allows researchers to focus their efforts on understanding or describing the ecosystem in areas at risk through detailed analyses. There are specific types of ecological research that concentrate on areas undergoing or having undergone land cover change, such as gap analysis, dispersal of plant genetic

material, and migratory behaviour of birds, to name a few. These kinds of research would benefit from having an *a priori* indication of where change is likely to take place, such that the ecological condition of an area can be described in its undisturbed state before the change takes place. More in general, the ability to concentrate on areas of specific interest helps to employ resources where they are most effective. Particularly when complex biophysical models are used which require multiple inputs of hard to obtain data, or for which a numerical solution over large areas is computationally not feasible, the proper selection of a study area is of paramount importance. In those situations where land cover change – not only deforestation, but essentially any observable change in land cover – is a factor, the presented method could be a valuable tool.

B. The PARcalc method

The PARcalc method presented in Chapter 3 can also play an important role in enhancing biophysical models, but from a different perspective. Solar radiation is ultimately the source that drives all biological processes. To date, however, little spatially and temporally explicit data was available on the terrestrial PAR radiation regime. In the absence of such data biophysical models have tended to rely on field observations of PAR, which are expensive to obtain and which offer few options for scaling up from the field experiment to the regional scale, on the spatial and temporal extrapolation of spatially sparse observations of broad-band radiation at meteorological observation stations, or on the correlation between PAR and proxy parameters from remotely sensed imagery, such as broad-band irradiance or the normalized difference vegetation index (NDVI). None of these three options offer the array of properties that would make these approaches truly useful in biophysical models that operate at the landscape or regional level: spatially exhaustive, temporally exhaustive, and sensitive to actual atmospheric conditions or seasonal trends. The presented PARcalc method has these three properties, as well as the

ability to calculate irradiance in the PAR region (400 nm to 700 nm) in 52 distinct wavelength bands. This latter ability opens up the possibility to make the photosynthesis component of biophysical models more accurate by exploiting the differential radiation absorption characteristics of chlorophyll in green plant tissues (Gates, 1980; Leigh, 1999). The kinds of biophysical models that could benefit from such improved estimates of PAR include those used in agricultural studies to estimate crop production, but also in models of general vegetation growth which are employed in climate change modelling and carbon sequestration studies.

The PARcalc method is not a complete solution to model irradiance on the surface though. The PARcalc method accurately computes the attenuation of radiation through the atmosphere, but it does not account for the important processes of bidirectional reflectance off the vegetation or the surface, or for multiple scattering between vegetative or mineral surfaces. Solutions have been proposed for these processes (e.g., Gastellu-Etchegorry et al., 1999), and in combination with the presented PARcalc method these should provide a complete solution to model PAR irradiance on vegetative surfaces.

The ability to produce maps of PAR irradiance at a relatively high resolution of 1 km (compared to other sources of irradiance data) from the global MODIS data set opens up possibilities to create a climatology of PAR from multi-year observations, similar to the procedure presented in Chapter 5. While the current availability of data from the pair of MODIS sensors aboard the Terra and Aqua satellites is too small to produce statistically rigorous averages, this situation will improve over time. Furthermore, given that the PARcalc method estimates PAR with unparalleled precision, its application may be warranted even in the absence of long time series of observations.

The near real-time availability of the data also makes it valuable as a tool to monitor or forecast crop development throughout a growing season. In combination

with similar monitoring systems for other environmental variables, such as rainfall and NDVI in the Africa Real-Time Environmental Monitoring and Information System (ARTEMIS) in operation by the Food and Agriculture Organization of the United Nations, powerful tools could be developed to help mitigate the consequences of environmental disasters.

C. Bibliography

- Gastellu-Etchegorry, J.P., Guillevic, P., Zagolski, F., Demarez, V., Trichon, V., Deering, D., & Leroy, M. (1999). Modeling BRF and radiation regime of boreal and tropical forests: I. BRF. *Remote Sensing of Environment*, 68, 281-316.
- Gates, D.M. (1980). *Biophysical ecology*. New York, NY: Springer-Verlag.
- Leigh, E.G., Jr. (1999). *Tropical forest ecology: A view from Barro Colorado Island*. New York, NY: Oxford University Press.

Appendix A

ALGORITHMIC STRUCTURE OF THE PARCALC METHOD

The PARcalc method is written in object-oriented Pascal and it runs on the Windows and Linux operating systems. This appendix lists the core functions used in this thesis in pseudo-code.

At the core of the PARcalc method are two functions: one which calculates instantaneous PAR under cloudless conditions, and one where there is cloud cover. These two functions essentially implement Equations 3-1 to 3-16.

```
function ComputeClearSky(a : TAtmosphere; Io: TIoArray) : TInstantaneous;
var l : integer;
    mp, tauR, tauZ, tauA, tauW, kwm: double;
begin
    mp := a.m0 * a.pz;
    Result.beam := 0.0;
    Result.diffuse := 0.0;

    // Loop from 400nm to 680nm
    for l := 1 to 50 do begin
        tauR := Exp(Rayleigh[l] * mp);
        tauZ := Exp(O3[l] * a.ozone * a.m0);
        tauA := Exp(Angstrom[l] * a.angst * mp);
        Result.beam := Result.beam + Io[l] * tauR * tauZ * tauA * a.sinalfa;
        Result.diffuse := Result.diffuse + a.sinalfa * a.skyview * Io[l] * tauZ *
            (0.5 * tauA * (1 - tauR) + a.scatter * tauR * (1 - tauA));
    end;

    // 690nm, include water absorption
    tauR := Exp(Rayleigh[51] * mp);
    tauZ := Exp(O3[51] * a.ozone * a.m0);
    tauA := Exp(Angstrom[51] * a.angst * mp);
    kwm := WaterAbsorption[51] * a.water * a.m0;
    tauW := Exp(-0.2385 * kwm / Power(1 + 20.07 * kwm, 0.45));
    Result.beam := Result.beam + Io[51] * tauR * tauZ * tauA * tauW * a.sinalfa;
    Result.diffuse := Result.diffuse + a.sinalfa * a.skyview * Io[51] * tauZ * tauW *
        (0.5 * tauA * (1 - tauR) + a.scatter * tauR * (1 - tauA));

    // 700nm, include water absorption
    tauR := Exp(Rayleigh[52] * mp);
    tauZ := Exp(O3[52] * a.ozone * a.m0);
    tauA := Exp(Angstrom[52] * a.angst * mp);
    kwm := WaterAbsorption[52] * a.water * a.m0;
    tauW := Exp(-0.2385 * kwm / Power(1 + 20.07 * kwm, 0.45));
    Result.beam := Result.beam + Io[52] * tauR * tauZ * tauA * tauW * a.sinalfa;
    Result.diffuse := Result.diffuse + a.sinalfa * a.skyview * Io[52] * tauZ * tauW *
        (0.5 * tauA * (1 - tauR) + a.scatter * tauR * (1 - tauA));
end;
```

```

function ComputeCloudySky(a : TAtmosphere; Io: TIOArray) : TInstantaneous;
var l : integer;
mp, tauR, tauA, tauW, kwm, transmittance : double;
begin
  Result.beam := 0.0;
  Result.diffuse := 0.0;

  // Attenuation above the clouds and cloud top reflectance. Reduce Io
  // according to the cloud top reflectance.
  mp := a.m0 * a.prs;
  transmittance := InterpolateBeta(a.tau, a.sinalfa) * a.tau / a.sinalfa;
  transmittance := 1 - transmittance / (1 + transmittance);
  for l := 1 to 50 do begin
    tauR := Exp(Rayleigh[l]) * mp + O3[l] * a.ozone * a.m0;
    tauA := Exp(Angstrom[l]) * a.angst * mp;
    Io[l] := Io[l] * tauR * tauA * transmittance;
  end;
  tauR := Exp(Rayleigh[51]) * mp + O3[51] * a.ozone * a.m0;
  tauA := Exp(Angstrom[51]) * a.angst * mp;
  Io[51] := Io[51] * tauR * tauA * transmittance;
  tauR := Exp(Rayleigh[52]) * mp + O3[52] * a.ozone * a.m0;
  tauA := Exp(Angstrom[52]) * a.angst * mp;
  Io[52] := Io[52] * tauR * tauA * transmittance;

  // Attenuation below the clouds
  // Loop from 400nm to 680nm
  mp := a.m0 * (a.pz - a.prs);
  for l := 1 to 50 do begin
    tauR := Exp(Rayleigh[l]) * mp;
    tauA := Exp(Angstrom[l]) * a.angst * mp;
    Result.beam := Result.beam + Io[l] * tauR * tauA * a.sinalfa;
    Result.diffuse := Result.diffuse + a.sinalfa * a.skyview * Io[l] *
      (0.5 * tauA * (1 - tauR) + a.scatter * tauR * (1 - tauA));
  end;

  // 690nm, include water absorption
  tauR := Exp(Rayleigh[51]) * mp;
  tauA := Exp(Angstrom[51]) * a.angst * mp;
  kwm := WaterAbsorption[51] * a.water * a.m0;
  tauW := Exp(-0.2385 * kwm / Power(1 + 20.07 * kwm, 0.45));
  Result.beam := Result.beam + Io[51] * tauR * tauA * tauW * a.sinalfa;
  Result.diffuse := Result.diffuse + a.sinalfa * a.skyview * Io[51] * tauW *
    (0.5 * tauA * (1 - tauR) + a.scatter * tauR * (1 - tauA));

  // 700nm, include water absorption
  tauR := Exp(Rayleigh[52]) * mp;
  tauA := Exp(Angstrom[52]) * a.angst * mp;
  kwm := WaterAbsorption[52] * a.water * a.m0;
  tauW := Exp(-0.2385 * kwm / Power(1 + 20.07 * kwm, 0.45));
  Result.beam := Result.beam + Io[52] * tauR * tauA * tauW * a.sinalfa;
  Result.diffuse := Result.diffuse + a.sinalfa * a.skyview * Io[52] * tauW *
    (0.5 * tauA * (1 - tauR) + a.scatter * tauR * (1 - tauA));
end;

```

The calculation of instantaneous PAR, as well as its daily integration, requires the calculation of solar geometry for the given day and time. For the production of PAR maps from MODIS data (Chapter 5) this function is embedded in an external loop that calls this function for every pixel on the map.

```

function CalcPAR(const data: TDSprRaster; today: integer; time: double): TPAR;
var
  latitude, elev, direct: double;
  sinlat, coslat, sinhour, coshour, sindecl, cosdecl : extended;
  dt, sunset, hour, alfa, ecc: double;
  diff, beam: single;
  e: integer;
  Io : TIoArray;
  curr : TAtmosphere;
  radiation : TInstantaneous;
begin
  Result := 0;
  dt := time * 0.0043633;          // Time step in radians

  // Daily constants
  sindecl := SinDeclination[today];
  cosdecl := CosDeclination[today];
  ecc := Eccentricity[today];

  curr.pz := Exp(-0.0001184 * elev);
  SinCos(latitude, sinlat, coslat);
  hour := ArcCos(-sinlat * TanDeclination[today] / coslat); // = sunrise (rad)
  sunset := -hour;

  // Loop from sunrise to sunset
  while hour > sunset do begin
    for e := 1 to 52 do Io[e] := TOA[e] * ecc; // correct for eccentricity

    SinCos(hour, sinhour, coshour);
    sinalfa := sinlat * sindecl + coslat * cosdecl * coshour;
    if curr.sinalfa > 0.0 then begin
      alfa := ArcSin(curr.sinalfa);
      if alfa >= PI3 then curr.m0 := 1 / curr.sinalfa
      else curr.m0 := 1 / (curr.sinalfa + 0.15 * Power((3.885 + alfa), -1.253));
      scatter := DetermineScatter; // calculate forward scatterance from MODIS
                                   // aerosol properties
      tau > 0 then radiation := ComputeCloudySky(curr, Io)
      else radiation := ComputeClearSky(curr, Io);
      Result := Result + radiation;
    end;
    hour := hour - dt;
  end;
  diffuse := diff * 0.00006 * time;
  direct := beam * 0.00006 * time;
end;

```
